

Modelling Sequential
Biosphere Systems
under Climate Change
for Radioactive
Waste Disposal

EC-CONTRACT : FIKW-CT-2000-00024

Deliverable D4/5:

Global climatic characteristics, including vegetation and seasonal cycles over Europe, for snapshots over the next 200,000 years.



Work package 2: Simulation of the future evolution of the biosphere system using the hierarchical strategy

RESTRICTED

'All property rights and copyrights are reserved. Any communication or reproduction of this document, and any communication or use of its content without explicit authorization is prohibited. Any infringement to this rule is illegal and entitles to claim damages from the infringer, without prejudice to any other right in case of granting a patent or registration in the field or intellectual property.'



Foreword

The BIOCLIM project on modelling sequential BIOSphere systems under CLimate change for radioactive waste disposal is part of the EURATOM fifth European framework programme. The project was launched in October 2000 for a three-year period. The project aims at providing a scientific basis and practical methodology for assessing the possible long term impacts on the safety of radioactive waste repositories in deep formations due to climate and environmental change. Five work packages have been identified to fulfil the project objectives:

Work package 1 will consolidate the needs of the European agencies of the consortium and summarise how environmental change has been treated to date in performance assessments.

Work packages 2 and 3 will develop two innovative and complementary strategies for representing time series of long term climate change using different methods to analyse extreme climate conditions (the hierarchical strategy) and a continuous climate simulation over more than the next glacial-interglacial cycle (the integrated strategy).

Work package 4 will explore and evaluate the potential effects of climate change on the nature of the biosphere systems.

Work package 5 will disseminate information on the results obtained from the three year project among the international community for further use.

The project brings together a number of representatives from both European radioactive waste management organisations which have national responsibilities for the safe disposal of radioactive waste, either as disposers or regulators, and several highly experienced climate research teams, which are listed below.

-
- Agence Nationale pour la Gestion des Déchets Radioactifs (Andra), France – **J. Brulhet, D. Texier**
 - Commissariat à l’Energie Atomique/ Laboratoire des Sciences du Climat et de l’Environnement (CEA/LSCE) France – **N. de Noblet, D. Paillard, D. Lunt, P. Marbaix, M. Kageyama**
 - United Kingdom Nirex Limited (NIREX), UK – **P. Degnan**
 - Gesellschaft für Anlagen und Reaktorsicherheit mbH (GRS), Germany – **A. Becker**
 - Empresa Nacional de Residuos Radioactivos S.A. (ENRESA), Spain – **A. Cortés**
 - Centro de Investigaciones Energeticas, Medioambientales y Tecnológicas (CIEMAT), Spain – **A. Aguero, L. Lomba, P. Pinedo, F. Recreo, C. Ruiz**
 - Universidad Politecnica de Madrid Escuela Tecnica Superior de Ingenieros de Minas (UPM-ETSIMM), Spain – **M. Lucini, J.E. Ortiz, T. Torres**
 - Nuclear Research Institute Rez, plc - Ustav jaderného výzkumu Rez a.s. (NRI) – **Czech Republic – A. Laciok**
 - Université catholique de Louvain/ Institut d’Astronomie et de Géophysique Georges Lemaître (UCL/ASTR), Belgium – **A. Berger, M.F. Loutre**
 - The Environment Agency of England and Wales (EA), UK – **R. Yearsley, N. Reynard**
 - University of East Anglia (UEA), UK – **C. Goodess, J. Palutikof**
 - ENVIROS QuantiSci, UK – **B. Watkins, M. Egan**
-

For this specific deliverable, the main contributor is the CEA/LSCE. The GCM simulations were carried out by D. Lunt and the vegetation simulations by N. de Noblet. We are very grateful to S. Charbit for running the ice-sheet model off-line to provide us with the necessary ice-sheet boundary conditions to run the “no-greenland” simulations and the future glacial maximum (178 kyr AP).

Public should be aware that BIOCLIM material is working material.



Content List

1- Introduction	6
2 - Model description	7
2.1 - The Atmosphere: LMDz	7
2.2 - The Ocean: OCRA-LIM	7
2.3 - The ocean damping	8
2.4 - The Biosphere: ORCHIDEE	9
3 - Simulation “Baseline” – Present day control	11
3.1 - Air Temperature	11
3.2 - Precipitation	12
3.3 - Sea Ice and Snow cover	12
3.4 - Vegetation	13
4 - GCM future-climate simulations	19
4.1 - Boundary Conditions	19
4.2 - Simulation “A” – CO ₂ =1100PPMV	21
4.3 - Simulation “E” – 67KYR AP ORBIT	22
4.4 - Simulation “D” – 67KYR AP ORBIT, and melted Greenland ice sheet	23
4.5 - Simulation “C” – 67KYR AP ORBIT, melted Greenland ice sheet, and CO ₂ =550PPMV	24
4.6 - Simulation “B” – melted Greenland ice sheet, and CO ₂ =550PPMV	24
4.7 - Simulation “F” – increased northern hemisphere ice sheets, CO ₂ =280PPMV, and 178KYR AP ORBIT.	25
4.8 - Summary of results	26
5 - Timeseries over the european sites	27
5.1 - 2m air temperature	27
5.2 - Precipitation	28
5.3 - Snow fall	28
5.4 - Wind strength	29
6 - Vegetation characteristics over Europe	30
6.1 - Methodology	30
6.2 - Vegetation distributions at the European scale	30
6.3 - Changes in vegetation distribution and surface climate at the selected studied areas	32
6.4 - Summary of the changes in vegetation distribution	34
7 - Critical dicussion	38
7.1 - Uncertainty	38
7.2 - Comparison with previous work	39
7.2.1 - Simulation “A” - comparison with IPCC	39
7.2.2 - Simulation “A” - Comparison with UKCIPO2 and ICCF	40
7.2.3 - Simulation “D” - Comparison with Vavrus and Kutzbach (2002)	41
8 - Recommendations	43
9 - Data products	44
10 - References	45
List of figures	48



1. Introduction

The aim of the BIOCLIM project is to develop and present techniques that can be used to develop self-consistent patterns of possible future climate changes over the next million years (climate scenarios), and to demonstrate how these climate scenarios can be used in assessments of the long-term safety of nuclear waste repository sites.

Within the project, two strategies are implemented to predict climate change. The first is the hierarchical strategy, in which a hierarchy of climate models is used to investigate the evolution of climate over the period of interest. These models vary from very simple 2-D and threshold models, which simulate interactions between only a few aspects of the earth system, through general circulation models (GCMs) and vegetation models, which simulate in great detail the dynamics and physics of the atmosphere, ocean, and biosphere, to regional models, which focus in particular on the European region and the specific areas of interest. The second strategy is the integrated strategy, in which intermediate complexity climate models are developed, and used to consecutively simulate the development of the earth system over many millennia. Although these models are relatively simple compared to a GCM, they are more advanced than 2D models, and do include physical descriptions of the biosphere, cryosphere, atmosphere and ocean.

This deliverable, D4/5, focuses on the hierarchical strategy, and in particular the GCM and vegetation model simulation of possible future climates. Deliverable D3 documented the first step in this strategy. The Louvain-la-Neuve 2-D climate model

(LLN-2D) was used to estimate (among other variables) annual mean temperatures and ice volume in the Northern Hemisphere over the next 1 million years. It was driven by the calculated evolution of orbital parameters, and plausible scenarios of CO₂ concentration. From the results, 3 future time periods within the next 200,000 years were identified as being extreme, that is either significantly warmer or cooler than the present. The next stage in the hierarchical strategy was to use a GCM and biosphere model, to simulate in more detail these extreme time periods.

This deliverable starts with a description of the GCM and biosphere models used, and continues with an assessment of the models' performance in simulating the present day climate. It then gives a summary of the boundary conditions that constrain the model for the future climate simulations, as indicated by the LLN-2D model, and describes how these boundary conditions are implemented in the models. The majority of the deliverable is a description of the GCM results for the future climate simulations, and the resulting vegetation distributions. This is followed by a section focusing on the areas of specific interest. Finally, there is a critical discussion, which includes a comparison of some of the results with previous work, and an assessment of the uncertainty in the model results.

There are many figures in this deliverable, all of which are included at the back. However, not all of the potentially interesting data from the models is discussed or presented. Therefore, data from all the simulations are available on the business collaborator at <http://cobweb.businesscollaborator.com/bc/bc.cgi>.



2. Model description

The GCM results presented in this deliverable were obtained using the IPSL (Institut Pierre Simon Laplace, Paris) global coupled ocean-atmosphere model, IPSL_CM4_D. The biosphere model which is forced by the output from the GCM, is ORCHIDEE. This section briefly describes the different submodels that make up the GCM and biosphere model. Within IPSL_CM4_D, the atmosphere submodel is LMDz, the land surface submodel is SECHIBA (also used in the biosphere model), and the ocean submodel is ORCA-LIM. For the BIOCLIM GCM simulations, the

ocean model is modified from the standard GCM, IPSL_CM4, in that it contains a damping term in the deep ocean, which nudges the ocean temperatures and salinities towards those of present day observations. The damping, which is applied in order to minimize the time required to achieve equilibrium in the model, is also described in some detail in this section. Within ORCHIDEE, the land surface submodel is SECHIBA, the carbon cycle submodel is STOMATE, and the vegetation submodel is LPJ.

2.1. - The Atmosphere: LMDz

The atmosphere submodel is LMDz3.3 [Ref. 1]. It is run at a resolution of 72 gridboxes in longitude (5°), and 45 gridboxes in latitude (mean 4°), and 19 vertical sigma (terrain following) levels. Figure 1 shows the model resolution over the European region. The model has two main constituents: dynamical, and physical. The dynamical part solves the primitive fluid dynamical equations in three dimensions. The physical part includes the Tiedtke parameterisation of convection [Ref. 2], and a treatment of radiation following Fouquart and Bonnel [Ref. 3] in the short-wave, and Morcrette in the long-wave [Ref. 4]. Standard empirical thermodynamic

functions are used to calculate the value and temporal derivative of specific humidity [Ref.1]. Diffusion in the boundary layer due to sub-gridscale eddies is set proportional to the tracer gradient, with a coefficient depending on the atmospheric stability. There is specific treatment of the effect of sub-gridscale orography. The model includes vertically varying empirical distributions of saturation within each gridbox, which leads to a realistic distribution of cloudiness. Of particular interest for the BIOCLIM project, the user can prescribe the global mean CO₂ concentration, orbital forcing, orography, and the fraction of land covered by ice-sheets.

2.2. - The Ocean: ORCA-LIM

ORCA is the name given to a series of global ocean configurations, with differing resolutions, that use the OPA model [version 8.2, Ref. 5]. We use the ORCA4 model, which has a 4 degree mean zonal resolution, and a 2.5 degree meridional resolution. In order to overcome errors associated with advection close to the pole (present in nearly all advection schemes), the North Pole is shifted to lie over North America. In the vertical, there are 31 levels, with 10 levels in the top 100m of the ocean. The OPA model solves an approximate form of the Navier-Stokes equations and the equation of state. The Boussinesq, spherical earth, and thin-shell (that is, the depth of the

ocean is small in comparison to the radius of the Earth) approximations are applied, and the ocean is assumed to be incompressible, hydrostatic, and to have a rigid lid. Vertical turbulent fluxes are assumed to be proportional to the gradients of large-scale quantities, such as temperature. The ORCA4 configuration is non-eddy resolving; the model includes a parameterisation of mesoscale sub-gridscale processes [Ref. 6]. The equation of state comes from a look-up table [Ref. 7]. There is no flow of heat, salt, or momentum across solid boundaries; however, momentum is exchanged between the ocean and the earth through friction processes. There are fresh water fluxes at the mouths

of rivers. The ocean and atmosphere are free to exchange momentum and heat. Between sea-ice and the ocean, there is, in addition, an exchange of salinity. Downwards radiation penetrates the top few meters of the ocean.

LIM, the Louvain-la-Neuve sea-ice model [Ref. 8], is used in conjunction with ORCA. It contains both thermodynamic and dynamic processes. At the ice-ocean interface, the sensible heat flux is proportional

to the temperature difference between the surface layer and its freezing point and to the friction. The ice-ocean stress is taken to be a quadratic function of the relative velocity between ice and the uppermost level of the ocean. Considering salt and freshwater exchanges between ice and ocean, brine is released to the ocean when ice is formed, while freshwater is transferred to the ocean when sea ice or snow melts. (This description of the LIM model has been taken from <http://www.astr.ucl.ac.be/tools/clio.html>).

2.3. - The ocean damping

All the GCM simulations carried out as part of this project start from the same initial conditions, both in the atmosphere and in the ocean. These initial conditions are representative of the current climate. Therefore, for the present day simulation, the model equilibrates relatively quickly (a few years). However, if a change in forcing is applied (for example increased CO₂), or if the boundary conditions are changed (for example a change in the ice-sheet volume and extent), the GCM could take a very long time to equilibrate, especially in the deep ocean (of order hundreds of years). This long run time is prohibitive for the BIOCLIM project, where several simulations are required in a relatively short time. Traditionally, two alternative approaches have been used to overcome this problem, without running fully coupled simulations. Firstly, changes to the ocean can be completely neglected, and the sea surface temperatures (SSTs) held constant. Secondly, a slab ocean can be used, which neglects dynamical changes in the ocean circulation, but allows thermodynamic feedbacks to take place between the ocean and atmosphere. Slab oceans are typically about 50m in depth, and take just a few years to equilibrate. In the BIOCLIM project, we use an innovative approach, in which the ocean is coupled to the atmosphere, and has some dynamical freedom, but in which the deep ocean temperatures and salinity are constrained. This section describes this approach in more detail.

A Newtonian damping term is added to the equations of temperature and salinity evolution. This effectively 'nudges' the calculated temperature and salinity, in the

deep ocean, towards the observations. The damping means that the deep ocean comes into equilibrium much more quickly, but leaves the upper ocean free to interact with the atmosphere. However, it is likely that the damping precludes the model representing changes in the mode of the thermohaline circulation, although this is yet to be tested.

The time evolution of temperature $\partial T / \partial t$, (and similarly for salinity) in the ocean model, is given by the following equation:

$$\frac{\partial T}{\partial t} = \mathbf{u} \cdot \nabla T + Q + D$$

where $\mathbf{u} \cdot \nabla T$ is the advection term, Q is a heat exchange term, and D is a diffusion term. In the damped ocean, a further term is added:

$$\frac{\partial T}{\partial t} = \mathbf{u} \cdot \nabla T + Q + D + \frac{1}{\tau} (T_{obs} - T)G$$

where T_{obs} are observed ocean temperatures, τ is a time constant, G is a factor varying with position and depth.

The time constant, τ , varies with depth, to preserve a constant relation between the damping term and the advection, heat, and diffusion terms. τ varies between 50 days near the surface, to 1 year near the ocean floor. In the uppermost 100 metres of the ocean, there is no damping, as this allows the ocean to evolve high latitude sea-ice more freely under changes in forcing.

The damping is not applied in regions close to continental boundaries or at the ocean floor, as this allows the model to construct its own boundary structures, in equilibrium with its physics. Nor is it applied in the equatorial region, with low coriolis parameter, f , because inconsistencies between the dynamics of the model and the observed temperatures and salinities, can lead to unrealistic circulations, the magnitude of which scale with $1/f$. Furthermore, the damping is not applied in regions of strong vertical mixing, where the timescale of adjustment is small.

Regions of strong vertical mixing are defined to be where the eddy viscosity parameter, ν , is greater than $0.5\text{m}^2\text{s}^{-1}$; this region is called the turbocline. It is deepest in the North Atlantic and Southern Ocean, and is shallowest in the Arctic; however, there it has significant temporal and spatial variability. In the GCM simulations carried out in this project, with the damped ocean, it is found that 10 years of model time are sufficient for the ocean to come into equilibrium with the atmosphere.

2.4. - The Biosphere: ORCHIDEE

ORCHIDEE is a dynamical global vegetation model developed in France by Krinner et al. (in prep.) and thereby simulates the vegetation distribution responding to the input climate. It is principally designed to be coupled on-line to atmospheric general circulation models (AGCMs) or regional climate models, but it can also be used off-line, where the atmospheric forcing is imposed from either observations or any available climate simulation (as in BIOCLIM project). ORCHIDEE simulates the principal processes of vegetation functioning which influence the global carbon cycle (e.g. photosynthesis, autotrophic and heterotrophic respiration of plants and in soils) as well as latent, sensible, and kinetic energy exchanges at the surface of soils and plants. As a dynamical vegetation model, it explicitly represents competition processes such as light competition, gaps¹, and establishment². It can thus be used in transient simulations of climate change, but it can also be used with a prescribed vegetation distribution. The whole seasonal phenological cycle is calculated prognostically without any prescribed dates or use of satellite data.

ORCHIDEE includes three sub-models which address different time-scales (figure 2). The first, which interacts with the atmosphere, is named SECHIBA [Ref. 9; Ref. 10] and it computes all instantaneous fluxes at the land-surface / atmosphere interface. The second is STOMATE (Viovy et al. unpublished) which

computes the daily variations of the canopy (e.g. allocation processes and fire) and of all carbon reservoirs in both plants and soils. The last module comes from the dynamical model LPJ [Ref.11] and includes all slow processes (longer than 1 day), for example competition (for resources and differential responses to fire) and establishment, which allow for changes in vegetation distribution. In addition each PFT is assigned bioclimatic limits which determine whether it can survive and / or regenerate under the climatic conditions prevailing in a particular grid-cell at a particular time in the simulation (table 1).

In this project, the SECHIBA (fast processes) part of ORCHIDEE has been used on-line for the coupled IPSL_CM4_D simulations described prior in this section, while the full code has been used off-line to simulate the changes in vegetation resulting from the simulated climates, which have been run according to the definitions described in Deliverable 3 (table 1 in section 4).

The land-surface, in ORCHIDEE, is described as a mosaic of 12 Plant Functional types (PFTs) and bare soil (see table 1). Each of these 13 surface descriptors can simultaneously occupy the same area (grid box). Fluxes and soil moisture reservoirs are computed separately for each PFT (and bare soil), while only one surface temperature is computed for each grid-box³. Results from the model runs include 1) the partitioning of

1) gaps = bare soil spaces between plants

2) establishment = introduction of individual plants in the open space (gap)

3) The fluxes computed for each PFT are added to participate to the energy balance of the grid-box.

vegetation at each site and for each climate considered, 2) some annual values, including rainfall and total evapotranspiration, and 3) seasonal cycles of some chosen variables which, to our opinion, describe best the behaviour of land-atmosphere exchanges and of their effect on land status.

It is important to note that ORCHIDEE, when run with its dynamic mode turned on, does not account for the effects of humans on landscape. Therefore the output is the potential vegetation that would arise simply

due to climate influences i.e. a theoretical natural vegetation.

Climatological monthly data are prescribed to ORCHIDEE for all simulations described herein, and are interpolated by a weather generator (J. Foley pers. comm..) to provide the 1-hour time series of meteorological data required to run ORCHIDEE. The weather generator also generates an interannual variability necessary to drive the dynamic component of ORCHIDEE.

Plant Functional Types (PFTs) and non-vegetated surfaces	Abbreviation	Bioclimatic Limits ^{4,5}	
		Tmin ⁸	Tmin ⁹
Bare Ground	BG	-	-
Tropical broad-leaved evergreen	TBLE	0	-
Tropical broad-leaved raingreen	TBLR	0	-
Temperate needle-leaf evergreen	TeNLE	-45°	5°C
Temperate broad-leaved evergreen	TeBLE	-10°C	15.5°C
Temperate broad-leaved summergreen	TeBLS	-45°C	15.5°C
Boreal needle-leaf evergreen	BNLE	-60°C	-2°C
Boreal broad-leaved summergreen	BBLS	-60°C	5°C
Boreal needle-leaf summergreen	BNLS	-	-2°C
C3 ⁶ grass	C3g	-	-
C4 ⁷ grass	C4g	-	-
C3 agriculture (e.g. wheat)	C3a	-	-
C4 agriculture (e.g. corn)	C4a	-	-

Table 1: List of the thirteen land-surface types accounted for in ORCHIDEE: 12 Plant Functional Types plus bare ground.

4) For all PFTs a minimum of 150 degree-days is required to establish or regenerate (sum of daily temperature above 0°C).

5) Where no number is given, no threshold is being applied

6) Carbon fixation in C3 plants relies on ribulose 1,3-bisphosphate carboxylase, and the first product is 3-phosphoglycerate. Most plants in temperate regions are C3.

7) In C4 plants CO₂ reacts with phosphoenolpyruvate in a reaction catalysed by phosphoenolpyruvate carboxylase, producing oxaloacetate. Oxaloacetate is a 4C molecule. Most grasses in tropical regions are C4.

8) Tmin = critical minimum temperature (hourly computed) below which PFT cannot survive.

9) Tomin = critical temperature of the coldest month. If the coldest month temperature exceeds this value then the PFT under consideration will not establish nor regenerate.



3. Simulation “Baseline” - Present Day Control

In this section, the GCM results from the simulation “Baseline”, the present day control experiment, and the resulting vegetation distribution, are compared with observations. This provides an indicator of the accuracy of the models used in the future-climate simulations that follow. It is also useful because, in

the following sections, it is primarily anomalies, from the control or other simulations, that are discussed. The discussion evaluates the GCM simulation of temperature, precipitation, and sea ice, and the biosphere model simulation of vegetation type.

3.1. - Air Temperature

Figure 3(a) shows the annual mean ground level temperature (SSTs over ocean, soil temperature over land), as simulated by the BIOCLIM GCM, including nudging (IPSL_CM4_D). The hottest seasonal temperatures, of over 40°, are in Arabia in June-July-August (JJA). The hottest region annually is the Amazon (with maximum temperatures in September-October-November (SON)). The very hot Amazon is characteristic of the relatively simple Tiedtke convection scheme. It is partly for this reason that the latest version of the GCM (not used in this project), uses the [Ref. 12] convection scheme. The cooling effects of the high altitude Greenland, Himalayas, and Antarctica, can clearly be seen.

Figure 3(b) shows the difference between the modelled 2m air temperature, and observations from the Climatic Research Unit (CRU) dataset [Ref. 13]. In general, the continental temperatures are too warm; the mean global continental temperature is too warm by 2.3°. Over the Himalayas, the temperatures are too cool. Over Europe, shown in figure 3(c), the continental temperatures are too warm by an average of 2.0°, due mainly to too high temperatures over the Alps and other mountain ranges. Over lower ground, the temperature is much better simulated. This could be due to the low resolution of the GCM, which does not resolve sub-gridscale orography. The modelled and observed (at a 1/6° resolution) orography are shown in figure 4. This shows that European mountain ranges such as the Alps

and Pyrenees, are not at all well represented by the model. The global biases could be due to a number of reasons. The model does not explicitly calculate 2m temperatures; they are calculated offline using a simple linear extrapolation from the lowest two model levels (which are typically at heights of 67m and 230m over Europe). There are likely to be errors associated with this approach. Furthermore, the observational dataset does not have particularly good coverage, particularly outside Europe and North America. Where there is poor coverage, the temperatures are extrapolated as a function of the orography; this could explain some of the apparent cold bias over the Himalayas.

Figure 3(d) shows the difference in annual mean SSTs between the model, and an observational dataset based on measurements between 1985 and 1990. In general, the model is doing a very good job of simulating SST. The apparent cold bias at high latitudes is due to the fact that, in regions of sea-ice, the modelled temperatures are those of the ice itself, whereas the observed temperatures are of the ocean below the ice. Equatorwards of 60°, the SST bias is just +0.06°. There are too-warm regions off the west coasts of South America, North America, and Africa, which are most prominent in JJA and SON in both hemispheres. These may be due to advection of too-warm air off the continents. There is also a warm region off the eastern coast of North America, which may be associated with a mis-representation of the Gulf

Stream, resulting from the relatively low resolution of the ocean model (the OPA model is usually run at 2° compared with the 4o here). The seasonality of the SSTs is in general well simulated, in all oceanic regions, with maxima in the North Atlantic and Pacific in August, and maxima in the South Atlantic and Pacific in March. Over the North Atlantic, the oceanic region which most affects Europe, excluding the warm region off North America, the ocean temperatures are very well simulated, with a bias of just -0.003°.

In the vertical, the model does a good job of simulating the mean temperature throughout the lower troposphere; however, the GCM exhibits a cold temperature bias in the mid and high troposphere, and a warm temperature bias in the stratosphere. This could result from the relatively small number levels in the vertical [Ref. 14].

3.2. - Precipitation

Figures 5(a) and 5(b) show the annual mean global precipitation rate in the model, and the difference between this and observations. In general, the model is doing a good job of simulating precipitation, capturing all the large scale features. However, there is too much continental precipitation associated with the African and Asian monsoon, and the tropical precipitation over Indonesia is misplaced. Over India and the Indian Ocean, the model simulates well the monsoon seasonality and intensity, although it is a little late in the year, and rather too intense during the wet season. In the Equatorial Atlantic and in the East Pacific, the seasonality is again too pronounced, although the annual mean precipitation is well reproduced.

Globally, there is a mean precipitation bias of +0.16mmday⁻¹, relative to a mean observed precipitation of 2.6mmday⁻¹. The oversimulation is strongest in the tropics, in the summer hemisphere.

Over Europe, shown in figure 5(c), the precipitation bias is -0.16mmday⁻¹, or -10%. The model predicts a strong seasonal cycle of precipitation, with a maximum of 3mmday⁻¹ in the winter, and a minimum of 0.5mmday⁻¹ in the summer, whereas the data points to a fairly constant 2mmday⁻¹ throughout the year. This may be due to an underestimation of summer convective precipitation, a sub-gridscale process which is very dependent on the convection scheme used in the model, and the model resolution, and which is notoriously difficult to simulate.

3.3. - Sea Ice and Snow cover

Sea ice and snow cover are important model variables to evaluate, as they play an important role in the earth system as a positive feedback mechanism. Under positive climate forcing, an increase in temperature can lead to a decrease in sea ice or snow cover, which leads to a lower albedo, more absorption of solar energy, and, therefore, further increases in temperature.

of high latitude coastlines, due to the relatively low resolution of the model. In the Southern Hemisphere, there is not enough ice in the Ross Sea. In both hemispheres, the seasonality of the sea-ice distribution is well simulated, with the maxima and minima occurring in the correct months.

In general, the model is doing a good job of representing the fraction of sea-ice. In the Northern Hemisphere, the largest differences are in the regions

The snow cover is a harder variable to evaluate, due to the lack of data available. However, the IPSL_CM4_D modeled snowfall can be compared to the same variable in other GCMs. The snowfall shares general characteristics with that in the Hadley Centre

atmosphere-only model (HadCM3); however, the snowfall is in general lower in the IPSL_CM4_D simulation, in particular outside of very high latitudes. This is perhaps related to the oversimulation of ground

level temperature, or an underestimate of the effects of orography due to the relatively low resolution of the atmospheric component of the model.

3.4. - Vegetation

As pointed out in section 2.4, ORCHIDEE includes no component of the effects of humans on landscape. Therefore we cannot compare the vegetation map simulated using as input the simulated Baseline climate with the observed one since over Europe the IGBP-DIS vegetation map (combination of satellite and actual ground measurements, Ref. 15) shows that more than 70% of the landscape covered with agriculture and managed prairies (referred to on the map as C3a; figure 6). The solution to overcome this problem is to let ORCHIDEE build its own potential vegetation map under present-day conditions. Figure 7 shows the PFT distribution obtained when ORCHIDEE is forced by the observed climatology (from Climatic Research Unit dataset, Ref. 13). Most of the land in Europe which observations show to be currently cultivated, is occupied by areas of evergreen forests in the potential-vegetation simulation (mainly temperate needle-leaved evergreen except in more oceanic regions where temperate broad-leaved evergreen are more abundant).

This potential distribution was obtained after 1000 years of simulation starting from bare ground at all points in Europe. The plot on the lower right of figure 7 shows the time evolution of the fraction occupied by different PFTs over Europe (spatial average). Grasses start to grow very quickly and are slowly out-competed by trees. A very interesting feature of this graph is that true equilibrium is never reached. Close to year 800 of the simulation for example, a very cold winter was experienced¹⁰ which killed large fractions of temperate broad-leaved evergreen trees, allowing for the expansion of temperate broad-leaved summergreen¹¹ trees and C3 grass. The fraction occupied by these

PFTs then slowly decreases with time since evergreen trees are more competitive. Such climate variability exists in the real world, as in the world simulated by a GCM, and explains why true equilibrium can never be reached.

If we now use as input for ORCHIDEE the "Baseline" IPSL_CM4_D simulation described in the previous sections, we simulate a smaller proportion of evergreen trees (mainly temperate needle-leaved 'TeNLE') than in 'reality' (i.e. ORCHIDEE forced by observations), while deciduous trees (mainly temperate broad-leaved 'TeBLS') and grasses (mainly C3g) are more extensive (figure 8). This is mainly the result of a much drier atmosphere simulated by the IPSL_CM4_D, which leads to larger rates of evapotranspiration, drier soils and surface litter, and therefore larger fire frequency (figure 9) which regularly kills significant fractions of trees (mainly evergreen), thereby allowing the growth of grass. Evergreen trees do not have enough time to completely out-compete deciduous trees since fire regularly provides enough open space for the growth of both evergreen and deciduous trees¹². It is interesting to note on the lower right hand graph of figure 8 the much higher frequency variability of PFT distribution than when using the CRU climatology, due to the larger fire frequency discussed above.

To summarize the results of this baseline simulation at the different BIOCLIM study areas, we have listed in tables 2 to 6 a number of surface variables, and plotted in figures 11 to 15 the seasonal cycle of other variables. Ambient air temperature is well simulated by IPSL_CM4_D at all sites, as already discussed in section 3.1, although the simulated climate is slightly

10) This cold winter issued from the interannual variability generated by the weather generator. Although it is purely numerical here, such events can occur in reality as well.

11) summergreen trees = deciduous trees which are temperature dependent, i.e. which have no leaves during winter time, as opposed to raingreen trees which depend upon rainfall (i.e. no leaves during the dry season, mainly found in tropical regions)

12) To more fully demonstrate the significant role of relative air humidity on the dynamics of PFTs, we have carried out another 300 year-long simulation using the Baseline climate for most atmospheric variables, except for the air relative humidity, which is that observed from the CRU climatology. Figure veg.6 shows the significant impact of this variable on the redistribution of trees and grasses.

warmer in summer and winter. Rainfall shows larger departure from observations, with, however, less seasonal variability, except in Spain where the site is experiencing very dry summers and wet winters in the IPSL_CM4_D world. Differences in evapotranspiration are large, as reported earlier, and result from the very

large difference in ambient air specific humidity. The consequences on soil water content are enormous and lead to soils which are very dry in the IPSL_CM4_D world while they remain quite wet in the climatology, except in Spain where summers are also very dry in the CRU climatology due to low rainfall input.

Surface climate / Simulations	Observed	Potential Vegetation	Baseline Simulation
Vegetation composition (%)			
BG	17		
TeNLE		89.6	72.2
TeBLE	1.2		
TeBLS	6.3	6.8	24.6
BNLE			
BBLS		3.5	3.1
BNLS			
C3g	0.8	0.1	0.1
C4g			
C3a	74.7		
Annual rainfall (mm)	655	655	588
Annual evapotranspiration (mm)	497	463	800
Annual runoff (mm)	392	425	71
Mean annual ambient air temperature (°C)	9.2	9.2	9.4
Mean annual surface soil temperature (°C)	10.1	9.7	9.5
Air temperature of the coldest month (°C)	1	1	1.6
Air temperature of the warmest month (°C)	18.2	18.2	19.8
Annual GPP ¹³ (gC/m ²)	2490	2230	1804
Annual NPP ¹⁴ (gC/m ²)	1398	943	747
Total soil carbon (T/ha)	162	190	225

Table 2: Description of vegetation composition and surface climate at the French study area (48.5°N, 5.5°E) at present. Second column (observed) corresponds to observed climate and vegetation; third column corresponds to observed climate and simulated potential vegetation; fourth column corresponds to simulated present-day climate and vegetation (baseline from IPSL_CM4_D).

13) GPP = Gross Primary Production, i.e. product of photosynthesis alone

14) NPP = Net Primary Production = GPP – Plant Respiration

Surface climate / Simulations	Observed	Potential Vegetation	Baseline Simulation
Vegetation composition (%)			
BG	10		0.3
TeNLE		38.6	
TeBLE	2.5	25.5	66
TeBLS	21.5	31.3	11.1
BNLE			
BBLS	1.4	2.3	
BNLS			
C3g	14.6	1.6	19.5
C4g		0.7	3.1
C3a	50		
Annual rainfall (mm)	428	428	790
Annual evapotranspiration (mm)	500	557	802
Annual runoff (mm)	10.7	6	46
Mean annual ambient air temperature (°C)	12.7	12.7	14.7
Mean annual surface soil temperature (°C)	14	13.6	15.1
Air temperature of the coldest month (°C)	4.9	4.9	8
Air temperature of the warmest month (°C)	22.8	22.8	25.8
Annual GPP (gC/m ²)	1381	1765	1485
Annual NPP (gC/m ²)	705	645	440
Total soil carbon (T/ha)	85	192	102

Table 3: Description of vegetation composition and surface climate at the Spanish study area (38°N-41.5°N, 1.3°W-6.3°W) at present. Second column (observed) corresponds to observed climate and vegetation; third column to observed climate and simulated potential vegetation; fourth column corresponds to simulated present-day climate and vegetation (baseline from IPSL_CM4_D)

Surface climate / Simulations	Observed	Potential Vegetation	Baseline Simulation
Vegetation composition (%)			
BG	20.6		
TeNLE		87.8	63.3
TeBLE		0.2	0.1
TeBLS	2.3	4.8	20.4
BNLE	0.1		
BBLS		7.1	15
BNLS			
C3g	3.1	0.1	1.2
C4g			
C3a	73.9		
Annual rainfall (mm)	760	760	527
Annual evapotranspiration (mm)	388	376	677
Annual runoff (mm)	604	616	26
Mean annual ambient air temperature (°C)	8.3	8.3	8.8
Mean annual surface soil temperature (°C)	9.1	8.6	8.9
Air temperature of the coldest month (°C)	1.8	1.8	3.2
Air temperature of the warmest month (°C)	15.4	15.4	16.4
Annual GPP (gC/m ²)	2242	2056	1583
Annual NPP (gC/m ²)	1274	891	650
Total soil carbon (T/ha)	120	163	202

Table 4: Description of vegetation composition and surface climate at the English study area (51.5°N-54.5°N, 2.6°W) at present. Second column (observed) corresponds to observed climate and vegetation; third column to observed climate and simulated potential vegetation; fourth column corresponds to simulated present-day climate and vegetation (baseline from IPSL_CM4_D)

Surface climate / Simulations	Observed	Potential Vegetation	Baseline Simulation
Vegetation composition (%)			
BG			
TeNLE		77.3	16.4
TeBLE			
TeBLS	2	5.9	30.6
BNLE	3	12.2	17
BBLS	4.5	3.8	4.3
BNLS		0.2	
C3g	7.7	0.6	19.1
C4g			12.6
C3a			
Annual rainfall (mm)	490	490	379
Annual evapotranspiration (mm)	483	453	583
Annual runoff (mm)	175	201	0
Mean annual ambient air temperature (°C)	7.7	7.7	8.4
Mean annual surface soil temperature (°C)	8.7	8.2	8.8
Air temperature of the coldest month (°C)	-4	-4	-0.8
Air temperature of the warmest month (°C)	17.8	17.8	20.4
Annual GPP (gC/m ²)	2823	2091	1124
Annual NPP (gC/m ²)	1580	910	467
Total soil carbon (T/ha)	155	169	227

Table 5: Description of vegetation composition and surface climate at the Czech study area (48.9°N-49.5°N, 15°E-15.6°E) at present. Second column (observed) corresponds to observed climate and vegetation; third column to observed climate and simulated potential vegetation; fourth column corresponds to simulated present-day climate and vegetation (baseline from IPSL_CM4_D)

Surface climate / Simulations	Observed	Potential Vegetation	Baseline Simulation
Vegetation composition (%)			
BG	4.4		
TeNLE		90.6	3.1
TeBLE			
TeBLS	2.3	5.9	41.4
BNLE			1.7
BBLS		3.4	6.7
BNLS			
C3g	0.1	0.1	37.5
C4g			9.6
C3a	93.2		
Annual rainfall (mm)	460	460	323
Annual evapotranspiration (mm)	422	392	527
Annual runoff (mm)	205	230	0
Mean annual ambient air temperature (°C)	8.2	8.2	7.7
Mean annual surface soil temperature (°C)	9.2	8.6	7.9
Air temperature of the coldest month (°C)	-1.5	-1.5	-0,7
Air temperature of the warmest month (°C)	17	17	19.2
Annual GPP (gC/m ²)	2568	2089	1131
Annual NPP (gC/m ²)	1905	902	575
Total soil carbon (T/ha)	118	147	186

Table 6: Description of vegetation composition and surface climate at the German study area (52.2°N, 10.4°E) at present. Second column (observed) corresponds to observed climate and vegetation; third column to observed climate and simulated potential vegetation; fourth column corresponds to simulated present-day climate and vegetation (baseline from IPSL_CM4_D).



4. GCM Future-Climate Simulations

Table 7 shows a summary of the GCM future-climate simulations that were recommended in Deliverable D3.

Name	Time (kyrAP)	Insolation (Wm ⁻²)	CO ₂ (ppmv)	NH ice volume (106km ³)
“Baseline”	0	0	345	3.2
“A”	0	0	1100	3.2
“B”	0	0	550	0
“C”	67	+42	550	0
“D”	67	+42	345	0
“E”	67	+42	345	3.2
“F”	178	+25	280	17.4

Table 7: The BIOCLIM climate simulations, showing the name, time after present, the solar insolation at 65°N in June relative to present, the CO₂ concentration, and the northern hemisphere ice volume.

This section starts with a description of the boundary conditions in these experiments, and how they were implemented in the GCM. Following this, the results of these experiments “A” to “F” are described. The results are described as anomalies, and the baseline for the anomalies varies with each experiment, so that the effect of changing a minimum number of boundary conditions at a time can be examined. However, every experiment is also compared to the control. The order in which the models

are described is “A”, “E”, “D”, “C”, “B”, and finally “F”. This relates to the order in which these simulations are used in formulating narratives of environmental change in Work Package 4. The colour scales used in the plots are all the same, being -6 to +6°C for temperature, and -1 to +1mmday⁻¹ for precipitation, with line contours being drawn every 2°C for global temperature, 1°C for european temperature, and 0.4mmday⁻¹ for precipitation (the zero contour is always omitted).

4.1. - Boundary Conditions

In the BIOCLIM experiments, a number of perturbations are made to the boundary conditions which constrain the model. These can be divided into three types: orbital forcing, CO₂ concentration, and ice sheet characteristics.

Figure 16(a) shows the zonally averaged imposed change in incoming solar radiation at the top of the atmosphere at 67kyrAP compared to present. In the Northern Hemisphere, there is a positive forcing centered on June, and a negative forcing centered on September. In the Southern hemisphere, the positive forcing is in October, and the negative forcing in January. Averaged between 30°N and 70°N, the forcing change relative to present is -6.5% in DJF, +1.8% in

MAM, +5.4% in JJA, and -9.1% in SON. Averaged over the globe and over the year, the forcing is zero. This perturbation is applied in simulations “C”, “D” and “E”. Figure 16(b) shows the same plot but at 178kyrAP. In this case, there is a negative forcing in northern hemisphere autumn, and a positive forcing in northern hemisphere spring. Averaged between 30°N and 70°N, the forcing change relative to present is -1.4% in DJF, +7.2% in MAM, +0.4% in JJA, and -12% in SON. This perturbation is applied in simulation “F”.

In simulations “Baseline”, “D” and “E”, the CO₂ concentration is 345ppmv. In simulation “A” this is increased to 1100ppmv, in simulations “B” and “C” it is increased to 550ppmv, and in simulation “F” it is

reduced to 280ppmv. All these values are constant throughout the atmosphere, and do not vary seasonally.

In simulations “B”, “C” and “D”, the Greenland ice sheet is removed, to simulate melting. This has two effects, the orography is reduced, and the surface type changes. The new orography is given as the height of the underlying bedrock. Following the melting of any ice-sheet, there is a rebound of the bedrock. Simulation by an ice-sheet model (GREMLINS; Ref. 16), shows that the bedrock stabilises approximately 50,000 years after the melting of Greenland is complete (Sylvie Charbit, LSCE, personal communication). In the GCM ‘no-Greenland’ simulations, the altitude over Greenland is the altitude of the bedrock after stabilization, as given by this ice-sheet simulation. The surface type is changed from ice to tundra. This will not only affect the albedo, but also the roughness length and hydrological parameters. The original and perturbed Greenland orography are shown in figures 17(a) and 6(b), respectively. In reality, the melting of the Greenland ice sheet would result in a large input of fresh water into the North Atlantic and Arctic Oceans. This would result in a freshening of the oceans in this region, and possible resulting changes in oceanic circulation. However, such changes would be transitory, and cannot be captured by using the nudged ocean. Even with a fully coupled model, it would require a long (of order hundreds of years) simulation to allow the ocean to come into equilibrium. Furthermore, such a freshening would be likely to occur over a longer timescale than similar events from the Earth’s past (such as Heinrich events [Ref. 17], and so would have less of an effect (Didier Paillard, LSCE, personal communication). A further effect would be a sea-level rise of approximately 7m (Ref. 18, p648). This is also ignored, due to the difficulties involved in changing the land-sea mask. In terms of climate, the sea-level rise on its own should not have a large effect (at the Last Glacial Maximum (LGM), when sea level fell by approximately 120m, the land sea mask in the Hadley centre GCM, at a 3.75° longitude, 2.5° latitude resolution, changed at just 50 gridpoints between 40°S and 40°N.). However, it could have extremely severe consequences for coastal populations.

Simulation “F” applies 178kyr after present, a time at which the LLN-2D model predicts there will be extensive northern hemisphere glaciation. The amount of northern hemisphere ice is predicted to be $17 \times 10^6 \text{ km}^3$, compared with a prediction of about $40 \times 10^6 \text{ km}^3$ from the same model for the LGM, and significantly more than the $3.2 \times 10^6 \text{ km}^3$ of the present. However, the LLN-2D model can give little information as to the geographical distribution of these ice sheets. In order to predict the geographical distribution, and height, of the ice sheets at 178kyAP, it is assumed that the distribution will be similar to one that has occurred in the past, in which there was a similar quantity of ice, and global climate was moving in the same direction. Such a time period has been found by running a high resolution ice sheet model [Ref. 16] for a period of 100kyr, forced by observed changes in climate over the past glacial-interglacial cycle. This points to a time 69kyr before present (69kyrBP), when the northern hemisphere ice sheets were approximately $17 \times 10^6 \text{ km}^3$. Furthermore, at this time the earth was becoming more glaciated, rather than less glaciated, giving consistency with the BIOCLIM future-climate scenario. The ice sheet distribution at this time, as estimated by the ice sheet model, and interpolated onto the resolution of the GCM, is shown in figure 18(b), along with the control ice sheet distribution in figure 18(a). Due to the interpolation in both time and space between the ice-sheet model and GCM, it turns out that the actual volume of ice in the GCM simulation “F” is about $10 \times 10^6 \text{ km}^3$; there is a similar ice-deficit in the GCM “Baseline” (see table 8). It can be seen that there is extensive northern hemisphere glaciation, especially over North America. In Europe, there are ice sheets over much of Scandinavia, the Alps, and Northern Scotland, which are large enough to appear at the model resolution. The increased orography due to the growth of the ice sheets, is shown in a similar fashion in figure 19. The largest changes are south of the Hudson Bay, and over Greenland; the other increases in orography are all less than 400m. The sea level fall corresponding to the increased ice sheets is ignored in this simulation. Considering that the LGM sea level fall was about 120m, the expected sea level fall at 178kyrAP would be less than 60m, which is half that at the LGM. A check can be made on the consistency of the ice sheet implemented in the GCM

at 178kyrAP, and that originally from the LLN-2D simulation. As well as total Northern Hemisphere ice volume, LLN-2D also gives a volume for the Greenland,

American, and Eurasian ice sheets separately. This is compared to the ice volume in the same areas in the GCM “Baseline” and “F” simulations in table 8, below.

	Total (106km ³)	Greenland	America	Eurasia
LLN-2D 0kyrAP	3.16	97%	3.0%	0%
GCM “Baseline”	2.09	98%	1.9%	0.11%
LLN-2D 178kyrAP	17.4	29%	45%	26%
GCM “F”	10.1	28%	65%	7.3%

Table 8: Comparison of ice sheet volume in the LLN-2D model, at 0kyrAP and at 178kyrAP, with that in the GCM “Baseline” and “F” simulations. The total is in units of 106km³. The individual ice sheets are as a percentage of the total.

There are a number of interesting things to come out from this comparison. Firstly, it is clear from the total ice sheet volume, that in the GCM, the ice volume is underestimated. It is 66% of the LLN-2D model value in the control, and 58% in simulation “F”. This difference is due to the interpolation which takes place between the high resolution orography (from observations for the case of simulation “Baseline” and from the ice sheet model in the case of simulation “F”) and the low resolution GCM. For the present, both LLN-2D and the GCM have the majority of ice in Greenland. For 178kyrAP, both have a similar fraction of the northern hemisphere ice in Greenland. However, they differ for the American and Eurasian ice sheets. In the GCM, the American ice sheet is relatively larger (65% compared to 45% of the total in LLN-2D). This means that the volume of the Eurasian ice sheet is

underestimated in the GCM compared to LLN-2D. It is not surprising that there are differences between the two approaches, seen as the LLN-2D ice sheet is calculated rather empirically, whereas the ice sheet in the GCM is interpolated from results from a high resolution 3-D ice sheet model. Furthermore, the LLN-2D ice sheets are from a transient simulation which has previously experienced greenhouse warming, whereas those from the ice-sheet model are from a transient simulation which has only been run over one standard glacial-interglacial cycle. With transient simulations, the results at any instant do not depend solely on the forcing, but also on the memory of the system, that is, what has gone before. The fact that the two simulations have different pasts, could be contributing to their different ice-sheet characteristics.

4.2. - Simulation “A” – CO₂=1100ppmv

In this section, the results from simulation “A”, which has a CO₂ concentration of 1100ppmv, are compared to the control, which has a CO₂ concentration of 345ppmv. It is expected that the increase in CO₂ will cause a warming of the atmosphere, due to an increased greenhouse effect, with the CO₂ absorbing outgoing long wave radiation.

In this simulation, the annual mean 2m air temperature increases by 2.2° relative to the control. The change in

seasonal 2m temperature in DJF and JJA is shown in figures 20(a) and 20(b). The temperature increases are in general larger over the continents than over oceans, except for in the Arctic Ocean. This is likely to be because the ocean has an unlimited supply of water to provide latent cooling as the temperature increases, whereas the continents have a limited supply of soil moisture. The SST increase is very small in the Southern Ocean and the North Atlantic; this is due to the strong ocean mixing which occurs in these regions,

which can draw heat down from the surface.

The largest increases in ground level temperature (SST over ocean, soil temperature over land) are in high northern hemisphere latitudes in early winter, with a maximum temperature change of about 10° in the zonal mean in November. The high latitude temperature increases are strongly spatially and temporally correlated with changes in the simulated sea ice. The high-latitude sea-ice forms later and melts earlier in experiment “A” than in the control,. Similarly, there is a large increase in temperature over northern Siberia in June which correlates strongly with a decrease in the snow cover in this region. This is a clear demonstration of the sea ice and snow albedo feedback.

Figures 20(c) and 20(d) focus in on the temperature change over Europe, in DJF and JJA respectively. It can be seen that in both DJF and JJA, over the North Atlantic, the temperature change is relatively small,

less than 2°C, due to the deep mixing in the North Atlantic Ocean. Because of this effect, the temperature increase over northern Britain is limited. In DJF, the largest temperature increases are in Finland, of more than 5°C. In JJA, the largest increases are over western continental Europe, also of more than 5°C. In the annual mean, the 2m temperature change over Europe (defined as being between 20°W and 40°E, and 30°N and 70°N) is +3.0°C.

The annual mean global precipitation change is +0.023mmday⁻¹, or +0.82%. Figures 20(e) and 9(f) show the precipitation change over Europe. In DJF, the decrease in precipitation over Spain is part of a large region of decreased precipitation over the subtropical Atlantic. In JJA, the decrease over continental Europe is a local phenomenon related to the increase in surface temperature in the same region. The annual mean precipitation change over Europe is -0.16mmday⁻¹, or -9.7%.

4.3. - Simulation “E” - 67kyr AP orbit

Simulation “E” involves modifying the orbital parameters to be those expected at 67kyrAP. The resulting change in solar insolation forcing is shown in figure 16(a). From this forcing, it is expected that simulation “E” will be warmer than the control in the Northern Hemisphere in JJA, and cooler in both hemispheres in DJF.

The change in zonally averaged ground-level temperature reflects the forcing change. In the Northern Hemisphere, the maximum temperature changes are in June at around 70°N, and in July at 40°N. Although the largest changes in forcing occur at the North Pole in June, there is little temperature change here. This is because the sea-ice feedback mechanism is weaker there in summer because the sea ice is predominantly melted. The annual mean change of temperature with height is not very significant; however, there are large increases in air temperature in JJA throughout the troposphere in the Northern Hemisphere, and decreases in DJF in the Southern Hemisphere. The temperature changes are at a maximum in the upper troposphere. In the annual mean, and averaged over

the globe, the change in incoming solar radiation is zero. This is reflected in the change in annual mean global 2m temperature, which decreases by just 0.063°.

In DJF, shown in figure 21(a), there is a cooling over most continental regions in both hemispheres. However, north of Scandinavia, in the Barents Sea, there is a warming associated with melting of the sea ice. There is a slight increase in ground-level temperature over tropical Africa, where there is an associated decrease in precipitation.

In JJA, shown in figure 21(b), the largest temperature increases are over sub-tropical and mid latitude continents. There are no large associated changes in snow fall, so the predominant positive feedback mechanism is likely to be changes in the water vapour content of the atmosphere. As in the case of CO₂ increase in simulation “A”, the reasons for the stronger response over continents are likely to be reduced latent cooling effects, and ocean mixing. There are decreases in temperature in the Sahel and India, which

are in the opposite direction to the forcing. In these regions, there are also strong increases in precipitation.

Figures 21(c) and 21(d) show the change in temperature, focused on Europe. The annual mean 2m temperature change is +0.82. In DJF the average surface temperature change in Europe is minimal; however, in JJA, there is a significant warming, in particular over southern and eastern Europe, of more than 3°C. As in simulation “A”, it appears that in JJA the strong North Atlantic oceanic mixing, is limiting the temperature increase over northern Britain.

The precipitation for the same seasons is shown in figures 21(e) and 21(f). The annual mean precipitation change over Europe is +0.069mmday⁻¹, or +4.2% (compared with an annual mean global change of -0.0025mmday⁻¹ or -0.087%). In DJF, there is a slight increase in precipitation over Spain and the Mediterranean, which is perhaps propagating down from eastern Greenland. In JJA, there is a decrease in precipitation over France and Central Southern Europe, associated with the increase in temperature, and an increase in precipitation over Scandinavia.

4.4. - Simulation “D” - 67kyr AP orbit, and melted Greenland ice sheet

Experiment “D” takes place under orbital conditions of 67kyrAP. In addition, the Greenland ice sheet is removed, as described and illustrated in section 4.1. In this section, the anomalies are first presented as differences from simulation “E”, which is also at 67kyrAP, but includes a modern day Greenland, and from the control. The lowering of Greenland is expected to increase temperatures locally relative to simulation “E”.

Figures 22(a) and 22(b) show the modelled change in global 2m temperature in DJF and JJA, respectively. It can be seen that the temperature increases over Greenland are very local in nature. They persist throughout the year, but are greatest in JJA. There is a cooling north of Scandinavia, in the Barents Sea, with cooler SSTs persisting throughout the year, and which is associated with an increase in sea-ice. The Southern Hemisphere high latitude SST cooling is related to an increase in sea-ice around the Antarctica Peninsula in JJA, and could be linked to the high interannual variability in this region. Changes in the thermohaline circulation, which provide a possible mechanism for cross-equator connections, are another possible explanation, but are unlikely due to the fact that the model has a damped ocean.

The focus on changes to European temperature, is shown in figures 22(c) and 22(d), for DJF and JJA. The annual mean 2m temperature change over Europe is -0.13°C. The high latitude cooling north of Scandinavia extends into Scandinavia itself, and results in cooler temperatures over Britain throughout the year. In contrast, parts of Southern Europe experience warmer temperatures in DJF. In JJA, there is slight cooling over parts of Scandinavia, Britain, and Northern Europe.

The change of precipitation is shown in figures 22(e) and 22(f) for DJF and JJA respectively. In DJF, Southern Europe experiences an increase in precipitation, and Northern Europe a decrease. In JJA, there is also a localised increase in precipitation over Scandinavia, which extends into Britain. In the annual mean, the precipitation increases over Europe by +0.068mmday⁻¹, or +4.0%, compared with a global change of -0.0023mmday⁻¹ or -0.08%.

A comparison between experiment “D” and the control, over Europe, is shown in figure 23. The decrease in temperature in DJF over Scandinavia and is probably related to the removal of the Greenland ice sheet. The increase in temperature in JJA is probably due to the orbital forcing. On average over Europe, the DJF

temperature decreases by 0.22°C, and the JJA temperature increases by 2.5°C, thereby intensifying the seasonal cycle. The annual mean temperature increases by 0.69°C.

The precipitation changes relative to the control in DJF are very similar to those due only to a change in orbit, with a large increase in precipitation over Southern

Europe. In JJA, there is an increase over Scandinavia, related principally to the removal of the Greenland ice sheet, and a decrease over Southern Europe related to the change in orbit. On average over Europe, the DJF precipitation increases by 7.3%, and the JJA precipitation shows no change. The annual mean precipitation increases by 8.4%.

4.5. - Simulation “C” - 67kyr AP orbit, melted Greenland ice sheet, and CO₂=550ppmv

Simulation “C” is identical to the one previously discussed, “D”, except that the CO₂ is increased from the standard 345ppmv to 550ppmv. In this section, the anomalies are first presented as differences from experiment “D”, and then as differences from the control.

As can be seen by a comparison of figures 24 and 20, the effect on temperature and precipitation of the increase of CO₂ from 345ppmv to 550ppmv, under the orbital conditions of 67kyrAP, is very similar in form to the change of CO₂ from 345ppmv to 1100ppmv, under present day orbital conditions and with no Greenland ice sheet. The most important difference is that the magnitude of the changes is less, in particular the increases in precipitation over Southern Europe in JJA.

The annual mean temperature increases by 0.83°C globally, and by 1.1°C over Europe relative to simulation

“D”. This is less than the values for experiment “A” relative to the control: 2.2°C globally and 3.0°C over Europe; however, the ratio of European to global temperature change is relatively unchanged.

The annual mean precipitation changes by +0.12% globally, and by -1.7% over Europe, compared to +0.82% and -9.7% in simulation “A”.

A comparison between experiment “C” and the control over Europe, is shown in figure 25. This shows similar features to the difference between experiment “D” and the control, except that there is the added effect of the increased CO₂. The DJF temperature change averaged over Europe is no longer negative, it is +1.1°C. The JJA temperature change is also greater, rising from +2.5°C to +3.6°C. The annual mean precipitation change over Europe relative to the baseline simulation is +6.6%, compared to an annual change of -0.044%.

4.6. - Simulation “B” - melted Greenland ice sheet, and CO₂=550ppmv

Simulation “B” is similar to the previous simulation, “C”, except that it relates to present day orbital conditions, rather than those at 67kyrAP. It differs from the control in that it has

increased CO₂ and no Greenland ice sheet. The anomalies are presented first relative to simulation “C” (but in fact as “C”-“B”, to aid comparison with “E”-“Baseline”), and then relative to the control.

Figure 26 shows the results of simulation “C”, using “B” as the baseline. This shows the effect of a transition from present day to 67kyrAP orbital conditions, with CO₂ held at 550ppmv, and with no Greenland ice sheet. It is for comparison with figure 21, which shows the same transition, but with CO₂ held at 345ppmv, and a present day Greenland ice sheet. The strong similarity between the two figures shows that the orbital transition is largely insensitive to the CO₂ concentration and the ice-sheet boundary conditions. The most significant difference between the two figures is the extent of the DJF warming over Scandinavia, resulting from sea-ice changes, which are larger when there is no Greenland ice sheet and with increased CO₂ than under present day conditions.

Over Europe, the DJF temperature change relative to simulation “C” is +0.32°C, and the JJA temperature change is +2.5°C. This is for comparison with -0.024°C and +2.4°C for the “E”-“Baseline” case. The difference in DJF is due to the sea ice changes described in the previous paragraph.

For precipitation, the changes over Europe are +2.2% in DJF and -7.7% in JJA, compared with +1.6% and -6.8% for the “E”-“Baseline” case.

This simulation can also be compared directly to the control; this is done in figure 27. It displays characteristics of both the increase to CO₂, and the removal of the Greenland ice sheet. There are maximum increases in temperature in both the upper tropical troposphere and also at high northern latitudes.

Over Southern Europe, the temperatures are generally warmer than at present, but over Northern Europe in DJF they are cooler. This shows that the cooling in Northern Europe in DJF due to the removal of the ice sheet is more important than the warming due the CO₂ increase. The annual mean temperature change over Europe relative to the control is +0.94°C.

In terms of precipitation, there are decreases over northern France and southern Spain in DJF. In JJA, there are decreases over Southern Europe, and increases over Great Britain and Scandinavia. The annual mean precipitation change over Europe relative to the control is +2.3%.

4.7. - Simulation “F” – increased northern hemisphere ice sheets, CO₂=280ppmv, and 178kyrAP orbit.

In simulation “F”, the extent of the northern hemisphere ice sheets is increased, the CO₂ concentration is decreased and the orbital parameters are those of 178kyrAP, as shown in figure 16(b).

In the annual mean, the global 2m air temperature decreases by 0.95°C. Figures 28(a) and 28(b) show the surface temperature change, relative to present, in DJF and JJA respectively. In general, the air over land cools more than the land over ocean. In DJF, the

largest temperature decreases are over the “Laurentide” ice sheet, where the temperature decreases by over 12°C. There is also significant cooling in the Barents Sea, associated with an increase in sea ice, and over Greenland, of over 6°C. There are also localised SST increases east of Newfoundland, and on the Taymyr peninsula in arctic Siberia, which are associated with a decrease in sea ice, and snow cover respectively. In JJA, the largest cooling is again over the Laurentide ice sheet, where the temperatures are up to 20°C cooler than present. There is also significant

cooling over the other northern hemisphere ice sheets in Scandinavia, arctic Siberia, and Alaska. In JJA, there is also significant warming in subtropical regions, associated with the drier climate.

Figures 28(c) and 28(d) show the temperature change over Europe. In DJF, the cooling over the Scandinavian glacier extends over Britain and northern Europe, but there is little temperature change over most of continental Europe. In JJA, the presence of European ice sheets results in a greater localised cooling than in DJF, and the cooling extend further south into continental Europe. The subtropical warming extends as far north as Spain, where the temperatures increase

by more than 1°C. Averaged over the whole of Europe, the 2m air temperature changes relative to present are -0.87°C in DJF, -0.33°C in JJA, and -0.85°C in the annual mean.

Figures 28(e) and 28(f) show the precipitation changes over Europe in DJF and JJA. In DJF, when average european precipitation increases by 5.3%, the changes are dominated by a localised increase in precipitation off the west coast of Spain, centered over the East Atlantic. In JJA, when the average change is an increase of 1.3%, there is however a decrease in precipitation over southern Europe. In the annual mean, the precipitation change is +7.7% over Europe, and -0.98% globally.

4.8. - Summary of results

For each future-climate simulations described in the previous sections, table 9 below summarizes the principal results, that is, the global annual mean temperature and precipitation change, and the

european annual, DJF, and JJA temperature and precipitation change, relative to the control simulation. “Europe” is defined as for the rest of this deliverable, as being between 20°W and 40°E, and 30°N and 70°N.

	Globe, ANN	Europe, ANN	Europe, DJF	Europe, JJA
	ΔT_{ANN} Δp_{ANN}	ΔT_{ANN} Δp_{ANN}	ΔT_{DJF} Δp_{DJF}	ΔT_{JJA} Δp_{JJA}
“A”	+2.2 +0.82	+3.0 -9.7	+2.7 -6.8	+3.3 -22.0
“B”	+0.77 +1.1	+0.94 +2.3	+0.75 +2.7	+1.1 +6.0
“C”	+0.69 -0.044	+1.8 +6.6	+1.1 +4.9	+3.6 -2.1
“D”	-0.14 -0.17	+0.69 +8.4	-0.22 +7.3	+2.5 +2.8e-4
“E”	-0.063 -0.087	+0.82 +4.2	-0.024 +1.6	+2.4 -6.8
“F”	-0.95 -0.98	-0.85 +7.7	-0.87 +5.3	-0.33 +1.3

Table 9: Summary of BIOCLIM future-climate simulations. All changes in the table are relative to the baseline simulation. Temperature changes are in °C, precipitation changes are in %.



5. Timeseries over the European Sites

In this section of the report, timeseries are presented of several variables, averaged over the different regions of interest to the BIOCLIM project. Figure 1 shows the resolution of the IPSL_CM4_D GCM over Europe, and the regions of “UK” (7W:2E, 50N:58N), “France” (2W:5E, 43N:50N), “Spain” (8W:1W, 36N:43N), and “Central Europe” (5E:13E, 46N:53N), as they are defined for this section. As can be seen, due to the low resolution of the GCM, the values in the timeseries in this section represent averages over only a very few number of gridboxes. All the results are given as anomalies from the control.

The variables presented are 2m air temperature, precipitation, snow fall and wind strength. Of these, the

2m air temperature is the one in which we have the most confidence. However, the 2m temperature is not explicitly calculated by the model, but is calculated off-line after the simulation is complete, by extrapolating from the lowest two model levels. We have less confidence in the precipitation, which results from sub-grid scale processes, and which is parameterised. We also have less confidence in the wind strength, which in reality depends very much on the local conditions, and also on sub-grid scale processes such as gusts. We have even less confidence in the snow fall, which is calculated rather empirically from the temperature profile and the precipitation rate.

5.1. - 2m air temperature

Figure 29 shows the simulated 2m air temperature change over the regions of the UK, Spain, France, and Central Europe. The control is zero throughout the year, as this is the baseline experiment.

In simulation “A”, there is a year round temperature increase in every region. The lowest annual increase is in the UK, which also has the most constant change. These are trends seen in every experiment, probably due to the damping effect of the North Atlantic Ocean. In France and Central Europe, and to a lesser extent Spain, the increase is greatest in summer, thereby increasing the summer-winter temperature difference. In all regions, there is a temperature change in March, which is greater than that in February and April. This is an effect which is common to the majority of the experiments, at both present and 67kyrAP, and both with and without a Greenland ice sheet. The effect is most prominent in Central Europe and least prominent in the UK. It is likely to be linked with a change in the local circulation.

Simulation “B” results in only small temperature changes over the UK, France, and Central Europe, but it has a year-round warming effect in Spain.

Simulation “C” exhibits large temperature increases relative to the control, and a strong seasonality of change, with maximum warming in July in all regions. It is the only experiment which produces temperature increases greater than those in experiment “A”, albeit only in Spain and the UK in July. This is the experiment with the greatest summer-winter temperature contrast.

Simulation “D” shows very similar changes to those in “C”, but with a consistently lower magnitude.

Simulation “E” is also similar to “C”, but again with a lower magnitude. Over Spain, the temperatures are cooler than in “D”, elsewhere they are warmer. The “March” effect is clearly visible in France, Spain, and Central Europe.

In simulation “F”, the temperature is reduced throughout the year in the UK, with a maximum cooling in October, of about 4°C. The minimum UK cooling is in June, by less than 1°C. In France and Central Europe, the results are similar, with a cooling in autumn of up to

4°C, and a warming in June, which is more important in France than in Central Europe. This warming is related to the band of subtropical warming, and is even more evident in Spain, where temperatures increase in May through to June.

5.2. - Precipitation

Figure 30 shows the simulated precipitation change over the regions of the UK, Spain, France, and Central Europe.

Simulation “A” increases the CO₂ concentration to 1100ppmv from 345ppmv. It results in a slight decrease in precipitation in summer over the UK and an increase in winter, with maxima of change of about 0.5mmday⁻¹. In France, there is a decrease in precipitation throughout most of the year, of about 0.5mmday⁻¹. In Spain, the precipitation is significantly decreased, by a maximum of more than 1.5mmday⁻¹, in winter. In Central Europe, the precipitation is also decreased significantly in this simulation, but in summer, by over 1mmday⁻¹.

In Simulation “B”, CO₂ is increased to 550ppmv, and the Greenland ice sheet is removed. This results in increased precipitation over the UK in late summer and early autumn. In France, there is a decrease in precipitation in June. In Spain, the change in precipitation in this simulation is similar to that in simulations “C” to “E”, with an increase in precipitation in February, and a decrease in April. Over Central Europe, there is significantly increased precipitation in August and September.

As for temperature, the three 67kyrAP simulations, “C”, “D”, and “E”, have very similar results. In the UK they show increased precipitation in SON, with a maximum in October, of about 1mmday⁻¹. There is also a secondary maximum in late winter to early spring. In France, they show increased precipitation in February and March, decreased precipitation in summer, with the greatest decrease in June, and another increase in precipitation in SON. In Spain, there is an increase in February, and a decrease in May and June. In Central Europe, the precipitation changes are smaller, but there is decreased precipitation in June.

In simulation “F”, over the UK there is an increase in precipitation in autumn, with a maximum in October, of more than 1mmday⁻¹. In France, there is a sharp decrease in the June precipitation, and a sharp increase in the October precipitation. In Spain, there are increases in precipitation in early spring and in autumn, and a decrease in April to June. In Central Europe, the precipitation decreases in June and July, and increases in August to October.

5.3. - Snow fall

Figure 31 shows the simulated snowfall change over the regions of the UK, Spain, France, and Central Europe.

The UK and France have similar results for the change in snow fall. Simulation “A” gives a decrease in snowfall of about 0.15mmday⁻¹ in winter. Simulation “B” and “C”

are similar, but with a smaller magnitude. Simulation “D” results in increased snow fall over the UK in January and February, but decreases snow fall in France. Simulation “E” increases snow fall in February in both regions. Not surprisingly, Spain has very little change to its snowfall.

Over Central Europe, there are large reductions in snowfall in all simulations except for “F”. In simulation “A” and “C”, the greatest decrease is in January. In simulations “B”, “D”, and “E”, the maximum decrease is in February or March.

In simulation “F”, unsurprisingly the snowfall increases in the UK, with a maximum increase in February of 0.3mmday^{-1} . A similar pattern, but of smaller magnitude, is seen in France. In Central Europe, the snowfall actually decreases in December and March.

5.4. - Wind strength

Figure 32 shows the simulated wind strength change over the regions of the UK, Spain, France, and Central Europe.

The monthly wind strength is calculated from the monthly mean zonal and meridional wind velocity. In the UK, the largest changes are a decrease in wind speed in March in experiments “B” and “C”, and an increase in wind speed in October in experiments “C”, “D”, and “E”. Over France, the changes in wind speed seem to depend on the orbital conditions, as experiments “A” and “B” show little change from the control, whereas simulations “C”, “D”, and “E” show increases in wind strength which peak in February and October. In Spain, experiment “A” shows a large reduction in wind strength in November and December. The other experiments

show an increase in February, the largest increase being for experiment “D”. Over Central Europe, the changes for the 67kyrAP experiments are all similar, with increases in wind strength in October. In simulations “A” and “B”, there is a decrease in wind strength in winter.

In simulation “F”, the UK has a large increase in surface windspeed in September of nearly 2ms^{-1} , and a decrease in February and March, of about 1ms^{-1} . In France, the windspeed stays nearly constant, except for increases up to a maximum of 1ms^{-1} in October to December. Spain has the largest increase in wind speed, of up to 2ms^{-1} in February. In Central Europe, the windspeed decreases in March, and increases in September.



6. Vegetation characteristics over Europe

This section describes the vegetation distribution simulated, at different time periods in the future, in response to the simulated climate changes discussed in previously (using the IPSL_CM4_D model).

We will first present how vegetation was computed, and then discuss the results at the European scale and at each selected study area.

6.1. - Methodology

Results from the 'Baseline' simulation have been discussed in section 3.4. For experiments 'A' to 'F' we have applied the so-called 'anomaly approach' adopted to study past climate changes. Differences between the climate simulated in the experiments and the 'Baseline' climate are computed and added to the CRU present-day climatology. These 'reconstructed' future climate changes are used to force the ORCHIDEE model. The main advantage of this approach is to smooth out the systematic biases of the climate model used. More discussion about this strategy can be found in [Ref. 19] and in articles cited therein.

All ORCHIDEE simulations, for BIOCLIM experiments 'A' to 'F', were run until a semi-equilibrium was reached, i.e. until the vegetation distribution simulated at the European scale was experiencing no major further changes from one year to another¹⁵. Here, we compare them with the simulated potential vegetation distribution obtained using the CRU climatology as atmospheric forcing (figure 7). They all start from the same initial state: year 400 of the present-day simulated potential vegetation distribution (which is rather close to equilibrium). The final length of the simulations is 900 years for experiment 'A', 'B' and 'F', and 600 years for all 67 kyr AP conditions.

6.2. - Vegetation distributions at the European scale

Simulation "A" – CO₂=1100ppmv

An almost three-fold increase in atmospheric CO₂ content (experiment 'A') leads to a major shift of evergreen trees in the western part of our European domain (figure 33(a), results summarized in table 15), from temperate needle-leaved to temperate broad-leaved, the latest being more adapted to warmer winters¹⁶. At present, broad-leaved evergreen trees are mainly found in coastal regions where the presence of the ocean prevents the winters from being very cold,

while the global warming simulated in 'A' enlarges the areas where those favorable warm winter conditions are met.

There is moreover a global decrease of evergreen trees over Europe (along the Atlantic façade of France and in the Pyrenees, and further East, inland), being replaced by deciduous trees and grasses. This results from the larger fire frequency experienced in this warmer climate (figure 33(b)) and induced by the drier litter resulting

15) excepting eventual abrupt changes due to much colder conditions resulting from the interannual variability, as experienced when using the CRU climatology.

16) Temperature of the coldest month more frequently goes above the 5°C threshold defined for TeNLE (see table 11 and table 12 for the Spanish and English studied areas).

from less summer rainfall. As already discussed in section 3.4, a higher fire frequency favors the installation of grasses which can occupy the open space

very quickly, and prevents the evergreen trees to completely out-compete deciduous trees and grasses since large portions of them are regularly killed by fire.

Simulation “E” – 67kyrAP orbit

Changing the Earth orbit from present to 67kyrAP (experiment ‘E’) leads to the replacement of some evergreen trees (TeNLE) by deciduous trees (TeBLS and BBLS) and grasses (C3g) over southern and western France, Portugal and southern Spain (figure 34(a), results summarized in table 15). This again results from an increase of the fire return frequency (figure 34(b)). But the reason for this increase

is not a decrease in summer rainfall as in experiment ‘A’, but a strong increase in the seasonality of air temperature (figure 34(c)). The warmer summers induced by more incoming solar radiation are accompanied by a rather large increase in summer evapotranspiration which dries out the soil and surface litter, thereby favoring fires at the end of the summer season.

Simulation “D” – 67kyrAP orbit, no Greenland

Melting the Greenland ice-sheet at 67kyrAP (experiment ‘D’) makes no significant further change to the climate (see section 4.4), nor to the vegetation distribution simulated over Europe, compared to simulation “E” (figure 35, results summarized in table 15). The biggest climate changes are indeed simulated further North (and also East) of

the geographical domain considered. Reconstruction of the vegetation distribution at the global scale (not shown) points to major changes occurring only over Greenland, where the grassy tundra initially prescribed is maintained and is even augmented by the growth of trees over southern Greenland (see Ref.20 for further discussion).

Simulation “C” – 67kyr orbit, no Greenland, CO₂=550ppmv

Interestingly, when CO₂ is increased by 200ppm at 67kyrAP with no Greenland ice-sheet (experiment ‘C’) to be compared to experiment ‘D’), the simulated changes in vegetation distribution are opposite to those obtained when CO₂ is increased under present-day orbital and ice-sheet configurations (i.e. when comparing experiment ‘A’ to present-day potential vegetation). Instead of decreasing, the area occupied by evergreen trees actually increases at the expense of deciduous trees and grasses (figure 36(a), results summarized in table 15), except in England. This occurs although all changes in the seasonality of surface climate variables, averaged over Europe, described for experiment ‘E’ (equivalent to experiment ‘D’) are quite similar and even

further enhanced (figure 36(b)), e.g. drier litter (including leaf and wood material) in summer, larger fire return frequency. This points to the greater regionalization of the climate change experienced in ‘C’ versus ‘D’ (or ‘E’) since more water is advected in winter in the western part of the domain where evergreen trees drive out deciduous trees. Figure 36(c) indeed shows that when we select a smaller geographical domain (the one showing the expense of evergreen trees in ‘C’, i.e. 40 to 50°N and 10°W to 5°E), the litter humidity is increased and the fire frequency decreased. For the same overall climate change, the spatial distribution of climate and vegetation changes can therefore be quite different.

Simulation “B” – present orbit, no Greenland, CO₂=550ppmv

Starting from experiment ‘C’ and changing the orbital configuration back to present-day’s is what we have done to run experiment ‘B’ which therefore is characterized by a CO₂ concentration of 550ppmv and no Greenland ice-sheet. Comparing ‘C’ to ‘B’ should therefore be equivalent to comparing ‘E’ to the potential vegetation map simulated using CRU climatology. The major differences between ‘B’ and ‘C’ are observed in the Pyrenees where temperate broad-leaved summer-green trees (more abundant in ‘C’) are

replaced by temperate broad-leaved evergreen trees in response to a more humid environment in ‘B’ in this area (figure 37, results summarized in table 15), and in England where needle-leaved evergreen increase in ‘B’ at the expense of deciduous trees in response to colder winters and more humid climate. All changes go in the same direction as when comparing ‘E’ to ‘Potential CRU’, but the magnitude of the changes is somewhat less as summarized in table 15.

Simulation “F” – 178kyr orbit, CO₂=280ppmv

At the time of the maximum of the next glaciation (simulation ‘F’) the largest changes in the geographical domain considered are in eastern Europe (while in all other simulations western Europe was the most sensitive), thereby pointing to more continentality in the simulated climate change. A large shift from temperate to boreal trees is predicted by ORCHIDEE, in response to colder conditions (figure 38, results summarized in table 15), together with the

enlargement of the area occupied with deciduous trees (boreal broad-leaved summer-green). Moreover in western France and the Pyrenees, there is a shift from broad-leaved to needle-leaved evergreen trees, in response to colder winters.

In southern Spain and Portugal a large change from trees to grass is also simulated in response to the rather large drying which favors the spread of fires (see figure 28 describing climate change).

6.3. - Changes in vegetation distribution and surface climate at the selected studied areas

Simulated changes in both vegetation distribution and surface climate at all sites are summarized in figures 39 to 43 and in tables 10 to 14.

France

The maximum change in vegetation distribution in France occurs when the atmospheric CO₂ concentration reaches its peak value (~three times its present-day concentration; simulation ‘A’). At this time, evergreen trees mostly disappear (from 89.6% to 16.6%), and are replaced with deciduous trees (63.2% compared to 10.3% at present) and grasses

(20.2%). This occurs because fires return much more frequently (~twice as much), despite the rather large increase in annual rainfall (but much less in summer). The length of the growing season is shortened due to the change in vegetation distribution (strong seasonal cycle of leaf area index) but the overall productivity is increased because deciduous trees are much more

productive than evergreen trees. At all other time periods, vegetation distribution is not markedly different from the present-day one although the changes experienced in experiment 'E' (67 kyr AP with

CO₂=350ppmv and presence of Greenland ice-sheet) is slightly larger and goes in the same direction as for experiment 'A' (but less in magnitude) pointing to the importance of summer warming.

Spain

The study area in Spain experiences the largest coverage by grasses in the future (in the absence of Human alteration), with more than 65% at 67 kyr AP (no Greenland, simulation 'D') and at 178kyrAP (next glaciation, simulation 'F'). It is also the site where the fire return frequency is the smallest, apart from the present and the coming global warming (simulation 'A'). The response of the seasonal cycles of evapotranspiration, soil water content and leaf area

index to climate change is more disperse than at all other sites implying that this Spanish site is the most sensitive. Soil water stress is maximum when atmospheric CO₂ concentration is tripled but still allows for the growth of trees rather than grasses. Surprisingly enough, fires are at their least at that time, due to the very small seasonal cycle of rainfall and other hydrological variables.

England

At the English study area, the changes simulated resemble the ones discussed for the French region of interest. The largest changes are obtained when atmospheric CO₂ is very large, while most other simulations are showing no significant changes in the vegetation distribution. In experiment 'C' though, there is a rather large decrease of evergreen trees (from ~85% to ~55%) while deciduous trees are

increasing in area by about the same amount. This contradicts the general trend over Europe discussed in section 6.3 but follows the impact of increasing CO₂ obtained when comparing experiment 'A' to present-day, i.e. increased annual rainfall, warmer temperatures, specially in summer, lower soil water content in summer and more frequent fires.

Czech Republic

In the Czech republic, the largest changes in vegetation distribution are obtained at the next glaciation (i.e. 178kyrAP, simulation 'F') with the maximum extent of boreal needle-leaved evergreen trees (~30%) and minimum extent of temperate needle-leaved evergreen trees (~57%) in response to rather

strong winter cooling. Grass cover is very low (less than 1%) at all times due to the strong summer rainfall which prevents the soil from drying out. The maximum extent of deciduous trees is obtained in experiment 'A' when atmospheric CO₂ concentration is tripled, as is fire frequency.

Germany

Results at the German study area resemble those described for the Czech Republic, albeit the cooling experienced during the next glaciation

(simulation 'F') is stronger, and results in a larger shift from temperate needle-leaved to boreal needle-leaved evergreen trees.

6.4. - Summary of the changes in vegetation distribution

Table 15 summarizes the main vegetation changes simulated over Europe at all time periods. The maximum extent of evergreen trees is obtained for present-day conditions, whilst in the future this area will decrease. The area of bare ground never exceeds 2% since no real dry conditions will ever be met (in the IPSL_CM4_D world, combined with the sensitivity of ORCHIDEE to rainfall and air humidity) in Europe throughout the following 178 kyr. The maximum extent of deciduous trees will be attained 67 kyr after present, while the maximum extent of grasses will be met sooner, once CO₂ concentrations have tripled, since this will be the time when fires will be most frequent.

In the present and future time periods, Europe will remain mostly covered with trees, neglecting human alterations of the potential vegetation distribution.

The study areas located in more continental regions (Germany and Czech Republic) will be more sensitive to the cooling during the next glaciation, while the sites located at more temperate (oceanic) regions (France and England) will react more strongly to increased atmospheric CO₂ (i.e. be sensitive to global warming). The region located at the southernmost latitude (Spain), is sensitive to all climate changes.

If vegetation had been allowed to feedback on climate in all these simulations, we may have ended up with different climate/vegetation equilibria than that discussed above. This has already been demonstrated for past climate changes [Ref. 21, Ref. 22] and should be accounted for in scenarios of future climate change.

Surface climate / Simulations	Potential Vegetation	Simulation A	Simulation B	Simulation C	Simulation D	Simulation E	Simulation F
Vegetation composition (%)							
BG							
TeNLE	89.6	10.6	87.7	88.4	87.5	73.9	90.2
TeBLE		6					
TeBLS	6.8	37.3	7	7.5	8.4	15.3	3.6
BNLE							
BBLS	3.5	25.9	4.1	4	3.9	10.7	6
BNLS							
C3g	0.1	13.4	1.2	0.1	0.2	0.1	0.2
C4g		6.8					
C3a							
Annual rainfall (mm)	655	801	780	760	706	675	666
Annual evapotranspiration (mm)	463	474	402	454	457	506	455
Annual runoff (mm)	425	407	532	466	434	375	416
Mean annual ambient air temperature (°C)	9.2	12.4	9.1	10.6	9.5	10.2	7.9
Mean annual surface soil temperature (°C)	9.7	13.1	9.7	11.1	10.1	10.7	8.4
Air temperature of the coldest month (°C)	1	3.8	1.5	2.1	-0.3	0.6	-0.3
Air temperature of the warmest month (°C)	18.2	21.9	16.9	22.4	19.9	21.8	16.8
Annual GPP (gC/m ²)	2230	3194	2562	2535	2227	2236	1903
Annual NPP (gC/m ²)	943	1626	1104	1044	946	957	820
Total soil carbon (T/ha)	190	191	219	199	189	185	187
Fire return frequency (years)	838	387	996	370	934	655	518

Table 10: Description of vegetation composition and surface climate at the French study area (48.5°N, 5.5°E) at all time periods.

Surface climate / Simulations	Potential Vegetation	Simulation A	Simulation B	Simulation C	Simulation D	Simulation E	Simulation F
Vegetation composition (%)							
BG		0.9	1.2				
TeNLE	38.6	3.3	25.5	23.2	15.7	40.1	14.3
TeBLE	25.5	69	19.5	16.6	1.6	1.7	2.1
TeBLS	31.3	13.5	18.1	21	13.6	19.2	14
BNLE							
BBLS	2.3		0.4	1.1	2.1	0.8	1.7
BNLS							
C3g	1.6	11.8	32.9	35.2	60.3	34.4	61.8
C4g	0.7	1.5	2.4	2.9	6.7	3.8	6.1
C3a							
Annual rainfall (mm)	428	292	342	390	436	421	408
Annual evapotranspiration (mm)	557	288	386	504	484	527	441
Annual runoff (mm)	6	0	4.4	63	171	77	45.9
Mean annual ambient air temperature (°C)	12.7	16.3	13.8	14.6	13.2	13.6	12.7
Mean annual surface soil temperature (°C)	13.6	17.6	15.3	15.9	15.2	15.1	14.6
Air temperature of the coldest month (°C)	4.9	7.4	6	5.3	3.5	3.7	4.7
Air temperature of the warmest month (°C)	22.8	26.9	23.9	28.2	25.4	26.8	24.2
Annual GPP (gC/m ²)	1765	1739	1442	1830	1158	1460	781
Annual NPP (gC/m ²)	645	532	520	735	503	590	317
Total soil carbon (T/ha)	192	143	150	134	75	115	69
Fire return frequency (years)	872	1000	28	22	10	23	94

Table 11: Description of vegetation composition and surface climate at the Spanish study area (38°N-41.5°N, 1.3°W-6.3°W) at all time periods

Surface climate / Simulations	Potential Vegetation	Simulation A	Simulation B	Simulation C	Simulation D	Simulation E	Simulation F
Vegetation composition (%)							
BG							
TeNLE	87.8	20.5	84.5	53.2	87.6	87.6	79.2
TeBLE	0.2	60.1	0.1	0.6			
TeBLS	4.8	17.2	5.8	20.8	4.6	7.6	1.1
BNLE							
BBLS	7.1	2.1	9.1	24.8	7.7	4.4	19.3
BNLS							
C3g	0.1	0.1	0.5	0.6	0.1	0.4	0.4
C4g							
C3a							
Annual rainfall (mm)	760	931	750	804	817	835	674
Annual evapotranspiration (mm)	376	318	316	374	359	387	352
Annual runoff (mm)	616	700	605	609	677	659	607
Mean annual ambient air temperature (°C)	8.3	10.5	8	9.3	8.1	9	6.4
Mean annual surface soil temperature (°C)	8.6	11	8.5	9.8	8.5	9.4	6.8
Air temperature of the coldest month (°C)	1.8	5	2.8	1.9	0.5	2.2	-0.7
Air temperature of the warmest month (°C)	15.4	17.5	14.1	18.8	15.8	17.9	13.2
Annual GPP (gC/m ²)	2056	2719	2375	2384	2043	2079	1743
Annual NPP (gC/m ²)	891	1175	1056	1110	890	885	789
Total soil carbon (T/ha)	163	191	198	179	163	155	168
Fire return frequency (years)	967	826	937	199	980	834	948

Table 12: Description of vegetation composition and surface climate at the English study area (51.5°N-54.5°N, 2.6°W) at all time periods.

Surface climate / Simulations	Potential Vegetation	Simulation A	Simulation B	Simulation C	Simulation D	Simulation E	Simulation F
Vegetation composition (%)							
BG		1.7					
TeNLE	77.3	61.9	77.8	88.3	70.3	80.4	57.4
TeBLE							
TeBLS	5.9	18.9	6.5	7.7	6.9	7.7	1.6
BNLE	12.2		11		19.2	8.4	30.8
BBLS	3.8	17.2	3.9	3.6	3	3.4	9.5
BNLS	0.2						
C3g	0.6	0.3	0.8	0.4	0.6	0.1	0.7
C4g							
C3a							
Annual rainfall (mm)	490	555	570	569	553	510	487
Annual evapotranspiration (mm)	453	407	396	441	455	488	437
Annual runoff (mm)	201	242	326	259	272	152	208
Mean annual ambient air temperature (°C)	7.7	11.1	7.7	9.5	8.2	9	6.4
Mean annual surface soil temperature (°C)	8.2	11.7	8.3	10.1	8.7	9.5	6.9
Air temperature of the coldest month (°C)	-4	0.5	-2	-0.8	-4.1	-2.4	-3.9
Air temperature of the warmest month (°C)	17.8	21.2	16.5	21.8	19.4	21.2	16
Annual GPP (gC/m ²)	2091	2999	2430	2476	2091	2129	1777
Annual NPP (gC/m ²)	910	1362	1085	1057	915	906	803
Total soil carbon (T/ha)	169	186	196	178	160	156	165
Fire return frequency (years)	639	123	892	658	694	701	625

Table 13: Description of vegetation composition and surface climate at the Czech study area (48.9°N-49.5°N, 15°E-15.6°E) at all time periods.

Surface climate / Simulations	Potential Vegetation	Simulation A	Simulation B	Simulation C	Simulation D	Simulation E	Simulation F
Vegetation composition (%)							
BG							
TeNLE	90.6	80.4	90	89.1	89.9	89	40.7
TeBLE		0.4					
TeBLS	5.9	13	5.7	6.9	6.6	7.4	0.7
BNLE							39.6
BBLS	3.4	6.2	4	3.8	3.5	3.5	18
BNLS							
C3g	0.1		0.3	0.2		0.1	1
C4g							
C3a							
Annual rainfall (mm)	460	587	564	603	596	515	495
Annual evapotranspiration (mm)	392	332	347	378	392	421	378
Annual runoff (mm)	230	322	399	381	407	231	354
Mean annual ambient air temperature (°C)	8.2	11.3	7.9	9.5	8.1	9.4	5.7
Mean annual surface soil temperature (°C)	8.6	11.8	8.4	10	8.6	9.8	6.2
Air temperature of the coldest month (°C)	-1.5	3	0	0.5	-2.4	0.3	-3.1
Air temperature of the warmest month (°C)	17	20	15.9	21.1	18.5	20.5	14
Annual GPP (gC/m ²)	2089	2978	2403	2408	2062	2110	1704
Annual NPP (gC/m ²)	902	1289	1067	1026	901	890	790
Total soil carbon (T/ha)	147	162	172	151	142	134	152
Fire return frequency (years)	783	560	909	826	916	657	601

Table 14: Description of vegetation composition and surface climate at the German study area (52.2°N, 10.4°E) at all time periods

Vegetation types (%) / Simulations	Potential Vegetation	Simulation A	Simulation B	Simulation C	Simulation D	Simulation E	Simulation F
BARE GROUND	0	0.5	1.4	1.1	0.6	0	1.8
TREES	98.7	85.2	93	92.1	87.9	91.8	85.9
GRASS	1.3	14.3	5.6	6.8	11.5	8.2	12.3
Evergreen Trees	83	63.2	77.9	72.5	68.3	68.2	66.2
Deciduous Trees	15.7	22	15.1	19.6	19.6	23.6	19.7

Table 15: Summarizing the mean vegetation composition over Europe, at all time periods.



7. Critical discussion

This section provides a critical discussion of the results that have been presented. This is divided into a discussion of the major uncertainties in the

models and methodologies used, and a comparison of the results with previous work.

7.1. - Uncertainty

There are many uncertainties associated with the GCM simulations described in this deliverable. These arise from a number of sources.

Firstly, there are the boundary conditions which are used to constrain the GCM. The orbital conditions are well known at the snapshot time periods, but the CO₂ concentration and ice sheet distributions are not. However, because we have looked at a range of CO₂ concentrations, varying from 345 to 550ppmv, and one simulation at 1100ppmv, this gives an idea of the magnitude of errors associated with prescribing an erroneous CO₂ concentration. Averaged over Europe, the temperature increased by 1.1°C and 2.2°C, for CO₂ concentrations of 550 and 1100ppmv, respectively. For the ice sheets, we have not carried out any sensitivity studies to enable an assessment of the importance of their distribution or size. However, an estimate can be made of the sensitivity by considering that during the LGM, data points to an annual mean temperature over western Europe (40°N to 50°N, 10°W to 15°E) approximately 10°C cooler than present [Ref. 23], and that in simulation “F”, the modelled temperature decrease over the same region is 0.70°C. Part of this difference is due to the fact that in simulation “F”, there is only half the LGM ice volume, and a CO₂ concentration of 280ppmv compared with 200ppmv at the LGM. However, there is currently no model which correctly simulates the observed 10°C temperature decrease over western Europe at the LGM [Ref. 23], even given the correct boundary conditions. In order to investigate this further, an LGM simulation would have to be carried out, with the model used in this project. What we can say, is that the temperature change over Europe, relative to the present, during a “glacial” period is not particularly well constrained.

Other uncertainties come from the GCM itself. When given boundary conditions appropriate for the present day, the model does not perfectly reproduce present-day climate. An assessment of these errors has been carried out in Section 3, where the simulated present day climate is compared to observations. Here, the surface air temperature bias over Europe is found to be +2.0°C, and the precipitation bias to be -10%. Furthermore, even if the model did predict present day climate very well, there is no guarantee that it would correctly predict different climates. The predecessor of the GCM used in for the BIOCLIM simulations, the atmosphere-only model LMD5, was used in a model intercomparison project focusing on past climates (PMIP, Paleoclimate Modelling Intercomparison Project, Ref. 24), and it performed relatively well. However, neither the fully coupled GCM, nor the ocean-nudging method, have been tested under paleoclimate conditions. Initial experiments indicate that the climate changes predicted using the nudged ocean, are of a smaller magnitude than those predicted using a fully coupled ocean, at least for the increased CO₂ simulations.

Uncertainties also arise because of the methodology used in these simulations. The simulations are “snapshots”; they are run to equilibrium under constant forcing conditions, and they all start from the same initial conditions. In reality, climate change is a transient process, and the climate state cannot be predicted from knowledge of the boundary conditions alone. Carrying out simulations both with and without ice sheet changes goes some way to addressing this problem, but the ocean also plays an important role in producing multiple equilibria, for example through inputs of freshwater from melting ice sheets affecting the thermohaline circulation over timescales of centuries [Ref. 25]. An assessment

of this uncertainty is not possible without carrying out further simulations, preferably with the fully coupled version of the model. Another weakness of the methodology used for the GCM simulations, is that no account is made of possible future changes of vegetation. In reality, and as has been shown in the

vegetation sections of this deliverable, both 'warm' climates (eg simulation "A"), and 'cold' climates (eg simulation "F"), have significant associated changes in vegetation. To account for the resulting changes to climate, the GCM and vegetation model would have to be coupled together.

7.2. - Comparison with previous work

In this section, some of the BIOCLIM future-climate results are compared to similar previous work. Global results from Simulation "A" are compared to previous increased CO₂ simulations, which are summarised by the Intergovernmental Panel for Climate Change (IPCC). Local results from the same simulation,

over Britain and France, are compared to reports from the UKCIP02 (UK Climate Impacts Program 2002) and ICCF (Impacts potentiels du Changement Climatique en France en XXIeme siecle), respectively. Finally, a very qualitative comparison is made between simulation "D", and some previous paleoclimate simulations.

7.2.1 - Simulation "A" - comparison with IPCC

The IPCC have produced reports [Ref. 26; Ref.18] that summarise the current state of research into anthropogenic climate change. The following quotes taken from these reports, indicate the broad temperature and precipitation changes expected in an increased-CO₂ experiment:

"...all models produce a maximum annual mean warming in high northern latitudes." Ref. 25, p305.

"There is a minimum warming, or even regions of cooling, in the high latitude Southern Ocean." Ref. 25, p302.

"The surface air temperature [change] is smaller in the North Atlantic and circumpolar Southern Ocean regions relative to the global mean." Ref. 18, p528.

"Generally...the land warms more than the ocean after forcing stabilises." Ref. 18, p528.

"There is consistent mid-tropospheric tropical warming and stratospheric cooling" Ref. 25, p305.

"The globally averaged mean precipitation increases" Ref. 18, p528.

"Most tropical areas have increased mean precipitation, most sub-tropical areas have decreased mean precipitation, and in the high latitudes the mean precipitation increases." Ref. 18, p528.

All these changes from the IPCC reports are qualitatively consistent with the changes seen in simulation "A".

A quantitative comparison of the magnitude of the changes in simulation "A", with those found by previous workers is difficult, due to the fact that no one else has carried out an experiment with exactly the same forcing. In general, there are two types of forcing scenarios described by the IPCC: transient and equilibrium. In transient experiments, the CO₂ is increased gradually, for example scenario "IS92a" has a CO₂ concentration of 345ppmv at present, about 500ppmv at in the year 2050, and 700ppmv in the year 2100 (IPCC 1995, p23). IS92a also includes increases to other greenhouse gases, and to sulphate aerosols. Equilibrium experiments have a constant elevated CO₂ concentration, usually at double or quadruple the 'present' value (i.e. 690ppmv or 1380ppmv). The BIOCLIM experiment "A" is an equilibrium simulation, with a CO₂ concentration of 1100ppmv.

Table 16 summarises some results of global mean 2m temperature and precipitation changes from a selection of previous experiments, and compares them to those found in experiment "A".

Experiment Description	ΔT (°C)	Δp (%)
1% increase transient , at time of CO ₂ doubling	+1.8 (+1.1 to +3.1)	
Equilibrium twice-CO ₂ ensemble	(+2.0 to +5.1)	+2.5 (-0.2 to +5.6)
BIOCLIM simulation “A”	+2.2	+0.8

Table 16: Comparison of previous estimates of global temperature changes in increased CO₂ simulations, with that carried out for BIOCLIM. The transient data is from IPCC 2001, p527. The equilibrium data is from IPCC 2001, p537-540.

It shows that the “A” simulation, which is approximately a CO₂ tripling experiment, is reasonably similar to previous model results for a CO₂ doubling. The geographical distribution of the changes to temperature and precipitation, shown in IPCC 2001 (p546, p549), are also very similar, although the relatively large increases in precipitation over the Sahara seen in the IPCC ensemble are not reproduced in simulation “A”.

In summary, this comparison shows that the IPSL_CM4_D model is relatively insensitive to an increase in CO₂ concentration. The reason for this low sensitivity is likely to be related to the nudging of the deep ocean temperatures towards present day values. Although the ocean temperatures are never nudged in

the uppermost 100m, the nudging is nearest the surface at high latitudes, where the climate system is particularly sensitive, due to the sea ice and snow albedo feedbacks. The fact that the high latitude ocean temperatures are not being allowed to freely respond to the climate forcing could be leading to the low sensitivity of the model. However, without this ocean nudging, the model would take a long time (of order centuries) to spin up.

The fact that model is relatively insensitive to the CO₂ forcing, means that it is likely to be insensitive to other forcings, or changes in boundary conditions. This should be considered when interpreting all the GCM results presented in this deliverable.

7.2.2 - Simulation “A” - comparison with UKCIP02 and ICCF

The results from simulation “A”, can be compared to two reports, which have summarised possible future climate changes over the UK and France. These are the UKCIP02 [Ref. 27] report for Great Britain, and the ICCF [Ref. 28] report for France.

Table 17 shows the temperature change, ΔT , and the precipitation change, Δp , over the UK, in DJF and JJA, from simulation “A”, and from the UKCIP02 report. The values from the UKCIP02 report are from the “High Emissions Scenario”, in the 2080’s, for which the CO₂ concentration is approximately 800ppmv (see UKCIP02, p17, fig 20), compared with 1100ppmv in simulation “A”.

	UKCIP ΔT	“A” (UK) ΔT	UKCIP Δp	“A” (UK) Δp
DJF	+2.0 to +3.5	+2.5	+15% to +35%	+4.3%
JJA	+3.0 to +5.0	+2.7	-30% to -50%	-32%

Table 17: Comparison of temperature changes, ΔT (°C), and precipitation changes, Δp (%), over Great Britain, from the BIOCLIM simulation “A”, and from the UKCIP02 report. “UK” is taken to be 7°W to 2°E and 50°N to 58°N for the simulation “A” values, and the majority of the UK region for the UKCIP02 values. Values of UKCIP02 temperature change are from p32, fig 34, precipitation change from p36, fig 38..

The sign of all the changes is the same in the simulation and in the report; they both predict increases in temperature throughout the year, and a winter increase in precipitation and a summer decrease. Furthermore, the seasonal variations in change are also the same, with larger increase in temperature in summer than in winter, and a larger change in precipitation in summer than in winter.

However, the changes in simulation “A” are consistently of a smaller magnitude than the changes in the UKCIP02 report, or at least at the lower end of the range.

Table 18 shows the temperature change, ΔT , and the precipitation change, Δp , over France, in DJF and JJA, from simulation “A”, and from the ICCF report.

	ICCF ΔT	“A” (France) ΔT	ICCF Δp	“A” (France) Δp
DJF	+1 to +2	+2.8	+1 to +2	-0.52
JJA	+1 to +3	+4.8	0	-0.52

Table 18: Comparison of temperature changes, ΔT ($^{\circ}\text{C}$), and precipitation changes, Δp (mmday^{-1}), over France, from the BIOCLIM simulation “A”, and from the ICCF report. “France” is taken to be 2°W to 5°E and 43°N to 50°N .

The temperature changes from simulation “A” over France are in good agreement with the ICCF report findings. The temperature increases throughout the year, with a larger increase in summer than in winter. However, for precipitation, simulation “A” shows a decrease throughout the year, whereas the ICCF report indicates an increase in winter, and little change in summer. The magnitude of the temperature changes are greater in simulation “A” than in the ICCF report.

represented by just 1 whole gridbox, and 8 part-gridboxes. However, the GCMs used in the reports have a much higher resolution; the model used in UKCIP02 is the Hadley Centre regional model, running at a 50km resolution. Furthermore, the simulations in the reports do not have the same forcings as that in simulation “A”.

A comparison such as this has some limitations. The BIOCLIM GCM simulations are carried out at a relatively low resolution, and care must be taken when interpreting results that are averages over just a few gridboxes. In this case, both the UK and France are

However, despite the problems of the comparison, the results are encouraging. Over Great Britain, there is agreement over the general trends, if not magnitudes, of changes to both temperature and precipitation. Over France, there is good agreement over temperature, but not precipitation.

7.2.3 - Simulation “D” - comparison with Vavrus and Kutzbach (2002)

Vavrus and Kutzbach [Ref. 29] have carried out simulations with a fully coupled GCM, in which they reduce the height of the major mountain ranges (Tibetan plateau, Rockies and Andes), and remove the Greenland and East Antarctic ice sheets, replacing their surfaces with tundra vegetation. As well as a present day control, they carried out one simulation with increased CO_2 (3CO_2), and one with increased CO_2 and lowered topography (LT3CO2). This is in an attempt to recreate boundary conditions of 20-10MyrBP, preceding the development of extensive glacial ice on

Greenland. They present results of the difference in wintertime surface temperature between LT3CO2 and CO_2 . This can be compared to the difference between the BIOCLIM simulations “D” and “E”, which also only includes the effect of removing the ice sheet. They have a maximum local warming over Greenland of $+10$ to $+11^{\circ}\text{C}$, compared to the BIOCLIM $+13$ to $+14^{\circ}\text{C}$. They have a cooling centered over Iceland, of -4 to -5°C , which extends into northern Europe. This could be a similar feature to the warming centered in the Barents Sea in BIOCLIM simulation “D”, of -6 to -7°C .

The magnitudes of the changes in Vavrus and Kutzback are therefore similar to those in BIOCLIM. An extensive comparison is not possible, because the two experiments are not similar enough, but it is encouraging that the fully coupled system is reacting in a similar way to the nudged system.



8. Recommendations

This section provides some recommendations, which are to be considered in subsequent climate change experiments, carried out as part of safety assessments.

It is essential that the deep-ocean nudging technique be further validated. This should be carried out by initially performing a present-day fully coupled simulation, and then using the deep-ocean temperatures calculated in this simulation, to perform a present-day nudged simulation. This is to provide deep-ocean temperatures for the nudging which are in equilibrium with the model's physics. In this project, observed temperatures have been used, which may lead to some inconsistencies between the model physics and dynamics. Following this, a series of pairs of simulations need to be carried out, in which both a fully coupled and nudged simulation are carried out, for a variety of forcings and changes to boundary conditions. A comparison of the results in the fully coupled and nudged simulations, will reveal the strengths and weaknesses of the nudging technique. The nudging technique could be further evaluated by using different nudging temperatures, such as those from an LGM simulation, to test the model's sensitivity to the nudging temperatures. If the nudging proves satisfactory, then the technique can be applied in safety assessments. However, if it is found that the nudging technique fails to reproduce changes in SSTs, driven by changes to mechanisms such as the thermohaline circulation, then a fully coupled GCM would have to be used. At this point, no evaluation of the nudging technique has been carried out, except to say that the changes in SSTs due to an increase in CO₂, resemble those from a fully-coupled simulation more than those from a slab ocean.

A second recommendation is that the GCM and vegetation models described and used in this deliverable, be run in coupled mode for future safety assessments. This coupling could be asynchronous, whereby the GCM climate is used to produce vegetation maps, as is done here, but which are then put back into the GCM to provide the boundary conditions for a second GCM simulation. Otherwise the coupling could be complete, whereby the GCM and vegetation model are run simultaneously, but this approach requires much longer simulations (hundreds of years of simulation, as opposed to decades for the asynchronous case).

A third recommendation is that an ensemble of different GCMs be used, rather than just one as has been the case in this project. Model intercomparison projects, such as PMIP [Ref. 24], show that under identical forcings or changes to boundary conditions, different models can give very different results (e.g. Ref. 30). An ensemble of model simulations can therefore give a quantitative idea of the uncertainty of model predictions, which cannot be obtained by using just one model.

A fourth recommendation is that further validation of the model be performed, by carrying out paleoclimate simulations, such as the LGM and Holocene. These can be directly compared to paleoclimate proxies, and would give an idea of the model's performance under changes to radiative forcing, CO₂ concentration, and ice-sheet characteristics.



9. Data products

T This section provides a brief summary of how the results and data presented in this deliverable will feed into other parts of the project.

All the simulations that have been carried out have output 6-hourly data for at least one year of integration. These data will be used as boundary conditions to a high resolution model which can be run over Europe, the MAR atmosphere-only regional GCM. In this way, the one year of data can be downscaled, in a dynamical fashion.

The monthly mean temperatures and precipitation, will also be downscaled, but in a statistical fashion.

Empirical relationships between GCM-scale and local-scale climate variables will be formulated based on the present day results. The relationships will include parameters such as height above sea level, and distance from the coast. These empirical relationships will then be applied to the future climate simulations.

In addition to the dynamical and statistical downscaling procedures, the data from the GCM simulations is available to everyone in the BIOCLIM community, to use as they wish. Files of 2m air temperature, ground level temperature, precipitation, altitude, and land-sea mask, have been placed on the business collaborator, at <http://cobweb.businesscollaborator.com/bc/bc.cgi>



10. References

- Ref. 1:** Li, Z.L., 'Description algorithmique d'un ensemble de parameterisation physique - phylmd', 1998. Available from: <http://www.lmd.jussieu.fr/~lmdz/doc.html>
- Ref. 2:** Tiedtke, M., 'A comprehensive mass flux scheme for cumulus parameterisation in large scale models', *Monthly Weather Review*, 117, 1779-1800, 1989.
- Ref. 3:** Fouquart, Y. and Bonnel, B., 'Computation of solar heating of the Earth's atmosphere: A new parameterisation', *Beitr. Phys. Atmos.*, 53, 35-62, 1980.
- Ref. 4:** Morcrette, J.J., 'Radiation and cloud radiative properties in the ECMWF operational weather forecast model', *J. Geophys. Res.*, 96, 9121-9132, 1991.
- Ref.5:** Madec,G., Delecluse, P., Imbard,M. and Levy,C., 'OPA 8.1 Ocean General Circulation Model reference manual', Note du Pole de Modelisation, Institut Pierre-Simon Laplace (IPSL), France, No XX, 91pp, 1999.
- Ref.6:** Gent, P.R. and McWilliams, J.C., 'Isopycnal mixing in ocean circulation models', *J. Phys. Oceanogr., Notes and Correspondance*, 20, 150-155, 1990.
- Ref 7:** UNESCO, 'Algorithms for computation of fundamental property of sea water', Technical Paper in Marine Sciences, 44, UNESCO, 1983.
- Ref. 8:** Fichet, T., and Morales Maqueda, M.A., 'Modelling the influence of snow accumulation and snow-ice formation on the seasonal cycle of the Antarctic sea-ice cover', *Clim. Dyn.*, 15, 251-268, 1999.
- Ref. 9:** Ducoudré, N.I., Laval, K. and Perrier, A., 'SECHIBA, a new set of parameterizations of the hydrological exchanges at the land-atmosphere interface within the LMD atmospheric general circulation model', *J. Clim.*, 6, 248-273, 1993.
- Ref. 10:** Viovy, N., de Noblet, N., 'Coupling water and carbon cycle in the Biosphere' *Sci. geol. Bull.*, 1-4, 109-201, 1997.
- Ref. 11:** Sitch, S., Smith, B., Prentice, I.C, Arneeth, A., Bondeau, A., Cramer, W., Kaplan, J.O., Levis, S., Lucht, W., Sykes, M.T., Thonicke, K. and Venevsky, S., 'Evaluation of ecosystem dynamics, plant geography and terrestrial carbon cycling in the LPJ dynamic global Vegetation Model', *Glob. Change Biol.*, 9, 161-185, 2003.
- Ref. 12:** Emanuel, K., 'A scheme for representing cumulus convection in large-scale models', *J. Atmos. Science*, 48, 2313-2335, 1991.
- Ref. 13:** New, M., Hulme, M. and Jones, P.D., 'Representing twentieth century space-time climate variability. Part 1: development of a 1961-90 mean monthly terrestrial climatology', *Journal of Climate* 12, 829-856, 1999.
- Ref. 14:** Jourdan, L., 'Le bais froide a la troposphere', 2002.
Available from: <http://www.lmd.jussieu.fr/~lmdz/CRs/LMDZ/CR17012002>
- Ref. 15:** Eidenshink, J. and Faundeen, J., 'The 1 km AVHRR global land data set: First stages in implementation', *International Journal of Remote Sensing*, 15, 3443-3462, 1994.

- Ref. 16:** Ritz, C., Fabre, A. and Letreguilly, A., 'Sensitivity of a Greenland ice sheet model to ice flow and ablation parameters : consequences for the evolution through the last climatic cycle', *Clim. Dyn.*, 13,(1) 11-24, 1997.
- Ref. 17:** Broecker et al, 'Origin of the northern Atlantic's Heinrich events', *Clim. Dyn.*, 6, 265-273, 1992.
- Ref. 18:** IPCC, 2001, 'Climate Change 2001: The Scientific Basis', edited by Houghton et al., Cambridge University Press, 2001.
- Ref. 19:** de Noblet-Ducoudré, N., Claussen, N. and Prentice, C., 'Mid-Holocene greening of the Sahara: Comparing the response of two coupled atmosphere/biome models', *Climate Dynamics*, 16, 643-659, 2000.
- Ref. 20:** Lunt, D.J., de Noblet-Ducoudre, N. and Charbit, S., 'Effects of a melted Greenland ice sheet on climate, vegetation, and the cryosphere', in prep.
- Ref. 21:** Texier, D., de Noblet, N., Harrison, S., Haxeltine, A., Joussaume, S., Jolly, D., Laarif, F., Prentice, I.C. and Tarasov, P.E., 1997: Quantifying the role of biosphere-atmosphere feedbacks in climate change: a coupled model simulation for 6000 yr BP and comparison with paleodata for Northern Eurasia and northern Africa. *Climate Dynamics*, 13 : 865-882.
- Ref. 22:** De Noblet, N.I., Prentice, I.C., Joussaume, S., Texier, D., Botta, A. and Haxeltine, A., 'Possible role of atmosphere-biosphere interactions in triggering the last glaciation', *Geophys. Res. Lett.*, 23, 3191-3194, 1996.
- Ref. 23:** Kageyama, M., Peyron, O., Pinot, S., Tarasov, P., Guiot, J., Joussaume, S. and Ramstein, G., 'The Last Glacial Maximum climate over Europe and western Siberia: a PMIP comparison between models and data', *Clim. Dyn.*, 17, 23-43, 2001.
- Ref. 24:** Joussaume, S. and Taylor K.E., 'Status of the Paleoclimate Modelling Intercomparison Project (PMIP)', in *Proceedings of the first international AMIP scientific conference*, pp 425-430, 1995.
- Ref. 25:** Ganopolski, A., and Rahmstorf, S., 'Rapid changes of glacial climate simulated in a coupled model', *Nature*, 409, 153-158, 2001.
- Ref. 26:** IPCC, 1995, 'Climate Change 1995: The Science of Climate Change,' edited by Houghton et al., Cambridge University Press, 1995.
- Ref. 27:** Hulme, M., Jenkins, G.J., Lu, X., Turnpenny, J.R., Mitchell, T.D., Jones, R.G., Lowe, J., Murphy, J.M., Hassell, D., Boorman, P., McDonald, R. and Hill, S., 'Climate change scenarios for the United Kingdom: The UKCIP02 Scientific report', Tyndall Centre for Climate Change Research, School of Environmental Sciences, University of East Anglia, Norwich, UK, 2002. Available from: http://www.ukcip.org.uk/research_tools/research_tools.html

- Ref. 28:** Mousel et al, 'Impacts potentiels du Changement Climatique en France au XXIeme siecle', Seconde edition 2000.
Available from : <http://www.effet-de-serre.gouv.fr/main.cfm?page=fr/emissions/emissions.html>
- Ref. 29:** Vavrus, S. and Kutzbach, J.E., 'Sensitivity of the thermohaline circulation to increased CO₂ and lowered topography', *Geophys. Res. Lett.*, 29, doi 10.1029/2002GL014814, 2002.
- Ref. 30:** Masson, V., Cheddadi, R., Braconnot, P., Jousaume, S., and Texier, D., 'Mid-Holocene climate in Europe : what can we infer from PMIP model-data comparisons ?', *Climate Dynamics*, 15, 163-182, 1999.



List of figures

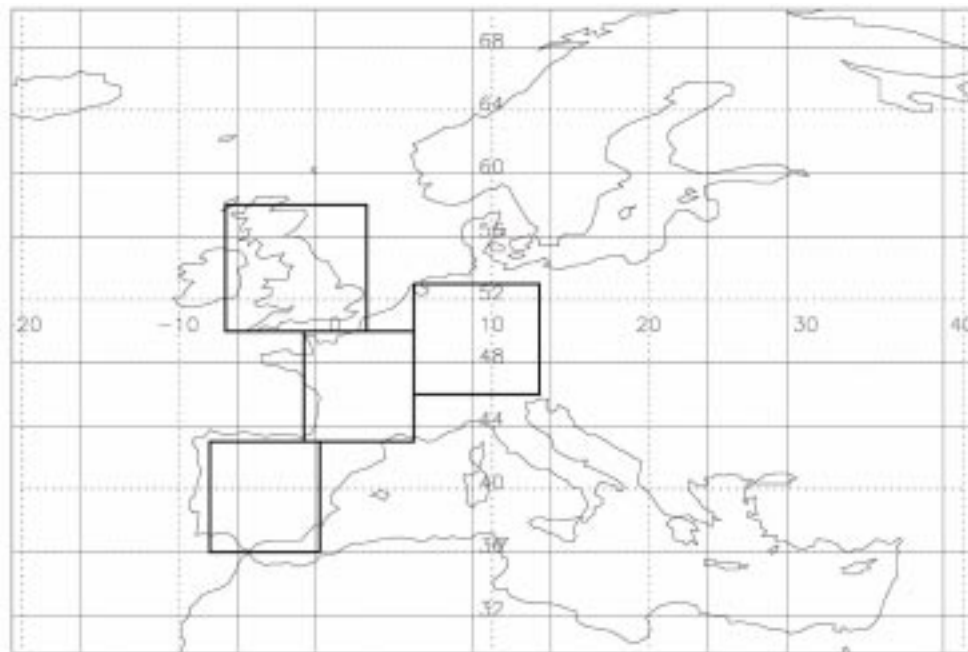


Figure 1: The european region. The thin lines show the GCM gridboxes. The dotted lines show the longitude and latitude. The thick lines show the regions defined as "UK", "France", "Spain", and "Central Europe", in section 5.

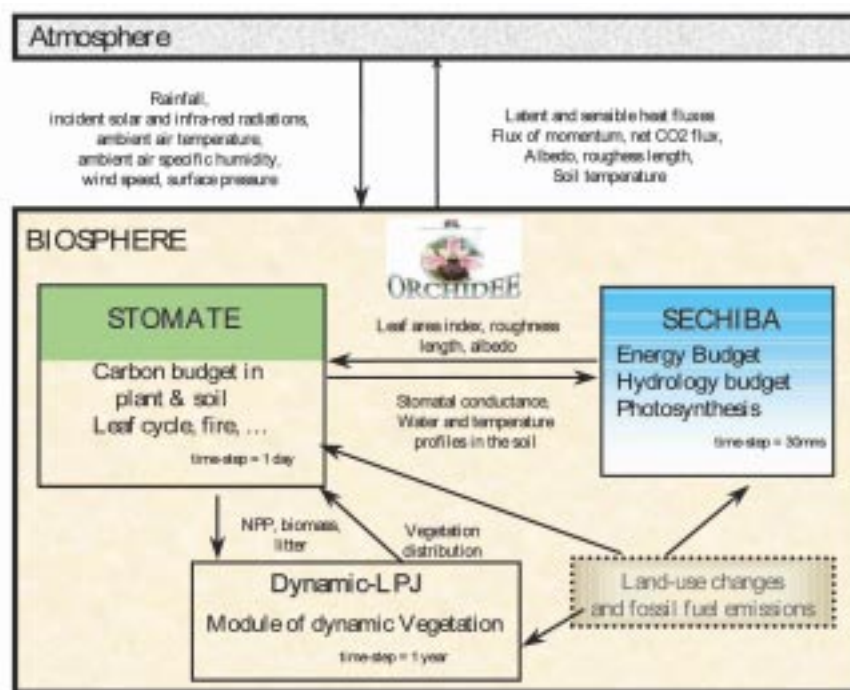
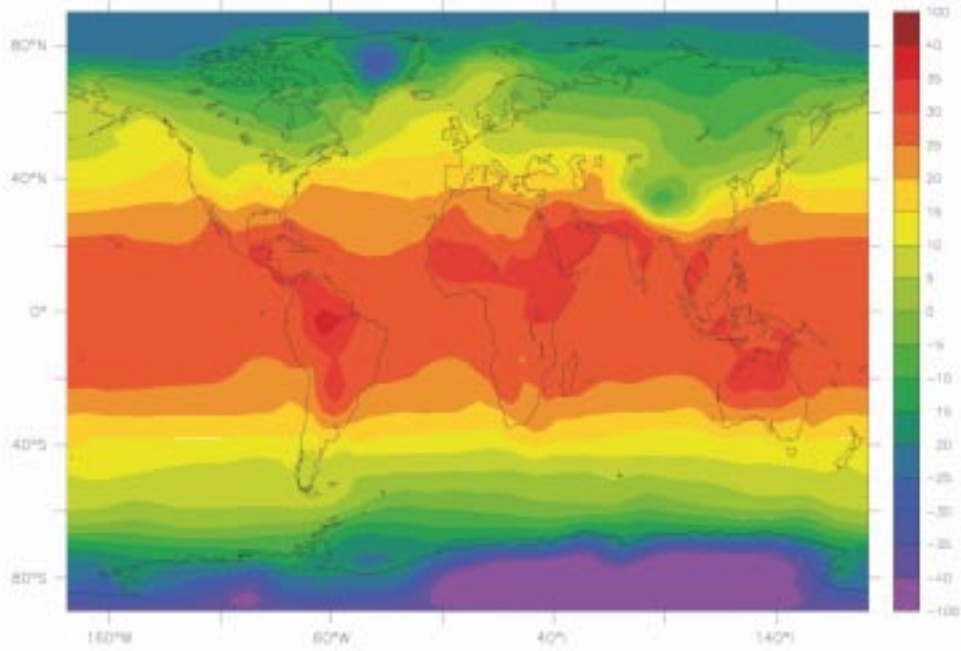
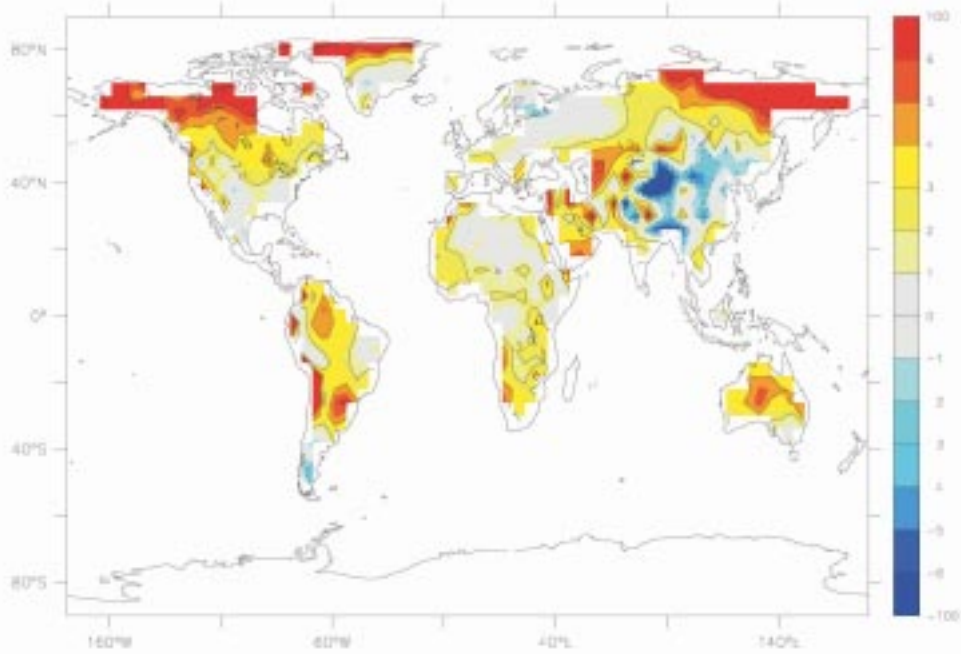


Figure veg.1: schematic diagram describing all components of ORCHIDEE, as well as its inputs from the atmosphere

Figure 2: Schematic diagram describing all components of ORCHIDEE, as well as its inputs from the atmosphere.

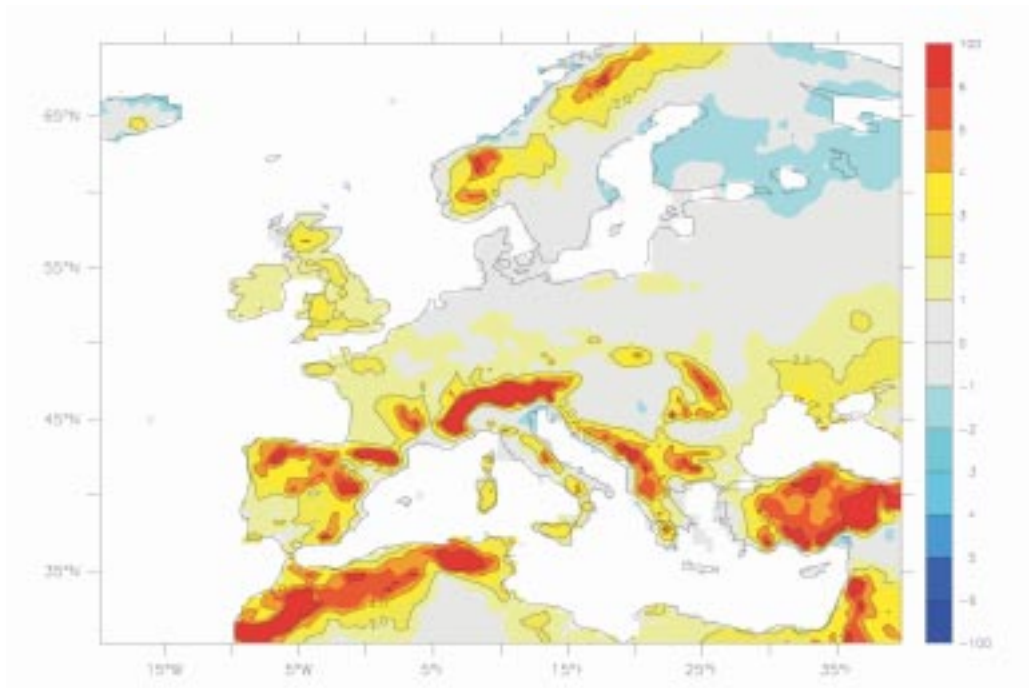


(a)

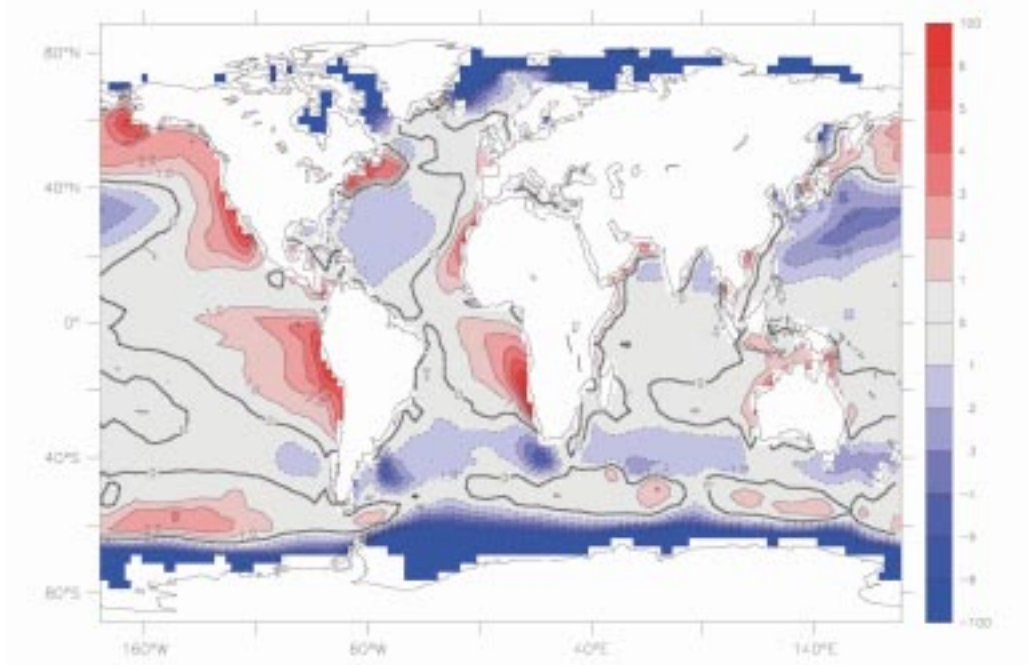


(b)

Figure 3: (a) Annual mean ground level temperature (SST over ocean, soil temperature over land), simulated by the IPSL_CM4_D model. (b) Simulated 2m temperatures minus observations (CRU climatology). (c) As for (b) but zoomed over Europe. (d) Simulated SSTs minus observations. All units are °C. Line contours are drawn every 2°C, zero contour omitted.

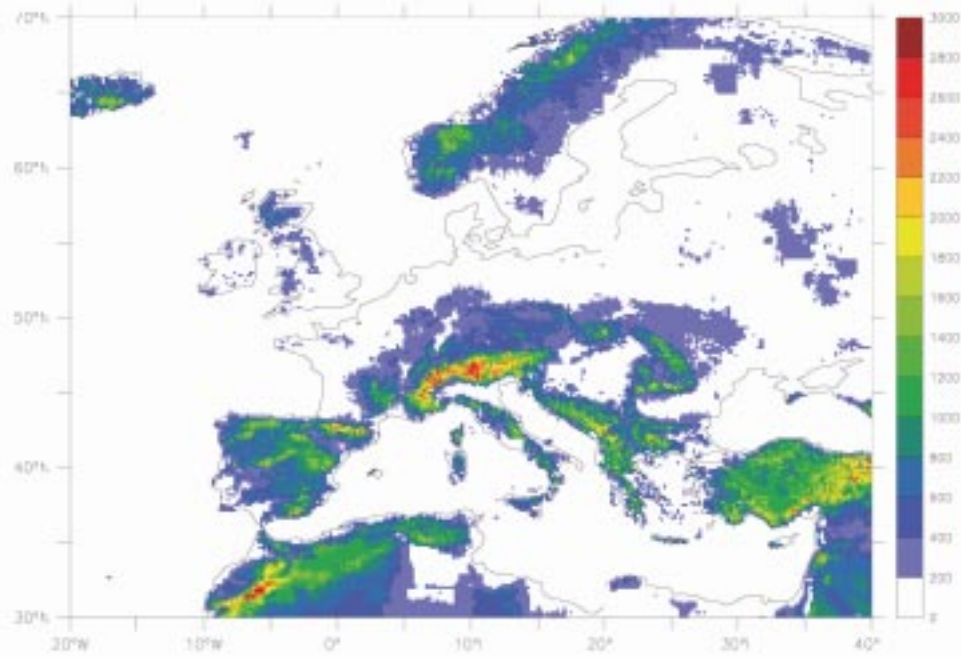


(c)

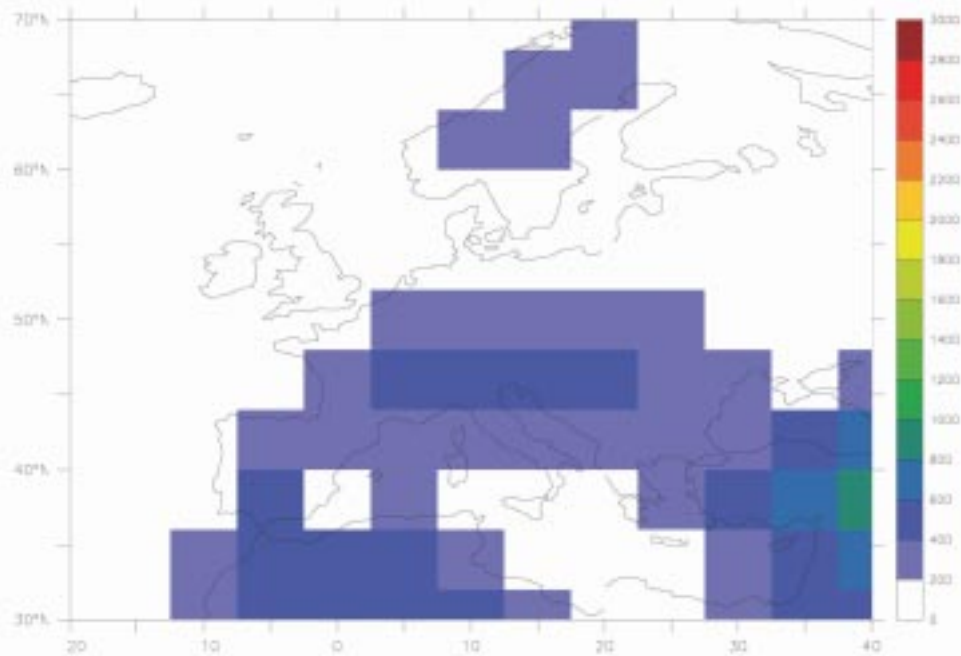


(d)

Figure 3: Caption at figure 3(a)

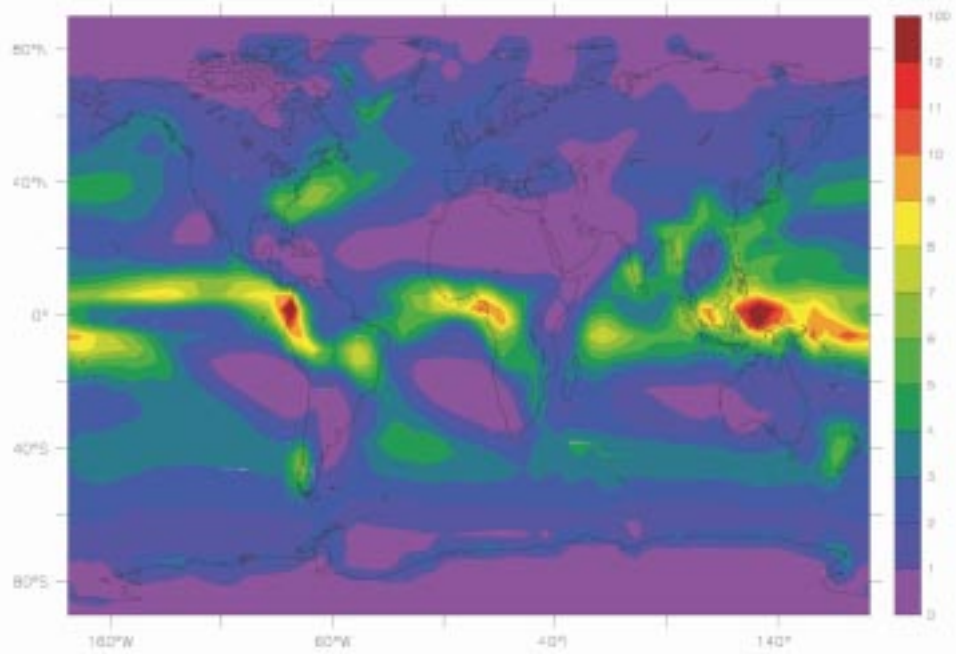


(a)

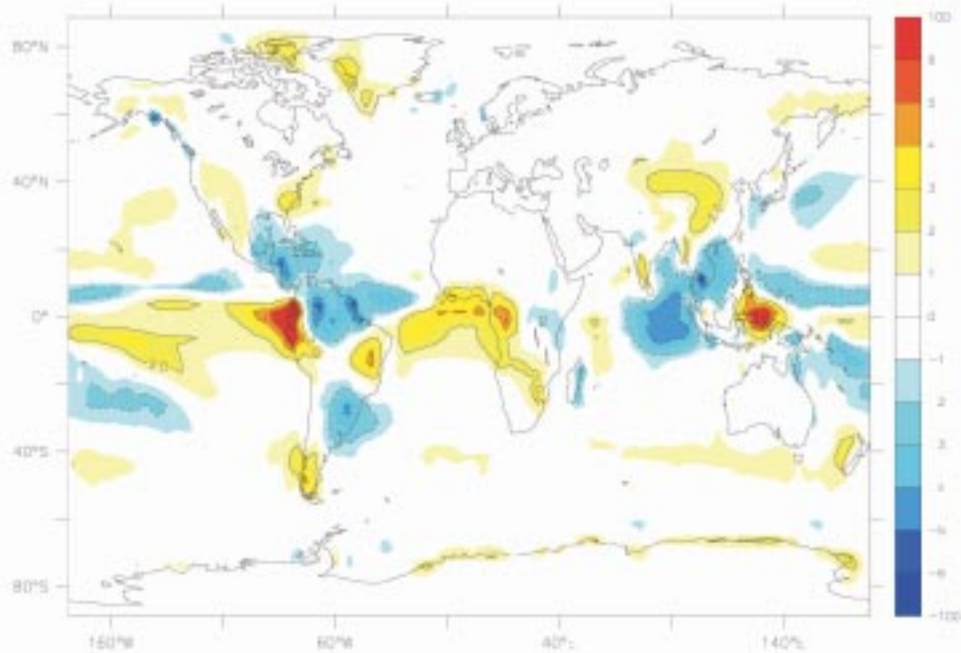


(b)

Figure 4: (a) Orography over Europe from an observational dataset, at a $1/6^\circ$ resolution. (b) Model orography over Europe.



(a)



(b)

Figure 5: (a) Annual mean precipitation rate as simulated by IPSL_CM4_D. (b) Modelled-Observed precipitation. (c) As (b), but zoomed over Europe. All units are mmday^{-1} . Line contours are drawn every 2mmday^{-1} in (b) and 0.4mmday^{-1} in (c), zero contour omitted.

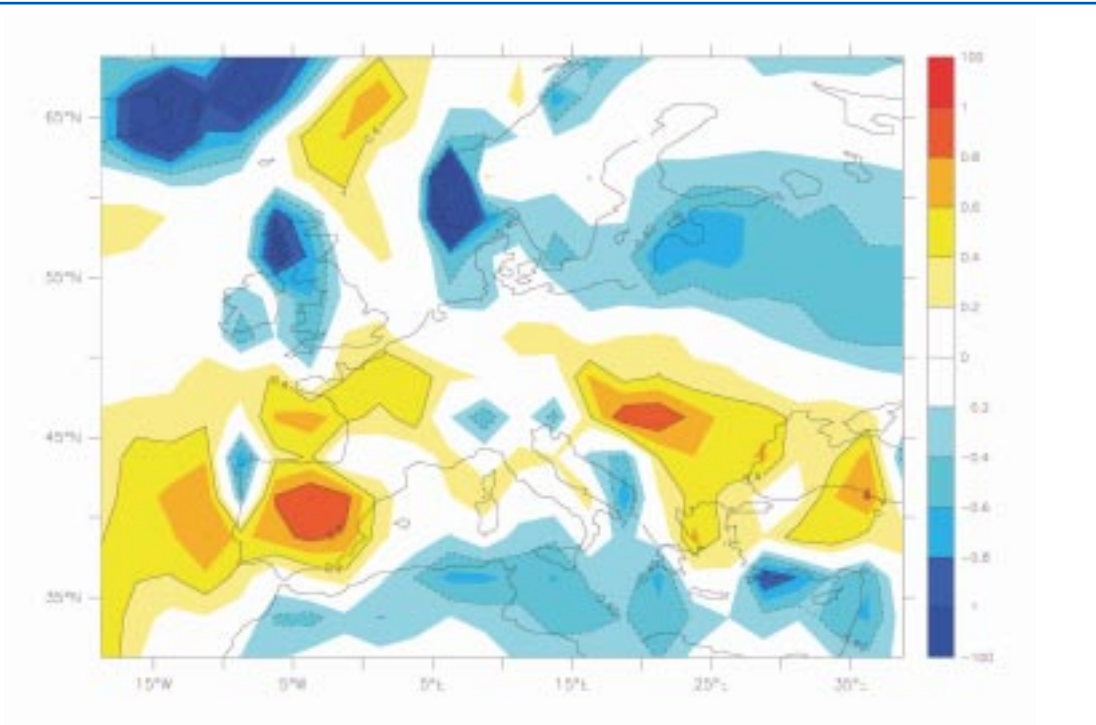
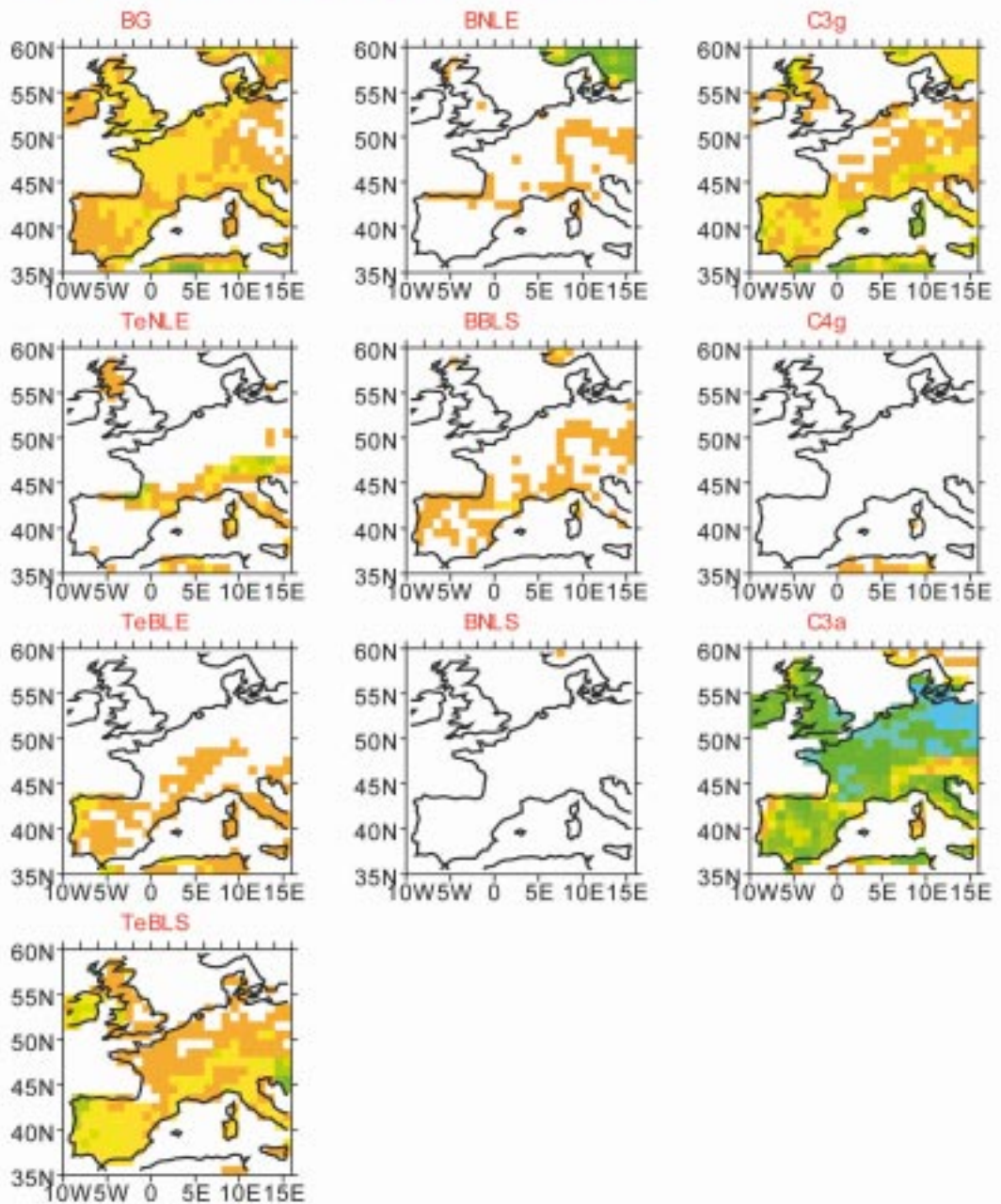


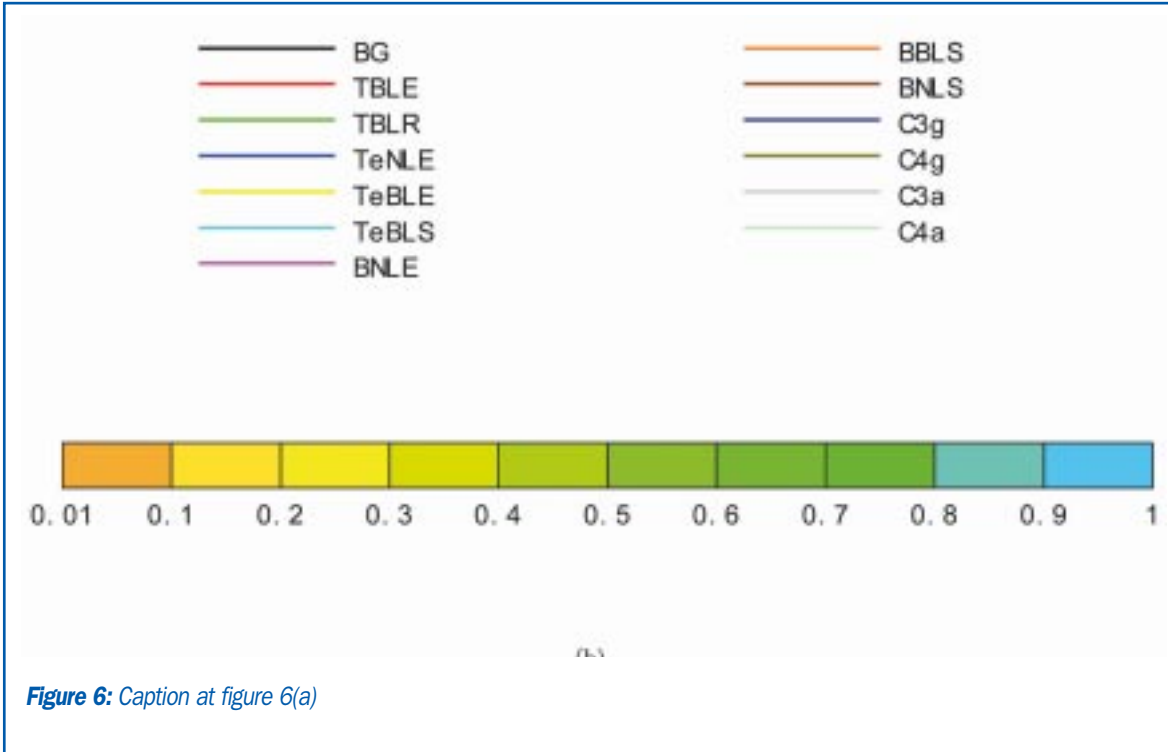
Figure 5: Caption at figure 5(a)

Observed Present-day Vegetation (from IGBP map)



(a)

Figure 6: (a) Observed present-day distribution of Plant Functional Types over Europe. (b) Color legend for figures 7 to 15, 33(a), 33(b), 34(a), 34(b), 35, 36(a), 36(c), 37 and 38. Lines correspond to different Plant Functional Types in the lower right graphic. Color boxes correspond to intervals of relative fractional coverage by any PFT (from 0 to 1 with 0.1 intervals).



Present-day Simulated Potential Vegetation (from CRU climatology)

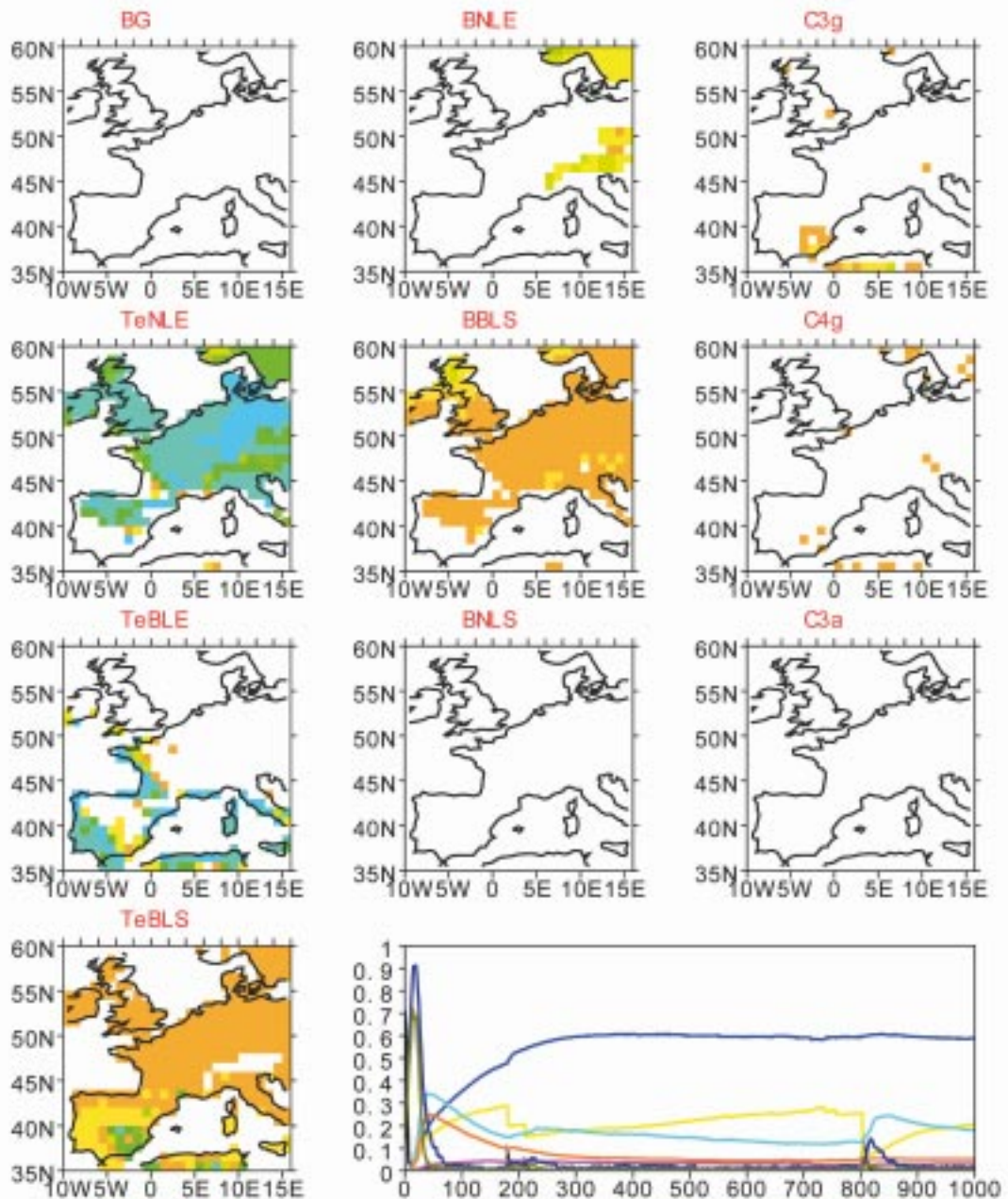


Figure 7: Simulated potential present-day distribution of Plant Functional Types over Europe (from the CRU climatology). The lower right graph corresponds to the time evolution of the area occupied by each PFT, averaged over Europe, for the 1000 years simulation. Color legend is displayed separately (figure 6(b)).

Present-day Simulated Vegetation (Baseline simulation)

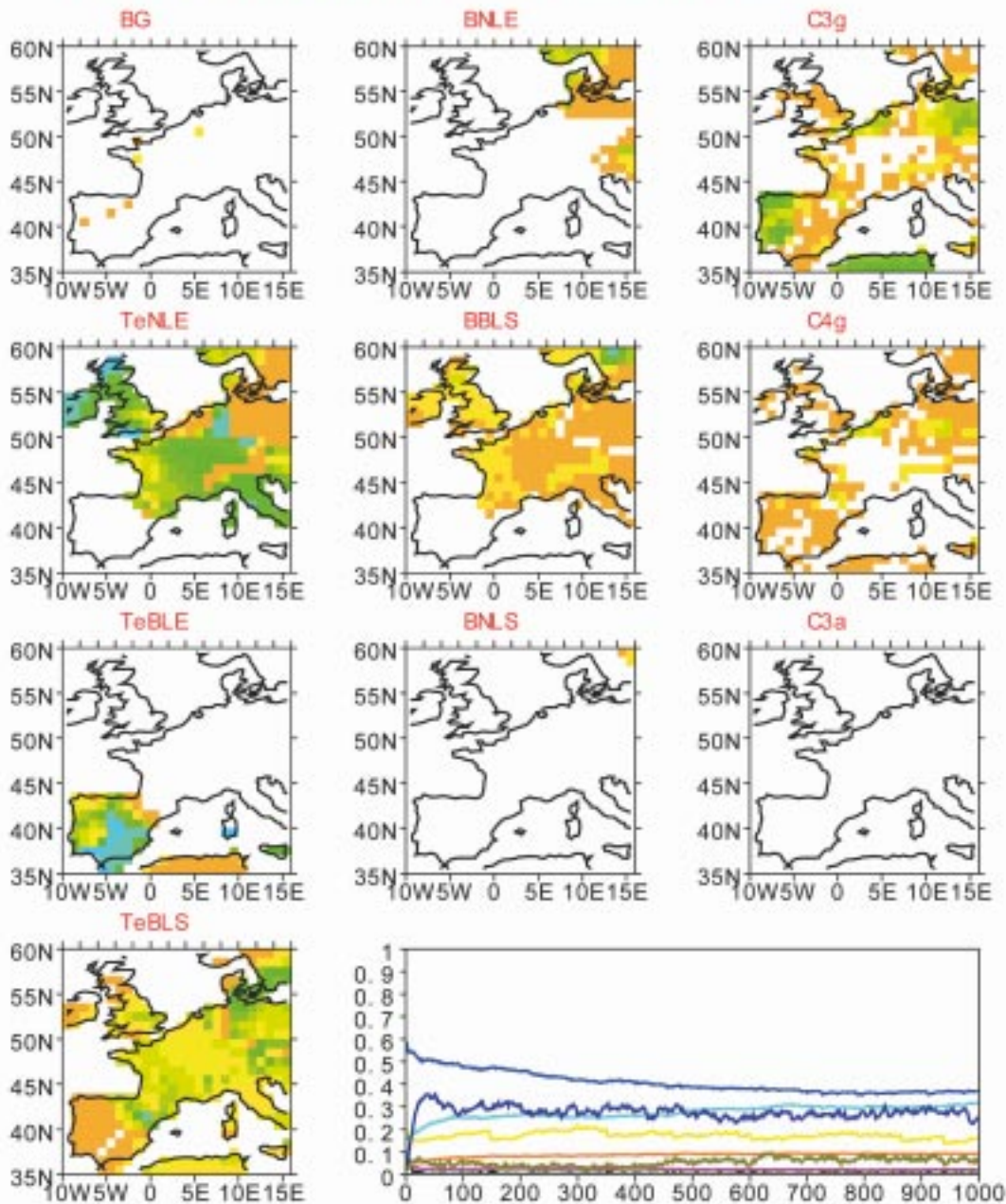


Figure 8: Simulated “Baseline” distribution of Plant Functional Types over Europe (from the “Baseline” IPSL_CM4_D simulation). The lower right graph corresponds to the time evolution of the area occupied by each PFT, averaged over Europe, for the 1000 years simulation (starting from the equilibrium vegetation distribution of the Baseline simulation). Color legend is displayed separately (figure 6(b)).

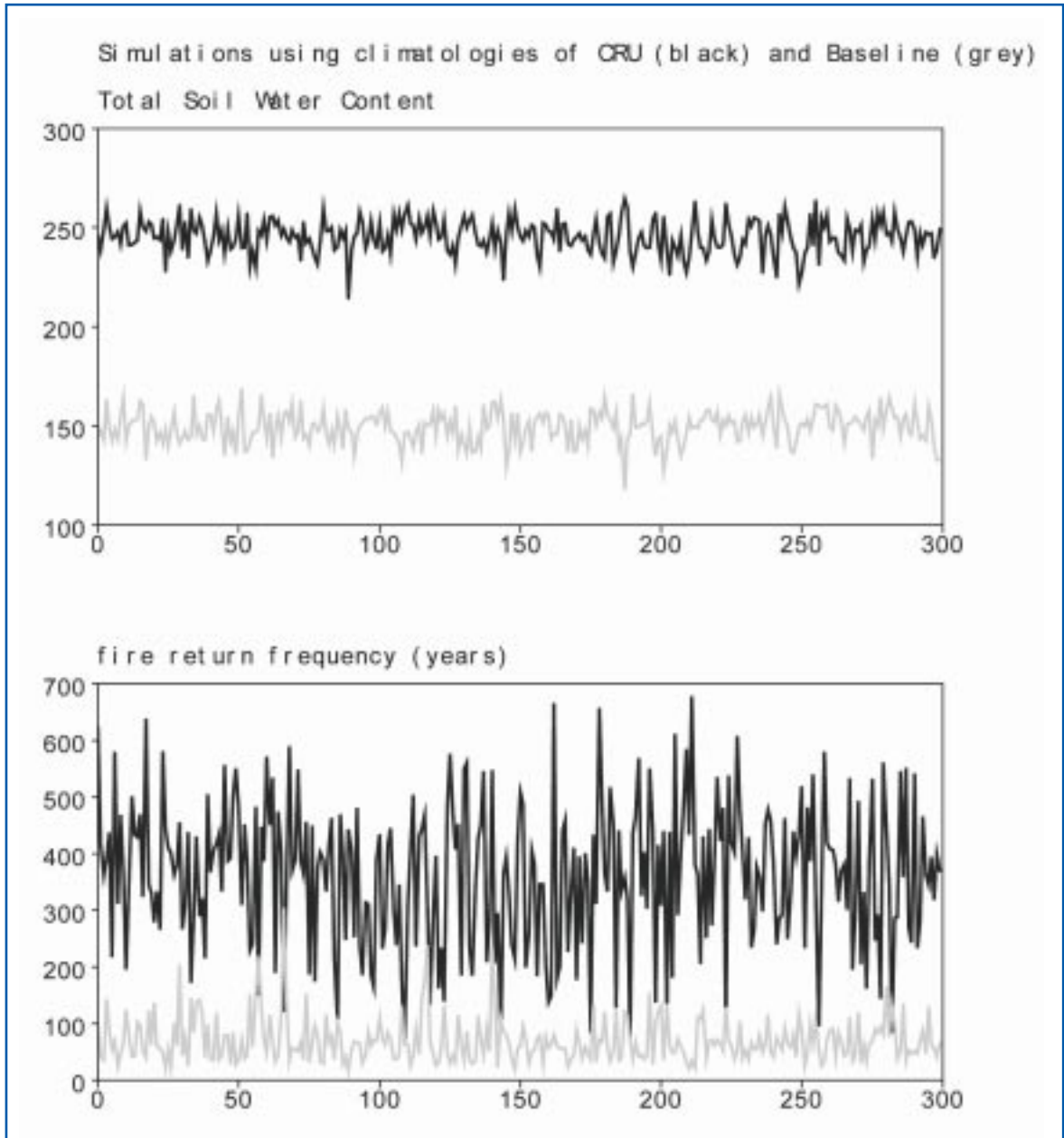


Figure 9: Time evolution of the soil water content (top graph) and the fire return frequency (bottom graph) simulated by ORCHIDEE using as atmospheric forcing the present day observed CRU climatology (black lines) and the IPLS_CM4_D simulated “Baseline” climate (grey lines).

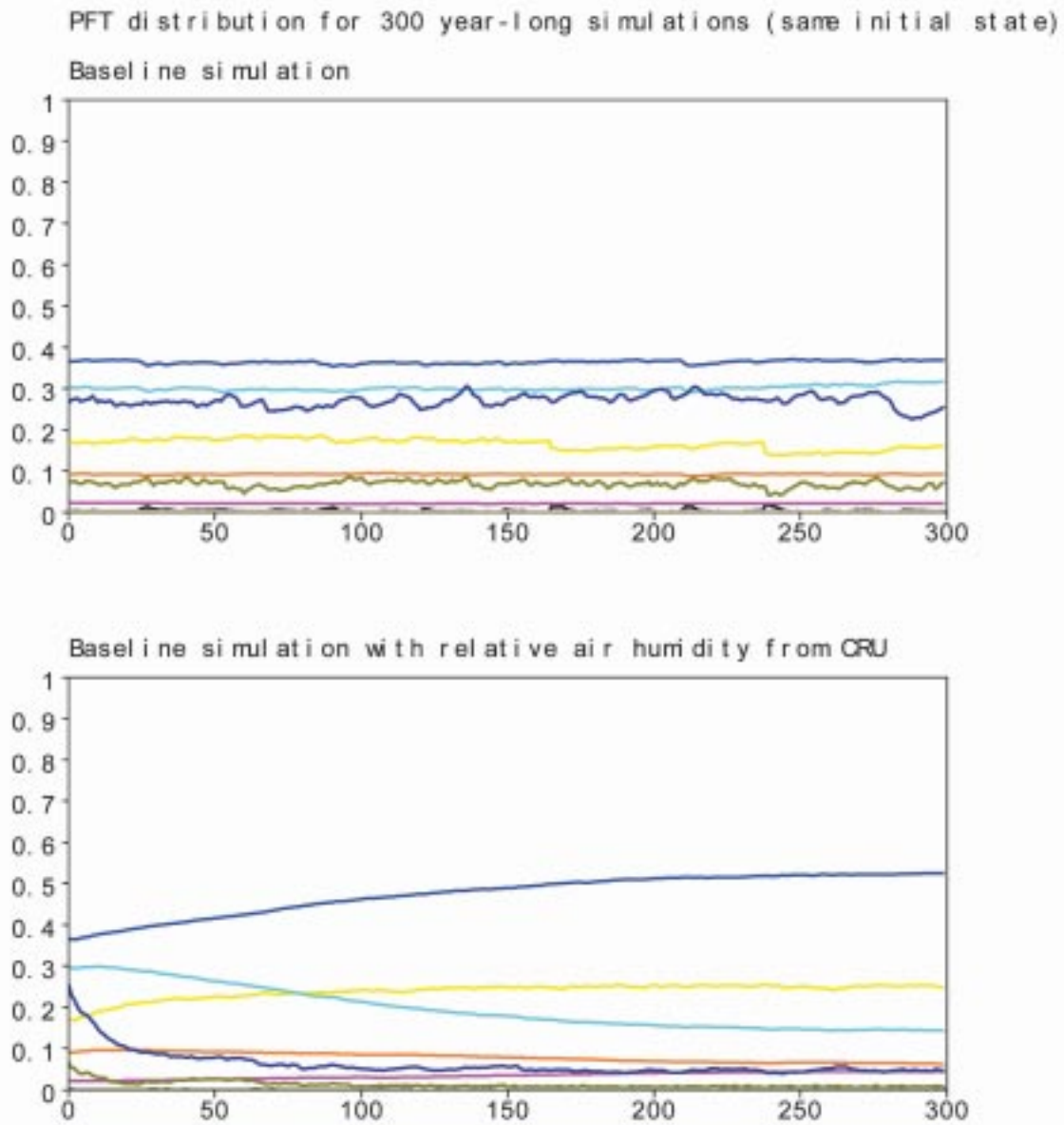


Figure 10: Time evolution of the distribution of different Plant Functional Types (legend can be found on figure 6(b)) simulated by ORCHIDEE using as atmospheric forcing the IPLS_CM4_D simulated “Baseline” climate (top graph) and the IPLS_CM4_D “Baseline” climate, albeit with relative humidity from the present-day CRU climatology (bottom graph). A moister air leads to larger fractions of trees at the expense of grasses.

Surface climate at site: FRANCE, for all simulations

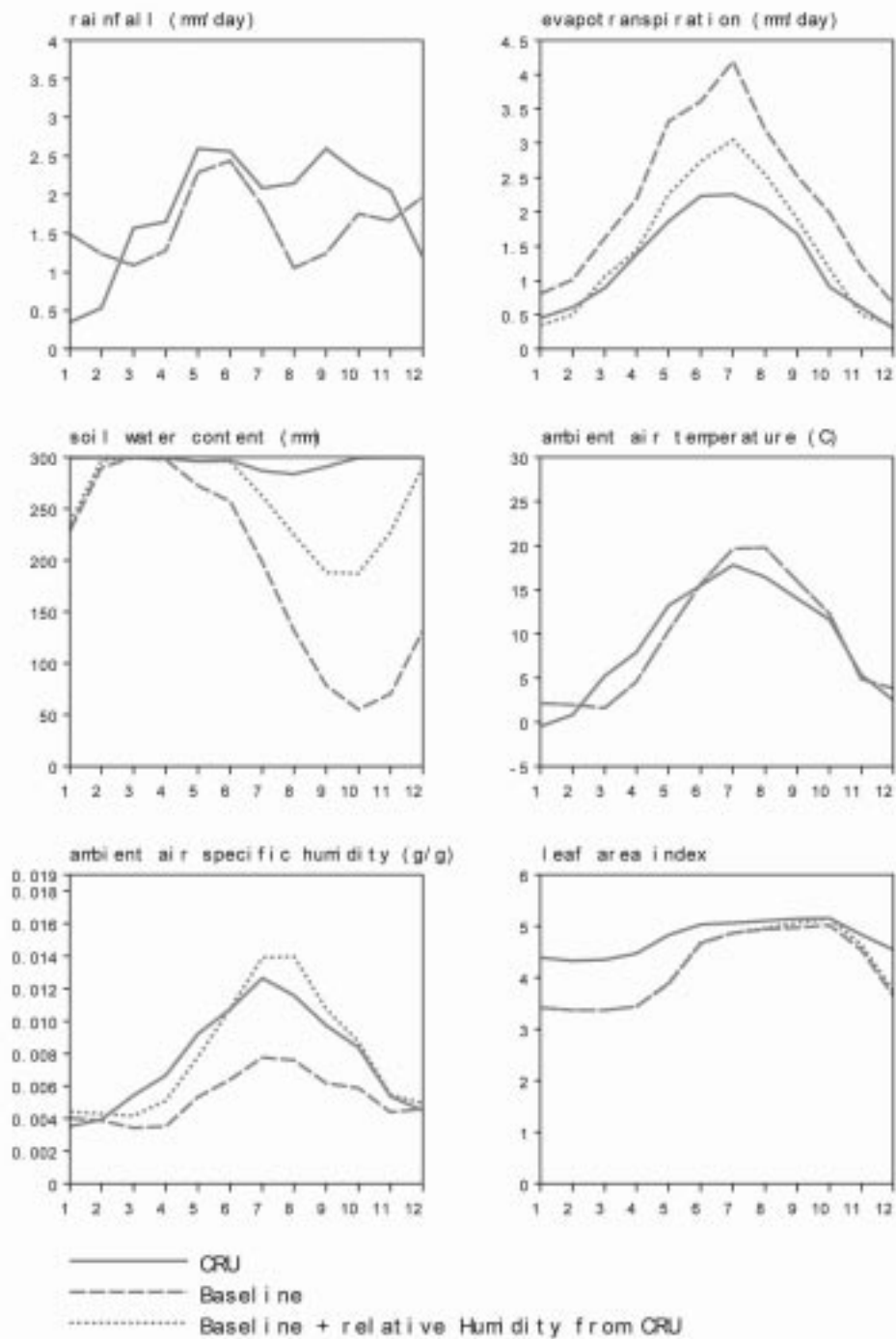


Figure 11: Surface climate at the French study area (48.5N, 5.5E): seasonal evolution of 6 surface variables simulated by IPSL_CM4_D (rainfall, ambient air temperature, ambient air specific humidity) or by ORCHIDEE (evapotranspiration, soil water content, leaf area index), for 3 different present-day climatologies. The dashed and dotted lines overlap for rainfall and ambient air temperature since they are from the same climatology.

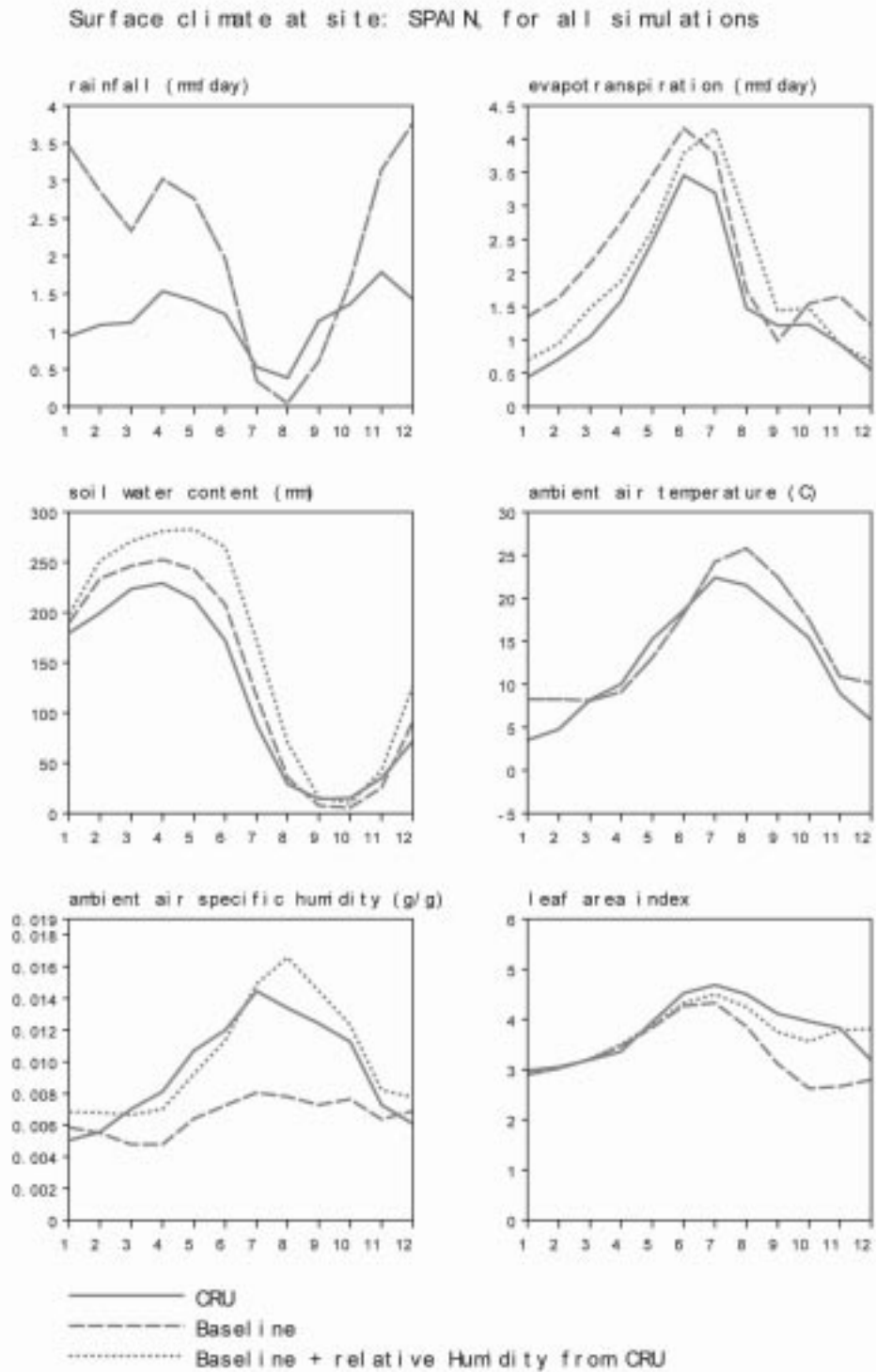


Figure 12: Surface climate at the Spanish study area (38N-41.5, 5N, 1.3W-6.3W): seasonal evolution of 6 surface variables simulated by IPSL_CM4_D (rainfall, ambient air temperature, ambient air specific humidity) or by ORCHIDEE (evapotranspiration, soil water content, leaf area index), for 3 different present-day climatologies. The dashed and dotted lines overlap for rainfall and ambient air temperature since they are from the same climatology.

Surface climate at site: ENGLAND, for all simulations

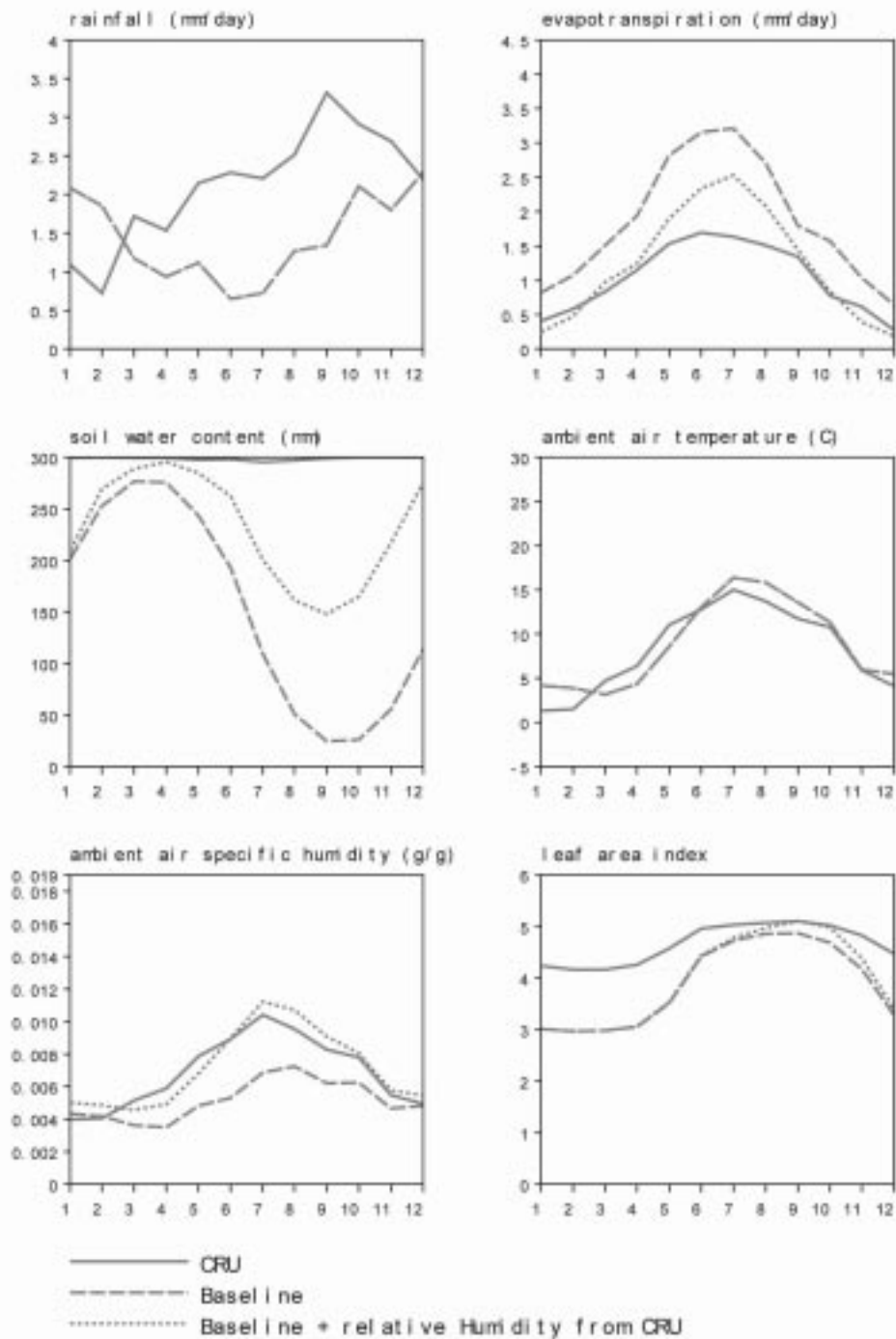


Figure 13: Surface climate at the English study area (51.5N-54.5N, 2.6W): seasonal evolution of 6 surface variables simulated by IPSL_CM4_D (rainfall, ambient air temperature, ambient air specific humidity) or by ORCHIDEE (evapotranspiration, soil water content, leaf area index), for 3 different present-day climatologies. The dashed and dotted lines overlap for rainfall and ambient air temperature since they are from the same climatology.

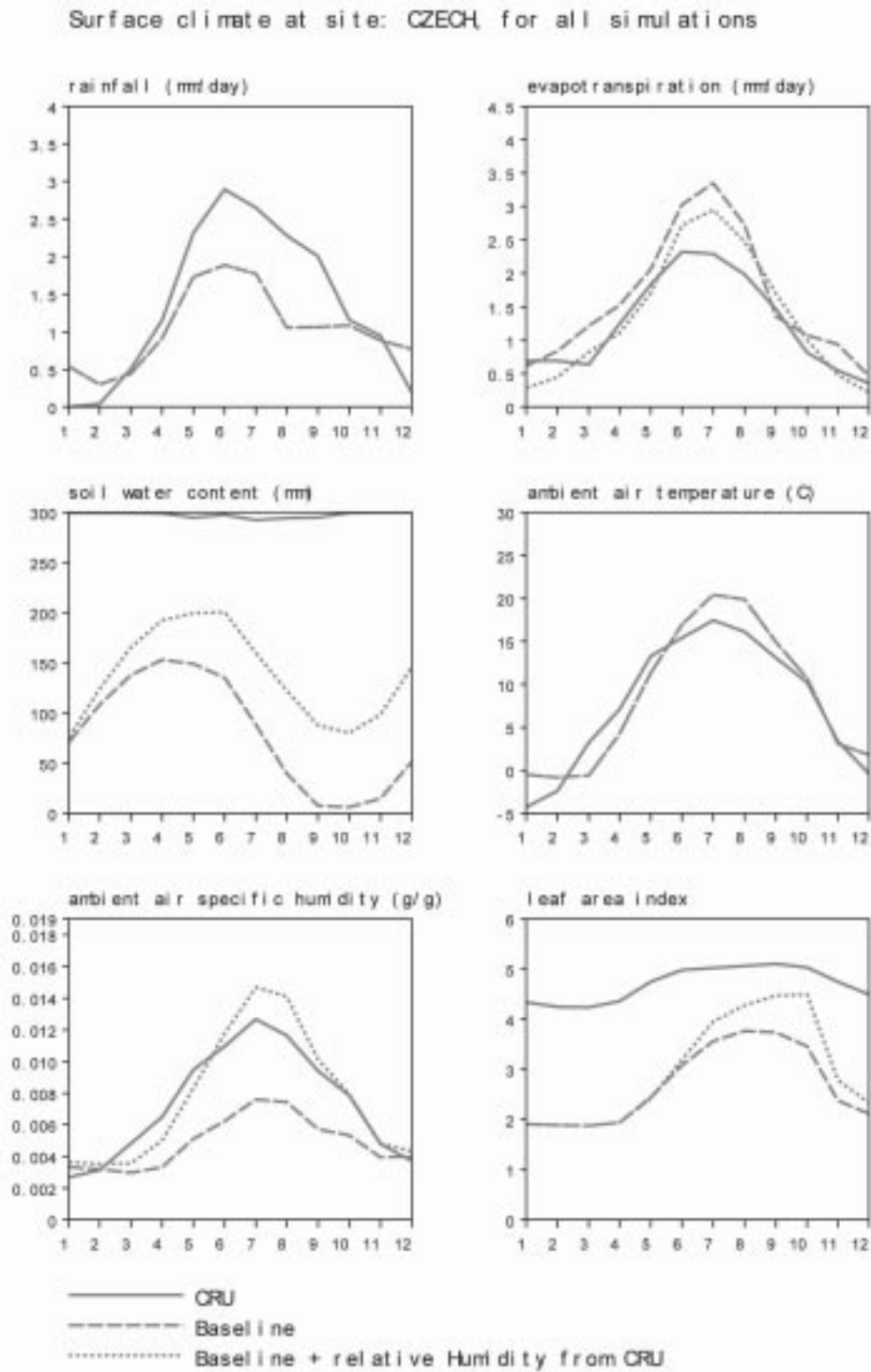


Figure 14: Surface climate at the Czech study area (48.9N-49.5N, 15E-15.6E): seasonal evolution of 6 surface variables simulated by IPSL_CM4_D (rainfall, ambient air temperature, ambient air specific humidity) or by ORCHIDEE (evapotranspiration, soil water content, leaf area index), for 3 different present-day climatologies. The dashed and dotted lines overlap for rainfall and ambient air temperature since they are from the same climatology.

Surface climate at site: GERMANY, for all simulations

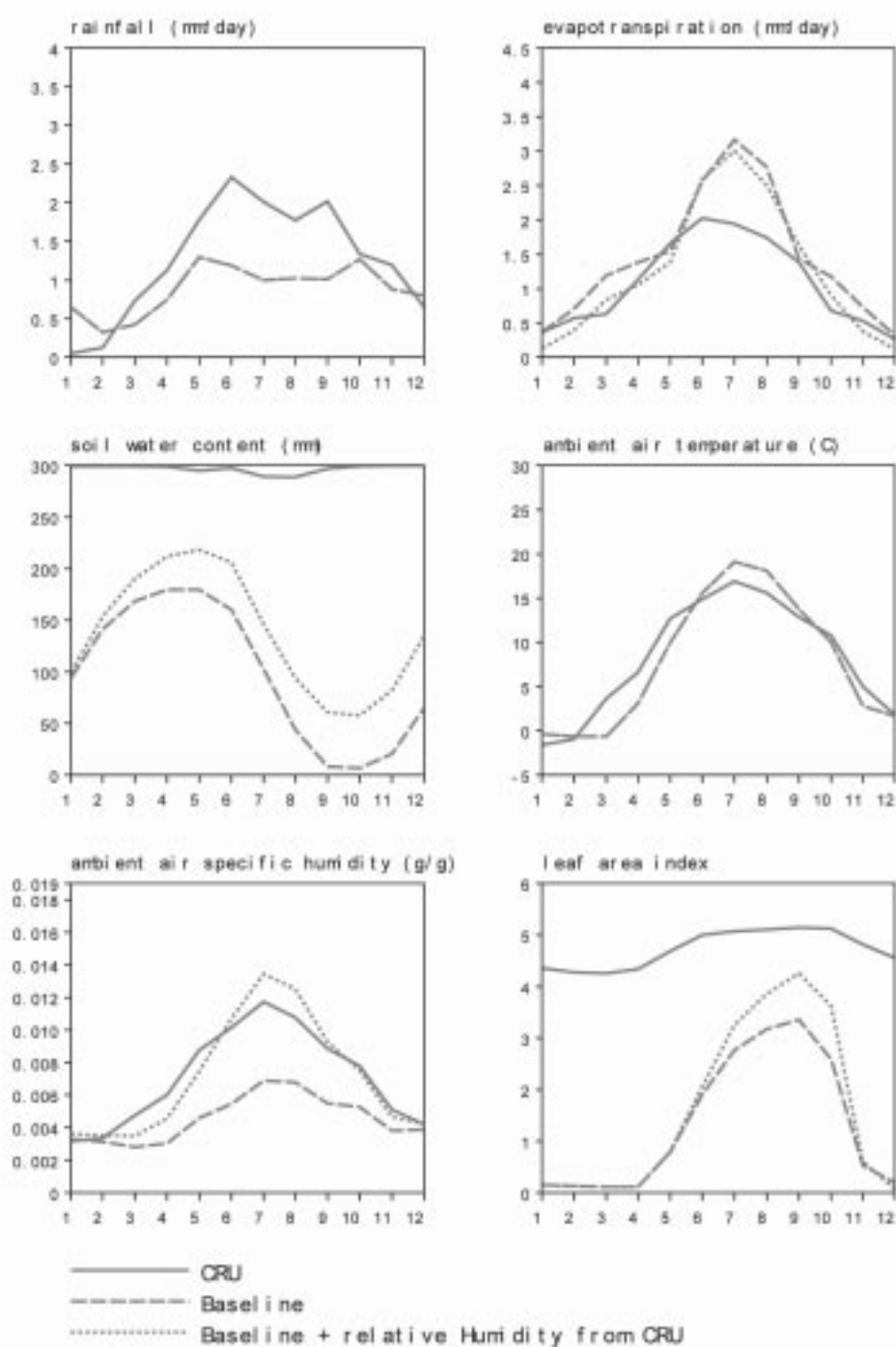
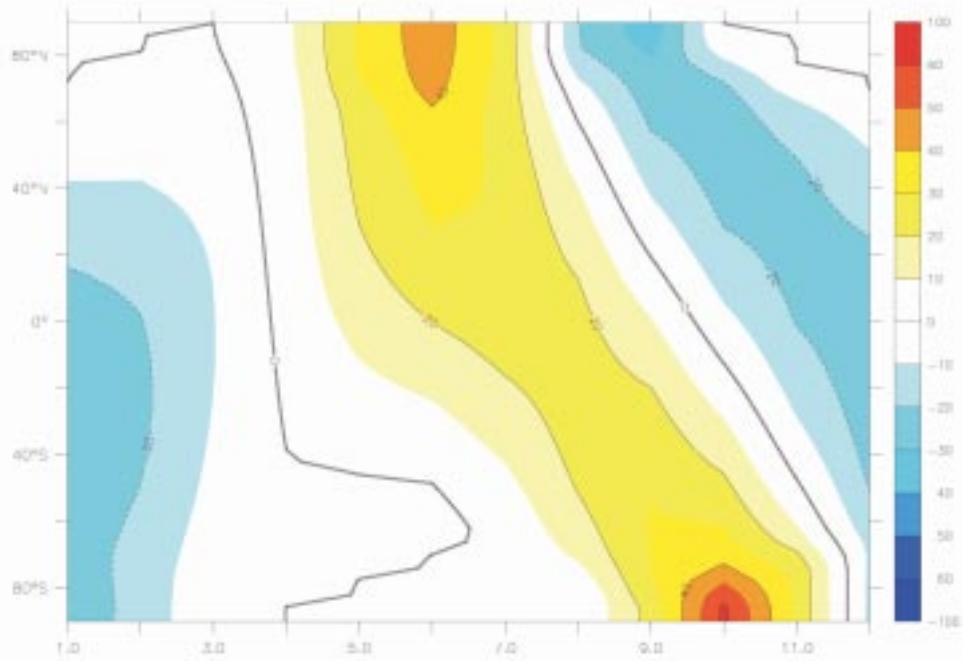
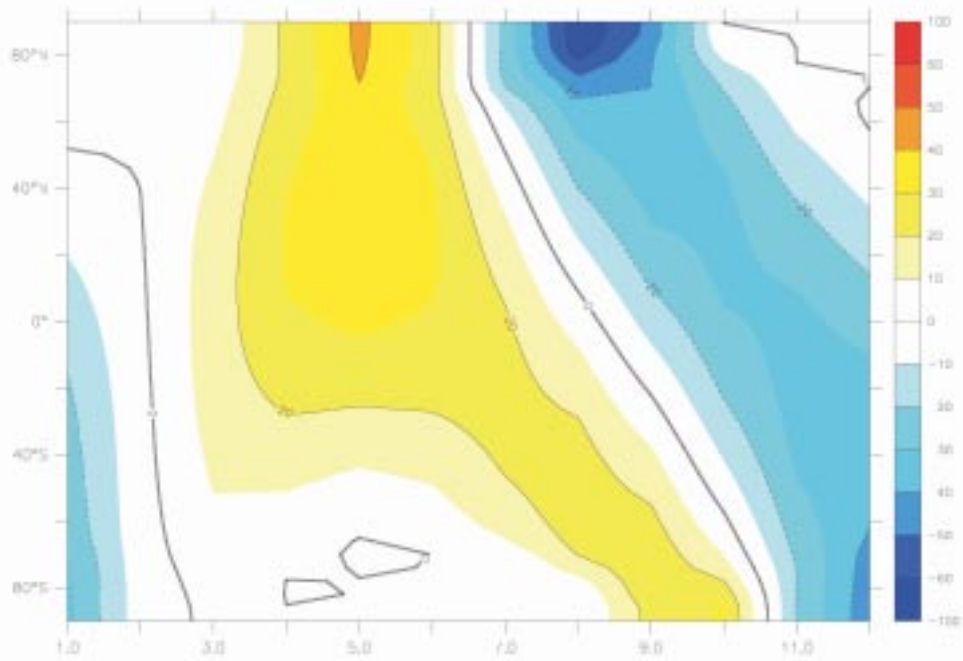


Figure 15: Surface climate at the German study area (52.2N, 10.4E): seasonal evolution of 6 surface variables simulated by IPSL_CM4_D (rainfall, ambient air temperature, ambient air specific humidity) or by ORCHIDEE (evapotranspiration, soil water content, leaf area index), for 3 different present-day climatologies. The dashed and dotted lines overlap for rainfall and ambient air temperature since they are from the same climatology.

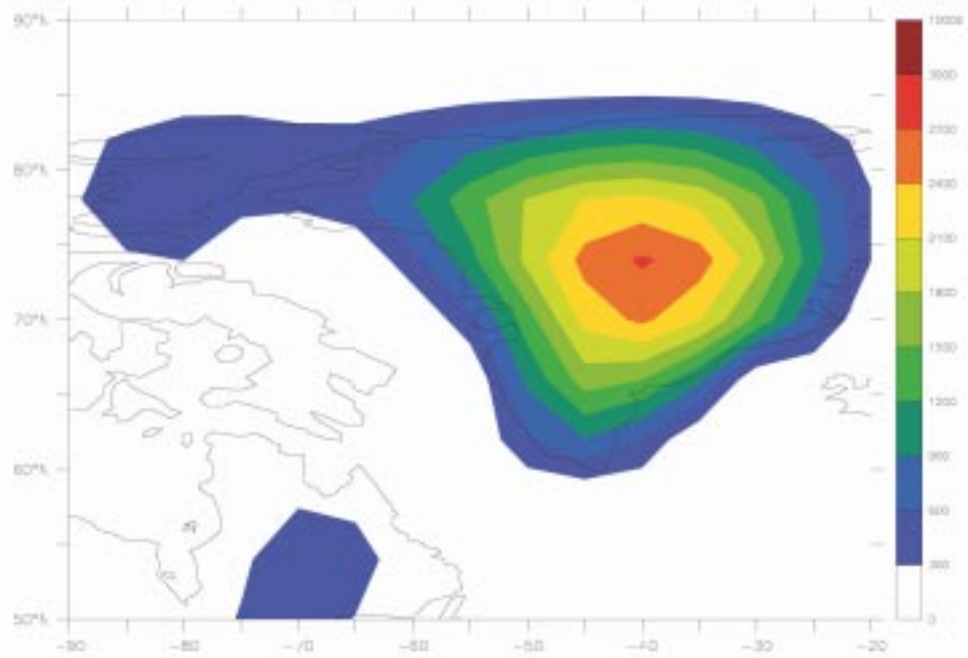


(a)

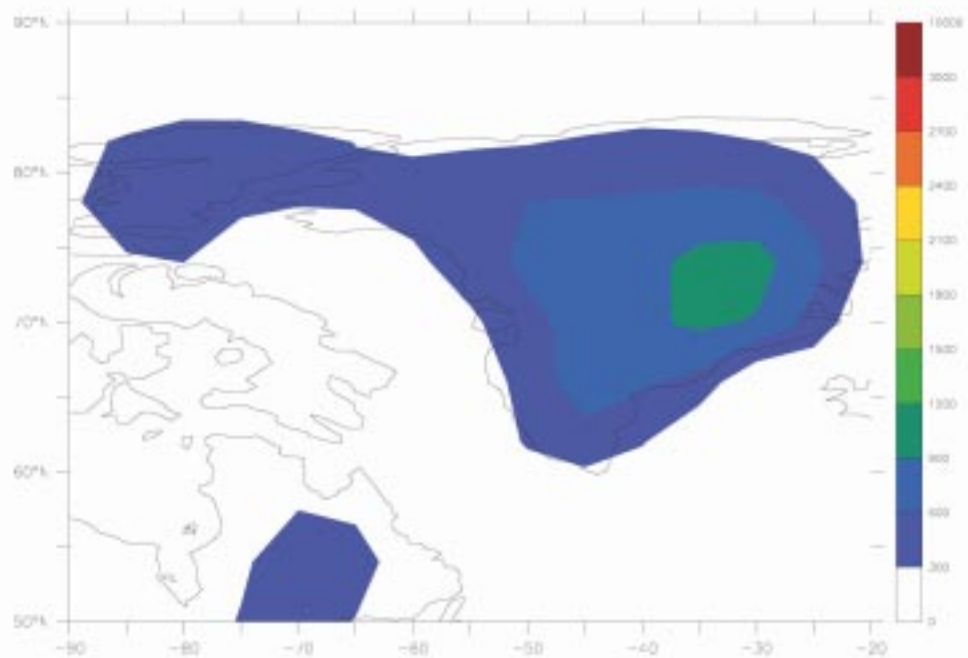


(b)

Figure 16: The change in incoming solar radiation at the top of the atmosphere compared to the present, at (a) 67kyrAP and (b) 178kyrAP. Units are Wm^2 .



(a)



(b)

Figure 17: (a) The orography over Grennland in the control. (b) The orography in the perturbed experiments, in which the ice sheet is melted. All units are metres.

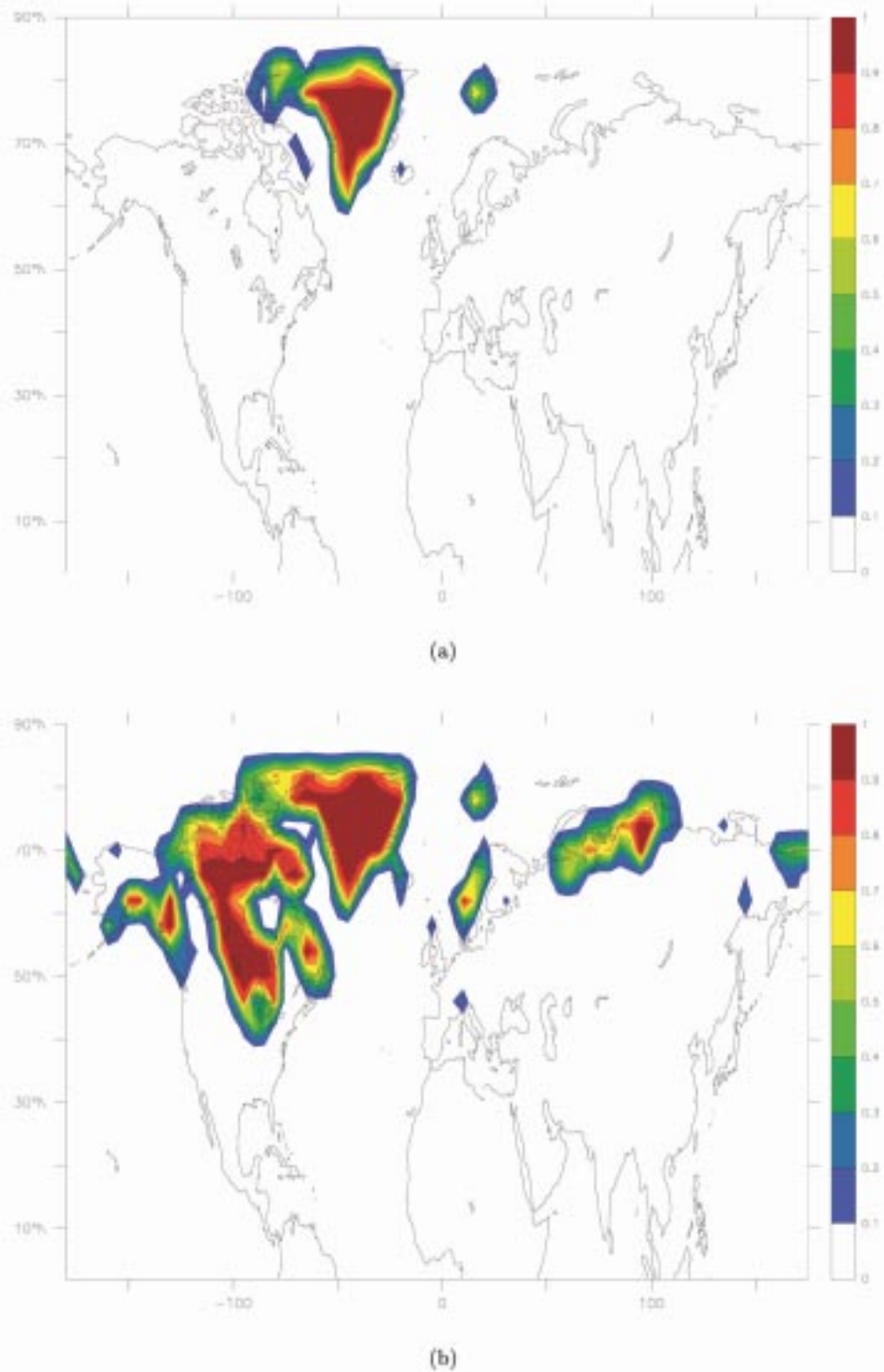
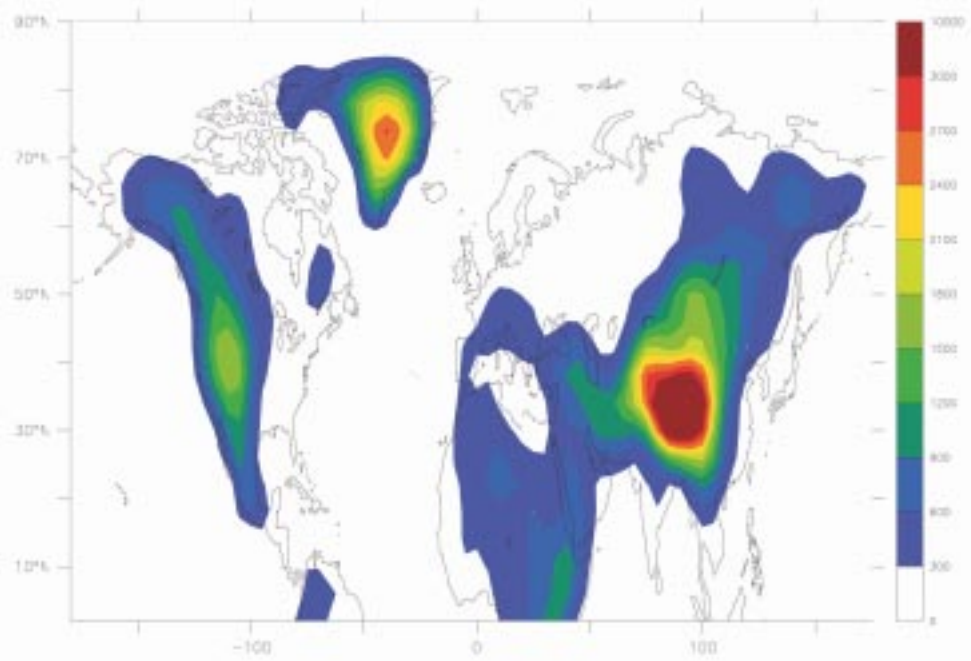
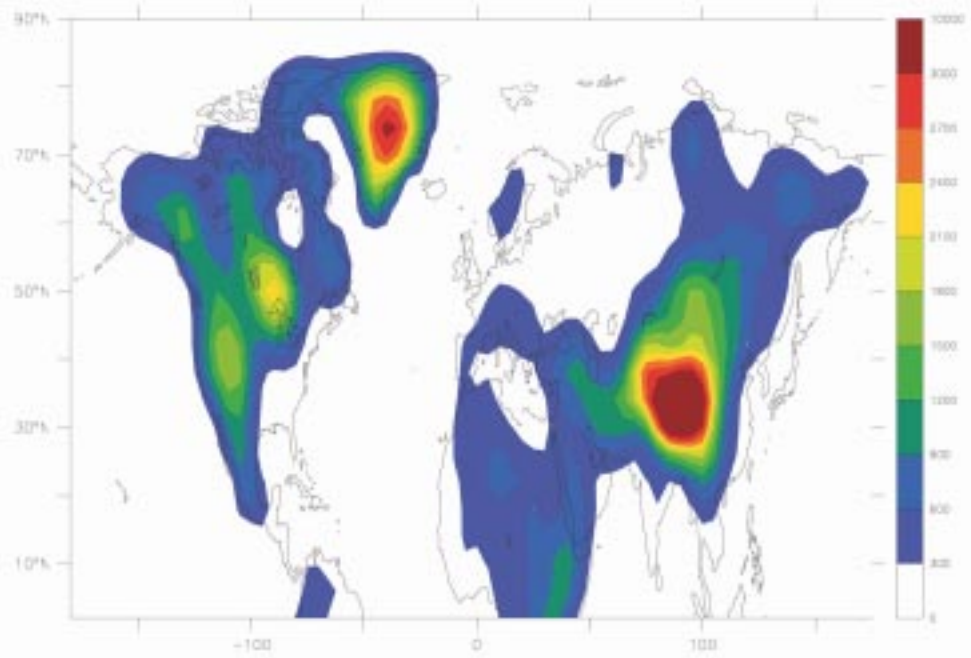


Figure 18: (a) The land ice fraction in the Northern Hemisphere in the control. (b) The land ice fraction in simulation "F" at 178kyrAP.

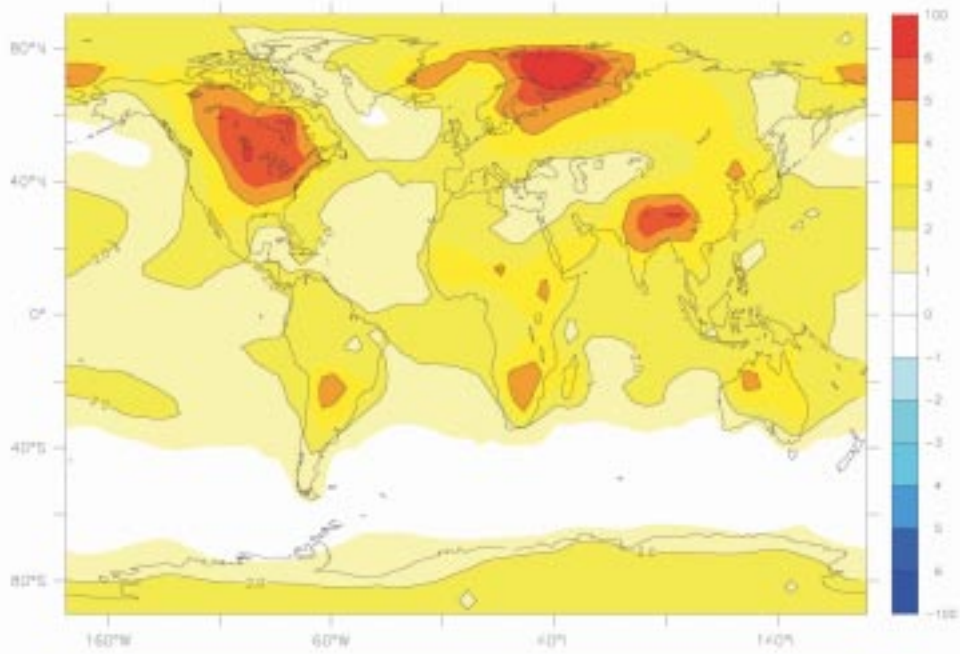


(a)

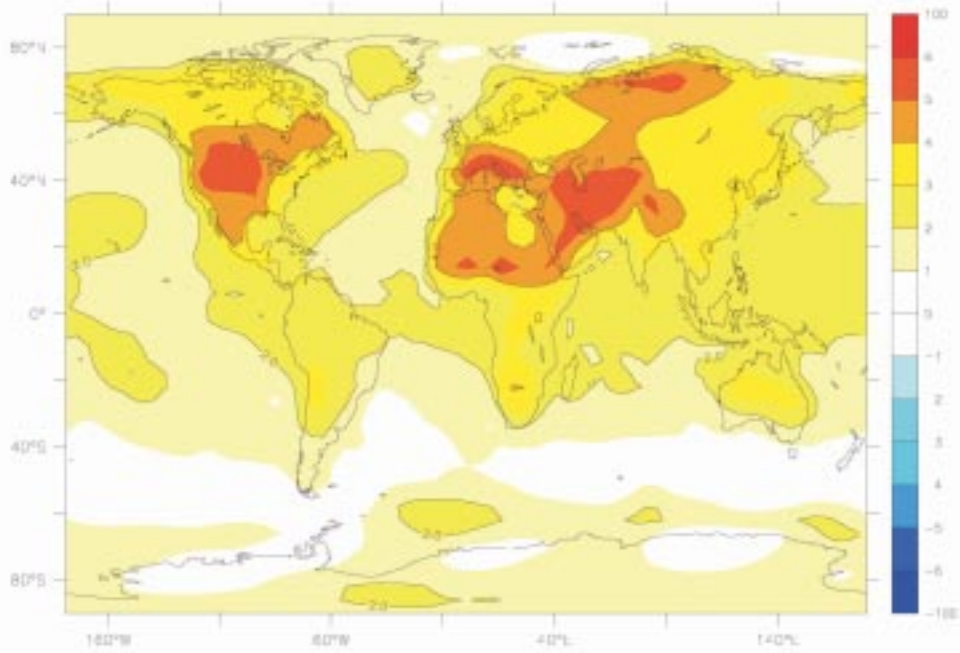


(b)

Figure 19: (a) The orography in the Northern Hemisphere in the control. (b) The orography in simulation "F" at 178kyrAP. All units are metres.

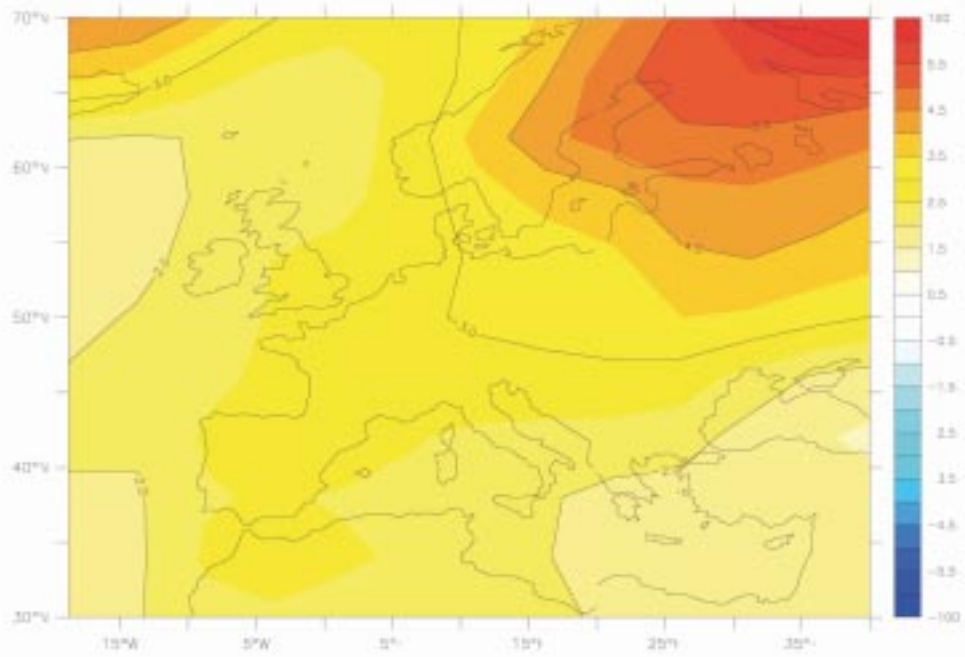


(a)

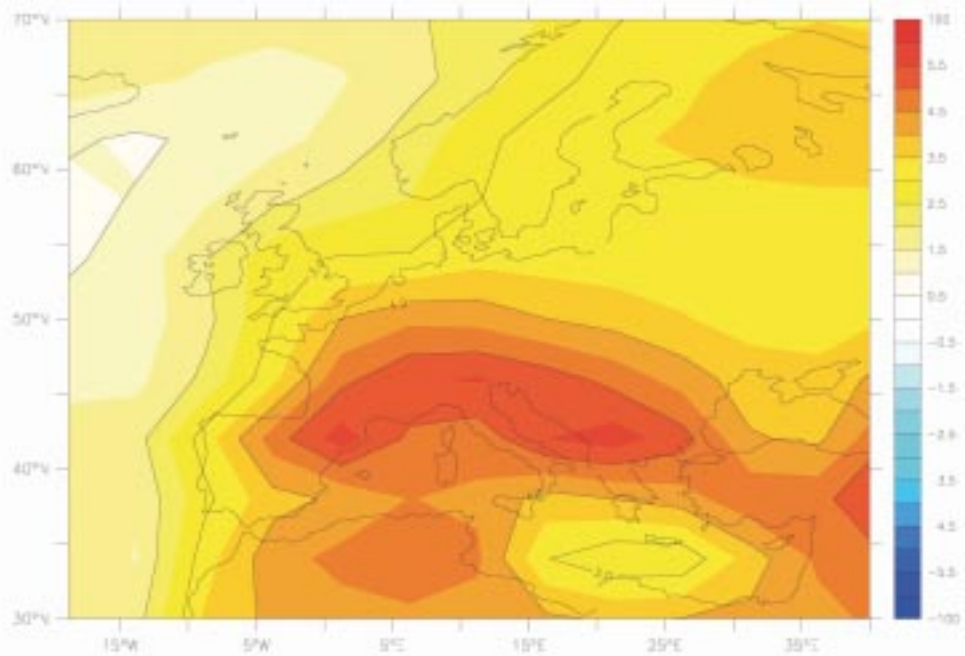


(b)

Figure 20: All fields are anomalies of experiment "A" (CO_2 increased to 1100ppmv from 345ppmv) minus control. (a) 2m temperature in DJF, and in (b) JJA. (c) 2m temperature over Europe in DJF, and in (d) JJA. (e) Precipitation over Europe in DJF and in (f) JJA. Temperatures are in $^{\circ}\text{C}$ and precipitation in mmday^{-1} .



(c)



(d)

Figure 20: Caption at figure 20(a)

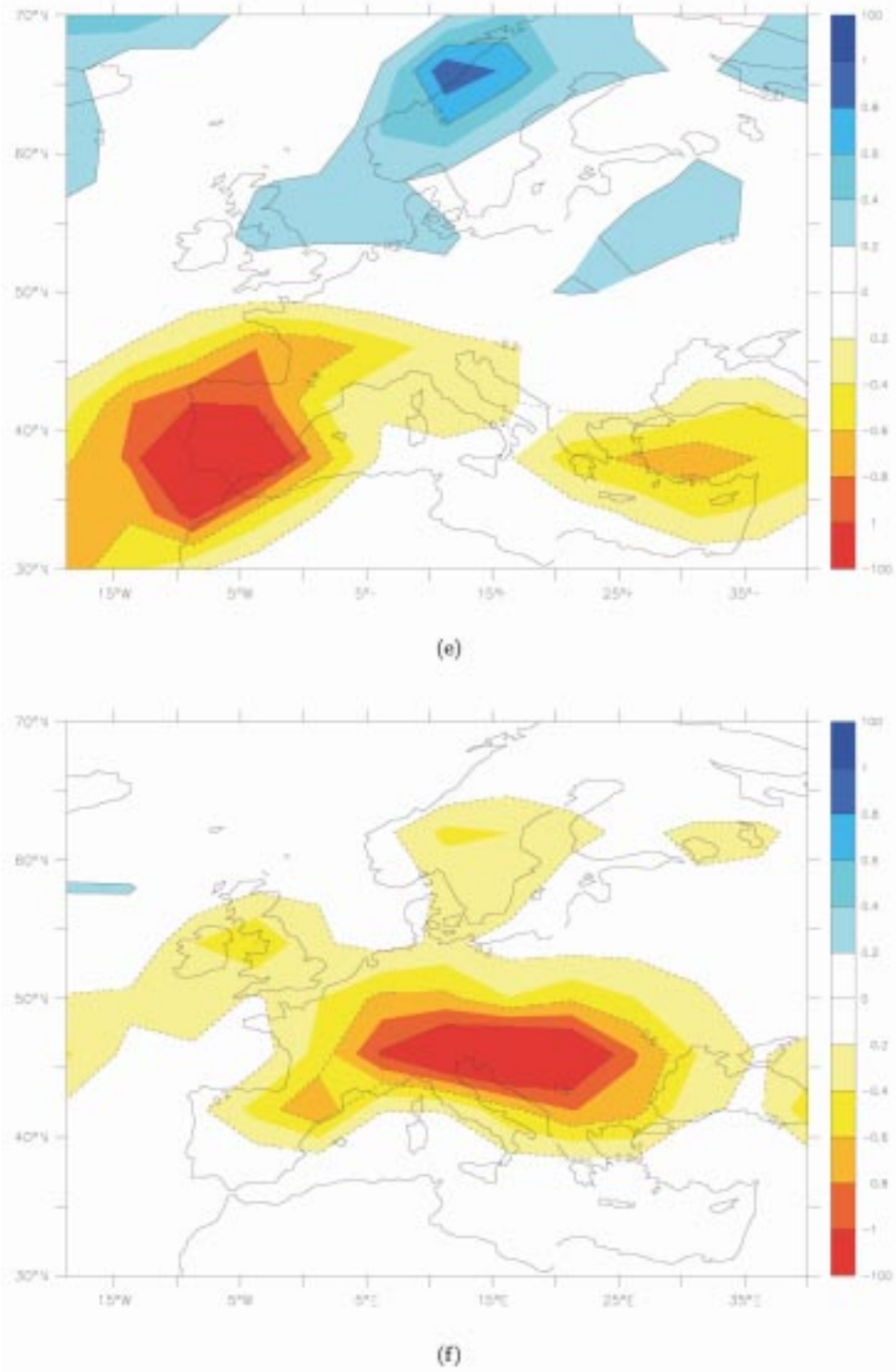
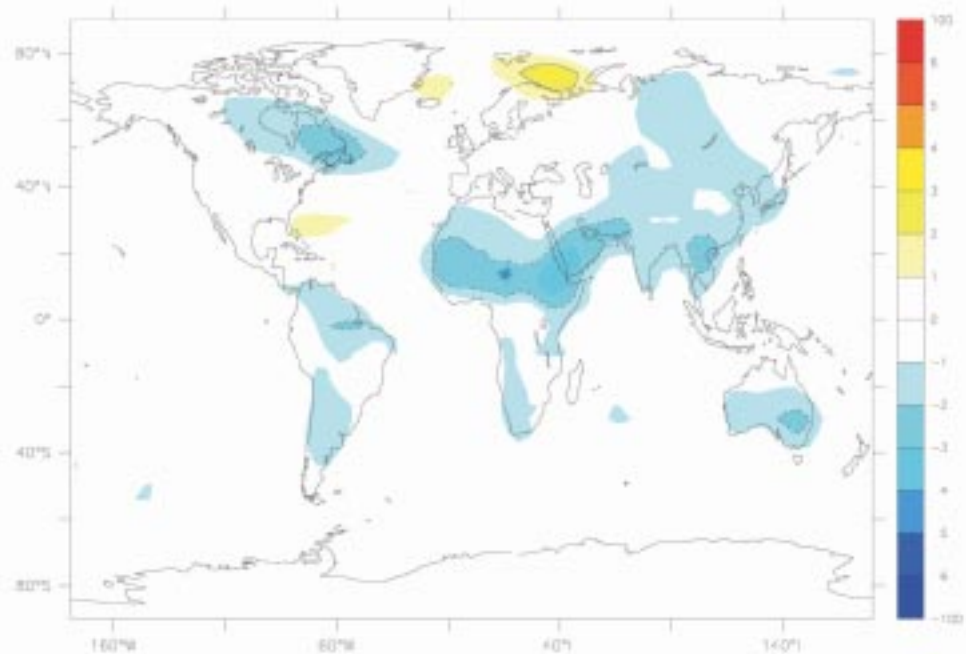
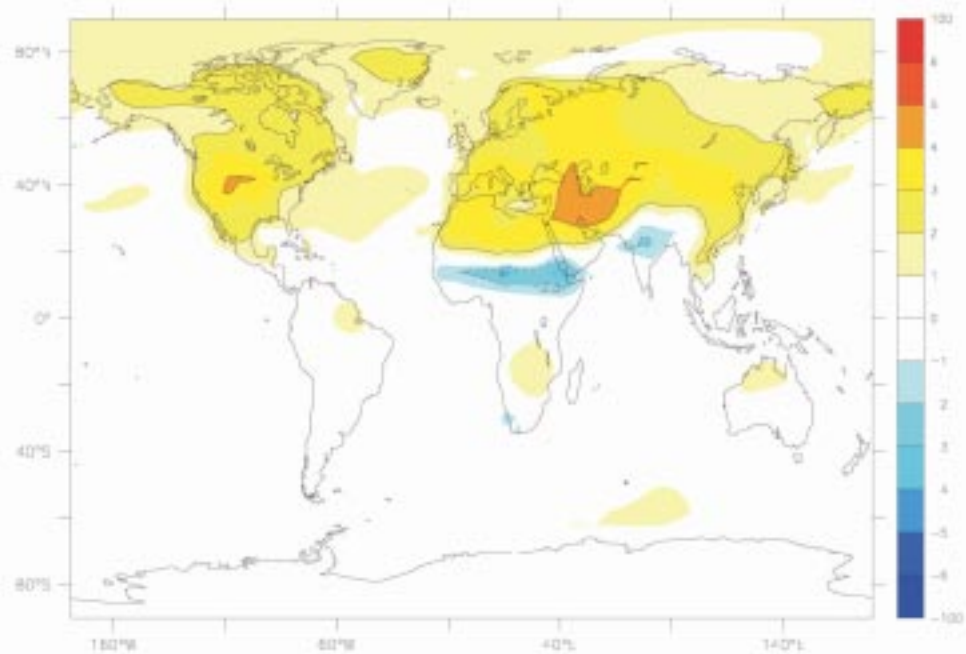


Figure 20: Caption at figure 20(a)

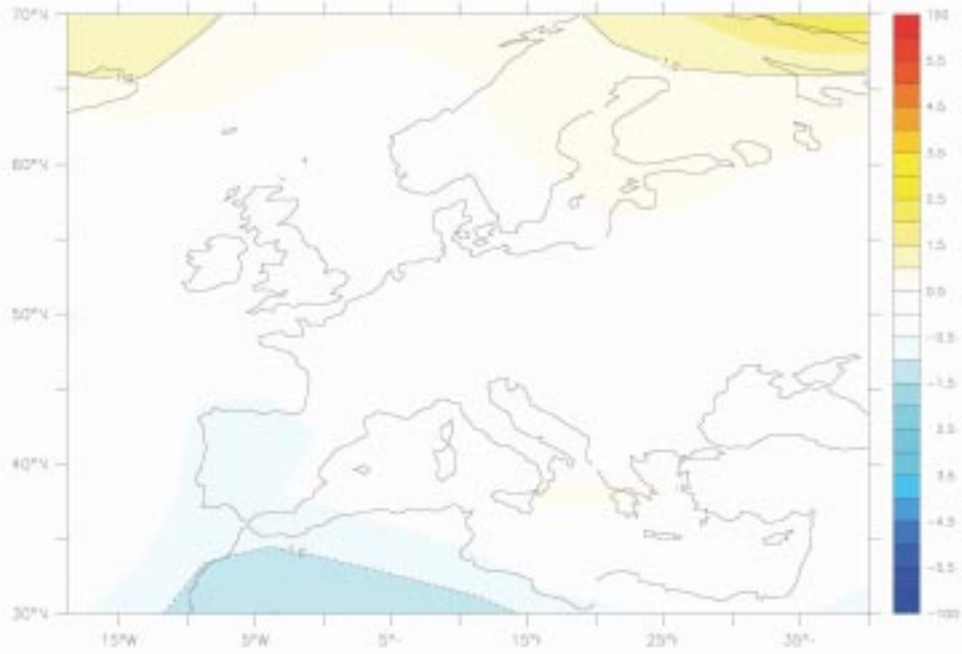


(a)

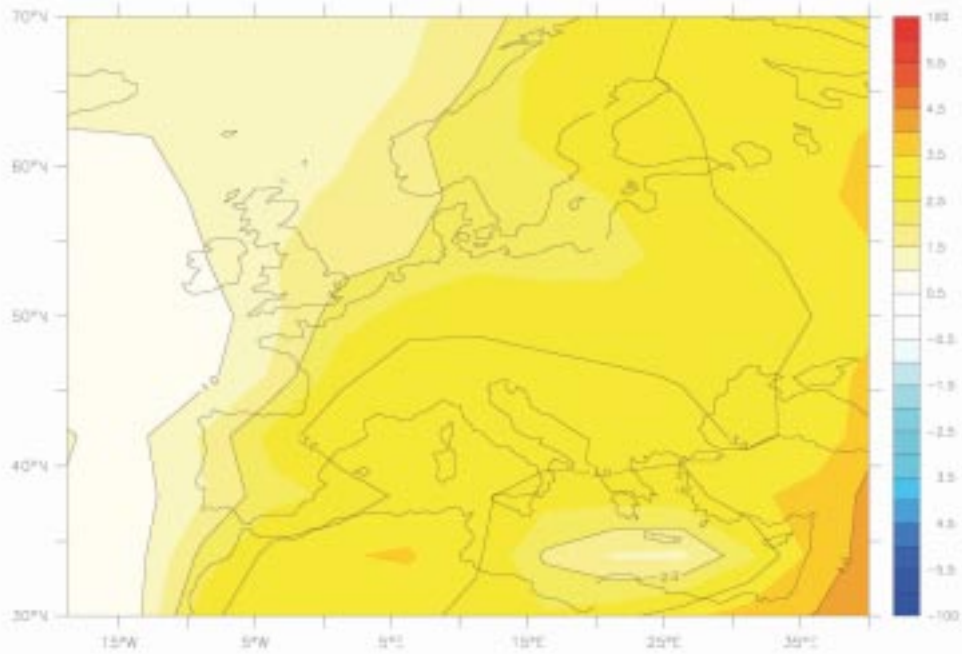


(b)

Figure 21: All fields are anomalies of experiment “E” (67kyr orbit) minus control. (a) 2m temperature in DJF, and in (b) JJA. (c) 2m temperature over Europe in DJF, and in (d) JJA. (e) Precipitation over Europe in DJF and in (f) JJA. Temperatures are in °C and precipitation in mmday^{-1} .

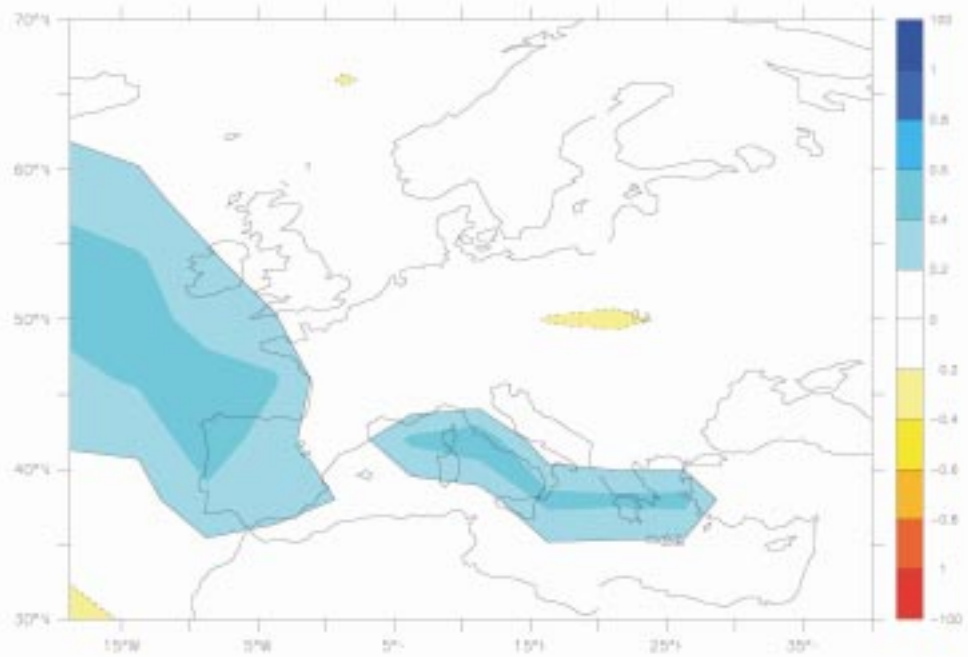


(c)

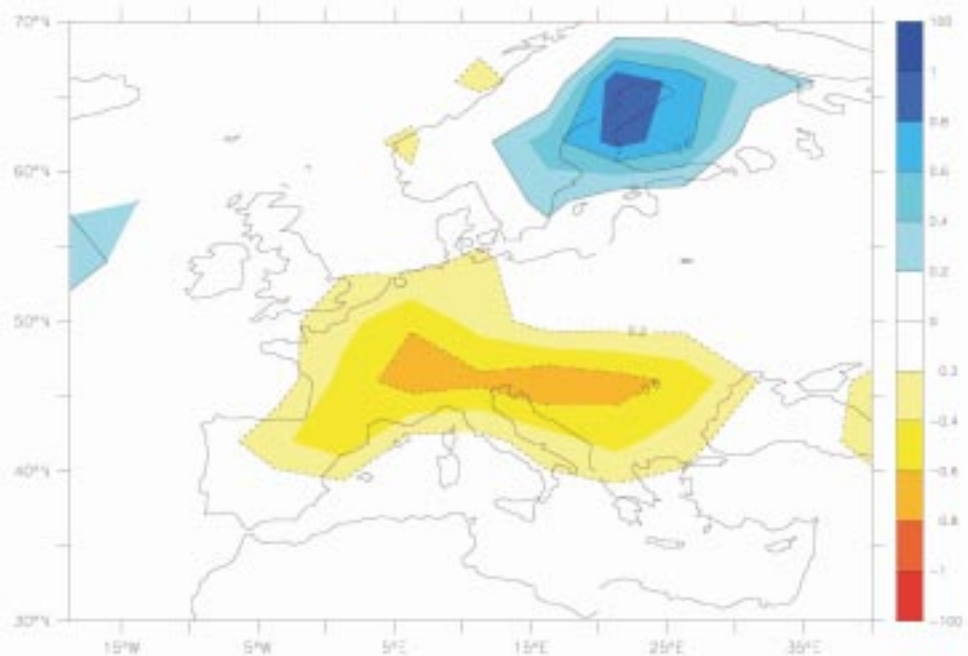


(d)

Figure 21: Caption at figure 21(a)



(e)



(f)

Figure 21: Caption at figure 21(a)

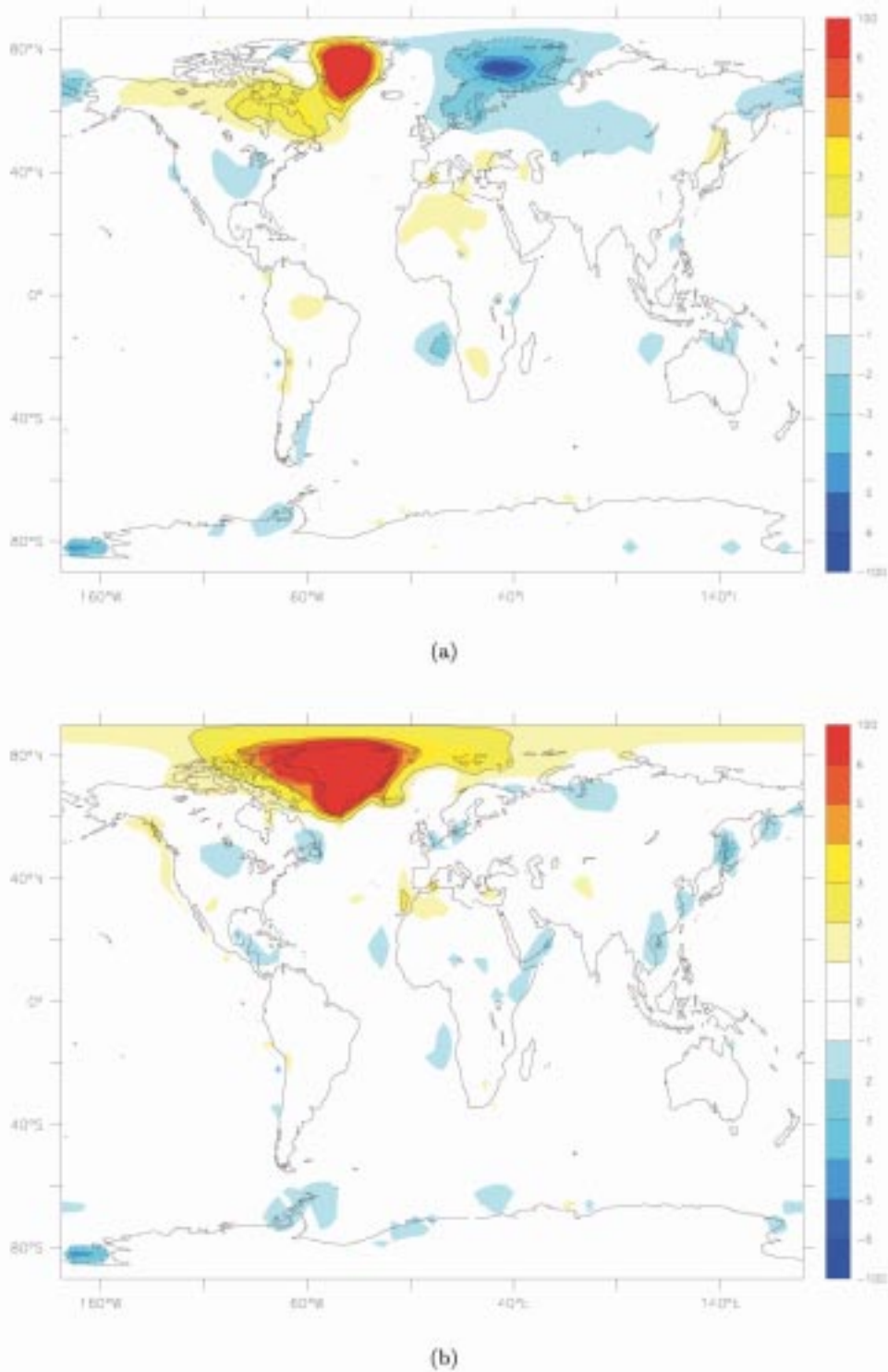
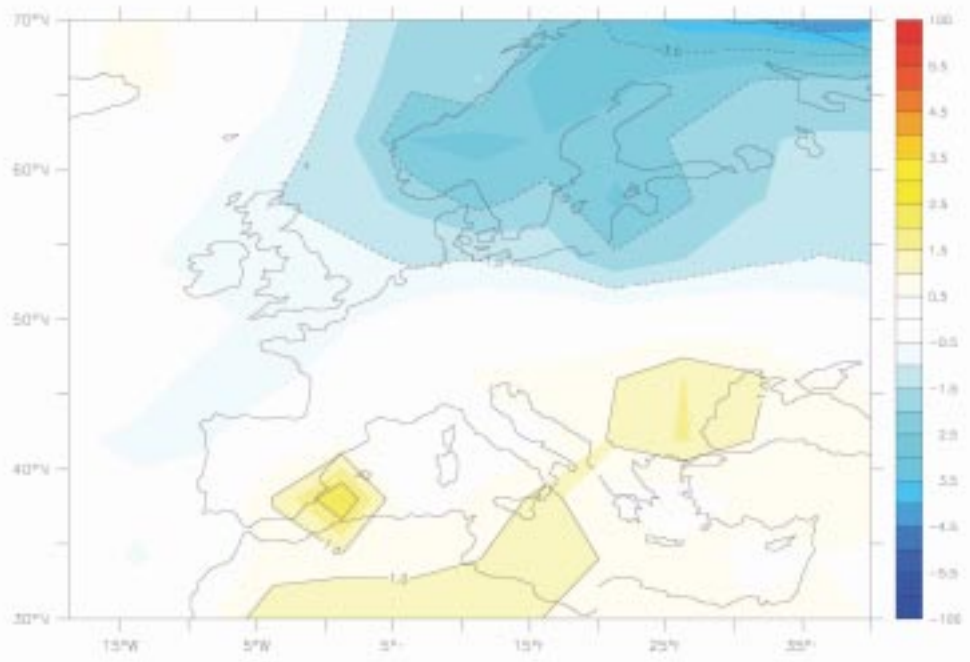
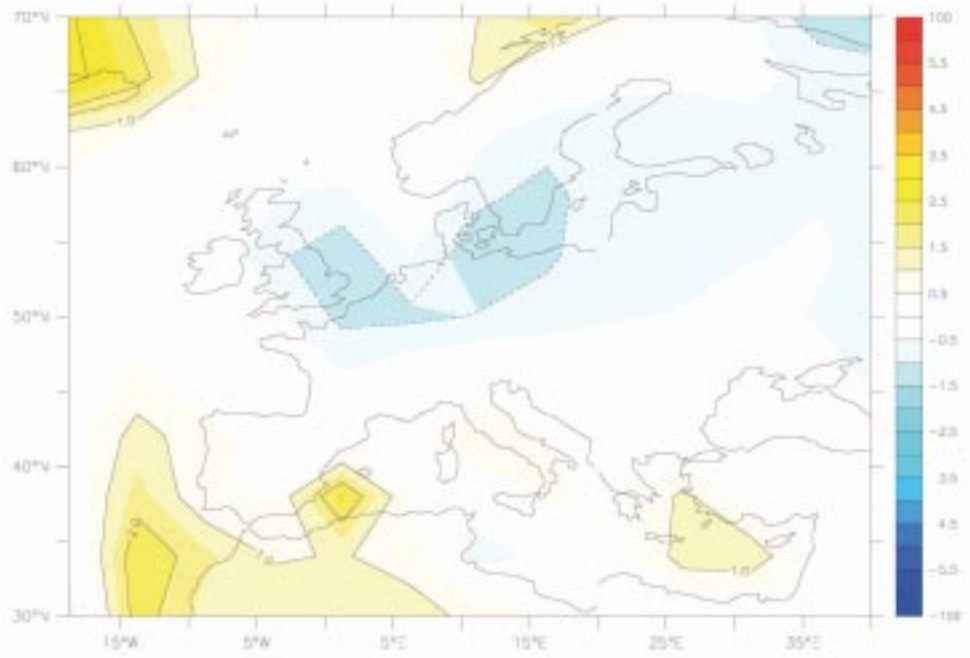


Figure 22: All fields are anomalies of experiment “D” (67kyr orbit and no Greenland ice sheet) minus experiment “E” (67kyr orbit). (a) 2m temperature in DJF, and in (b) JJA. (c) 2m temperature over Europe in DJF, and in (d) JJA. (e) Precipitation over Europe in DJF and in (f) JJA. Temperatures are in °C and precipitation in mmday^{-1} .



(c)



(d)

Figure 22: Caption at figure 22(a)

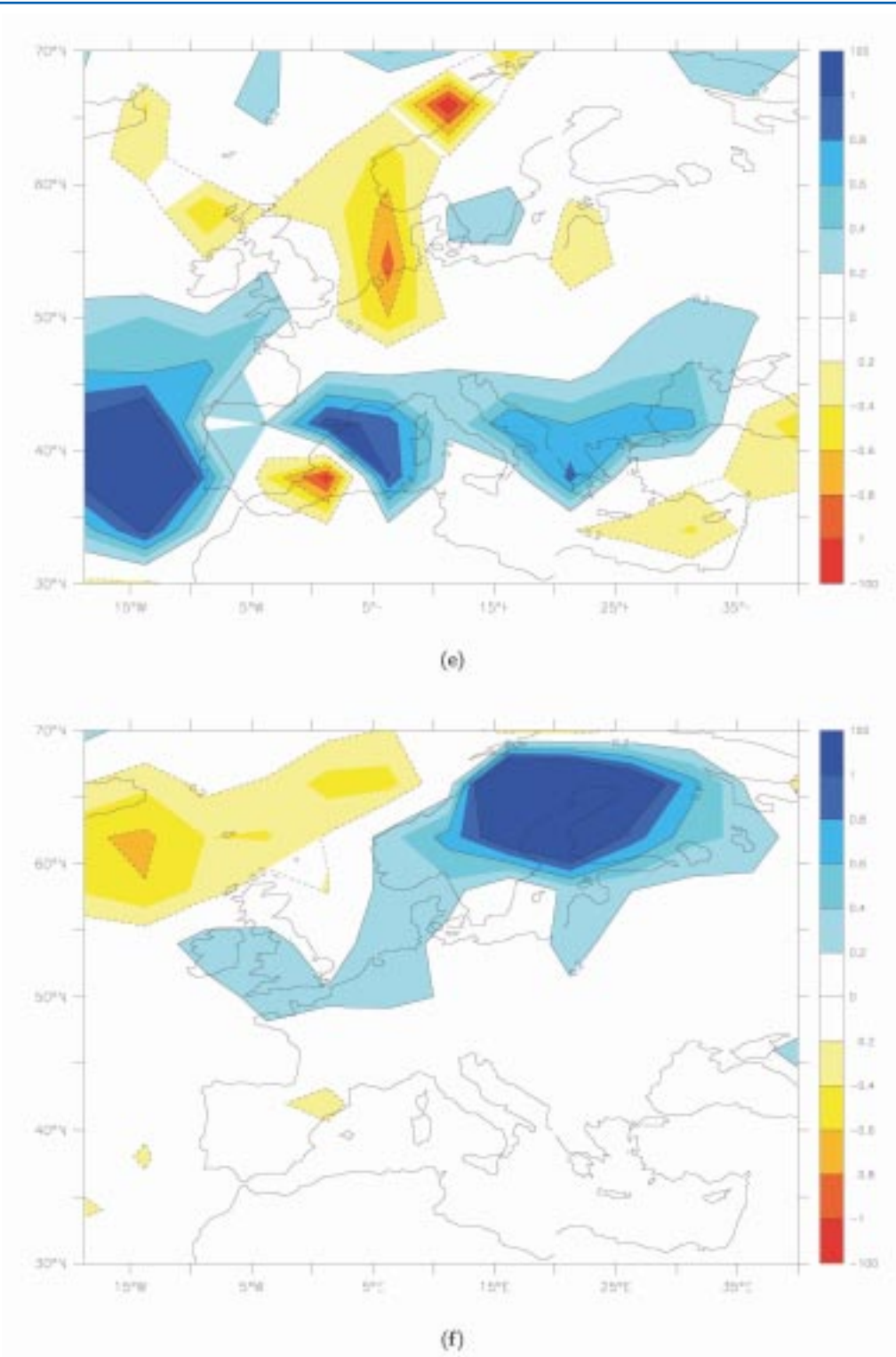
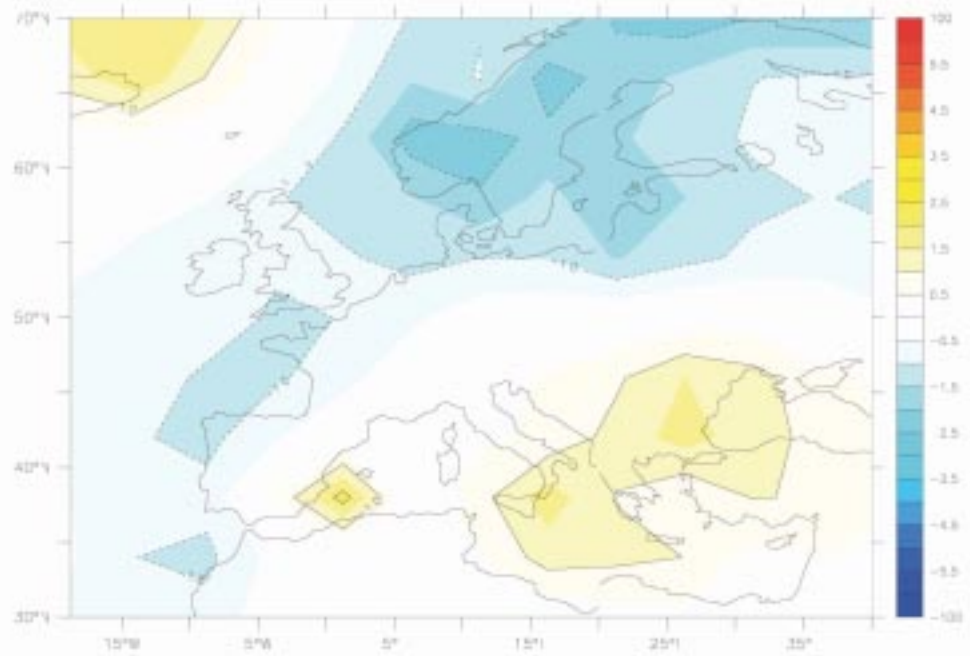
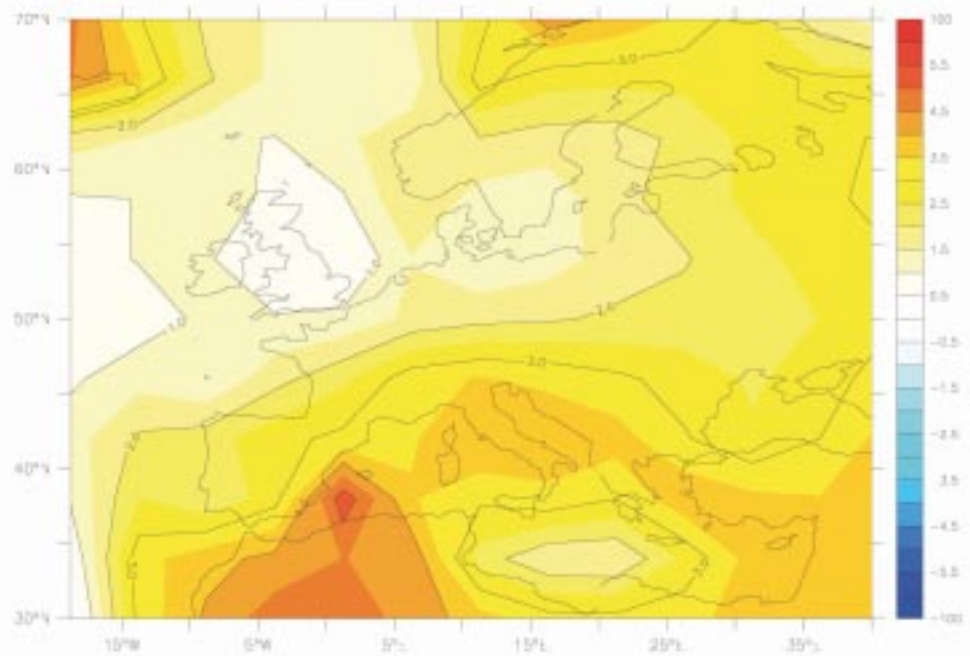


Figure 22: Caption at figure 22(a)

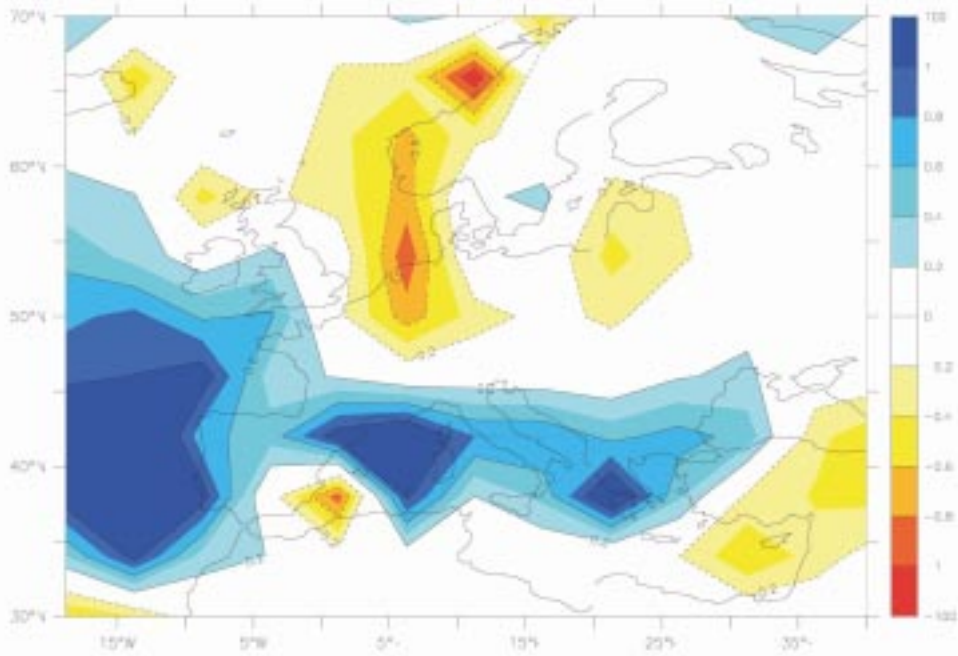


(a)

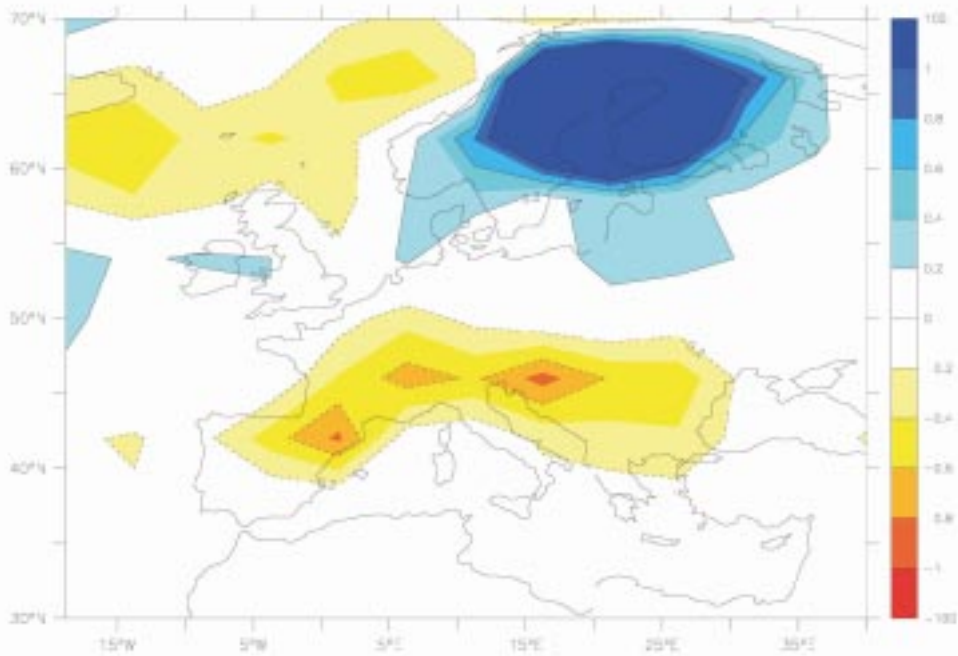


(b)

Figure 23: All fields are anomalies of experiment “D” (67kyr orbit and no Greenland ice sheet) minus experiment “Baseline”. (a) 2m temperature over Europe in DJF, and in (b) JJA. (c) Precipitation over Europe in DJF and in (d) JJA. Temperatures are in °C and precipitation in mmday^{-1} .

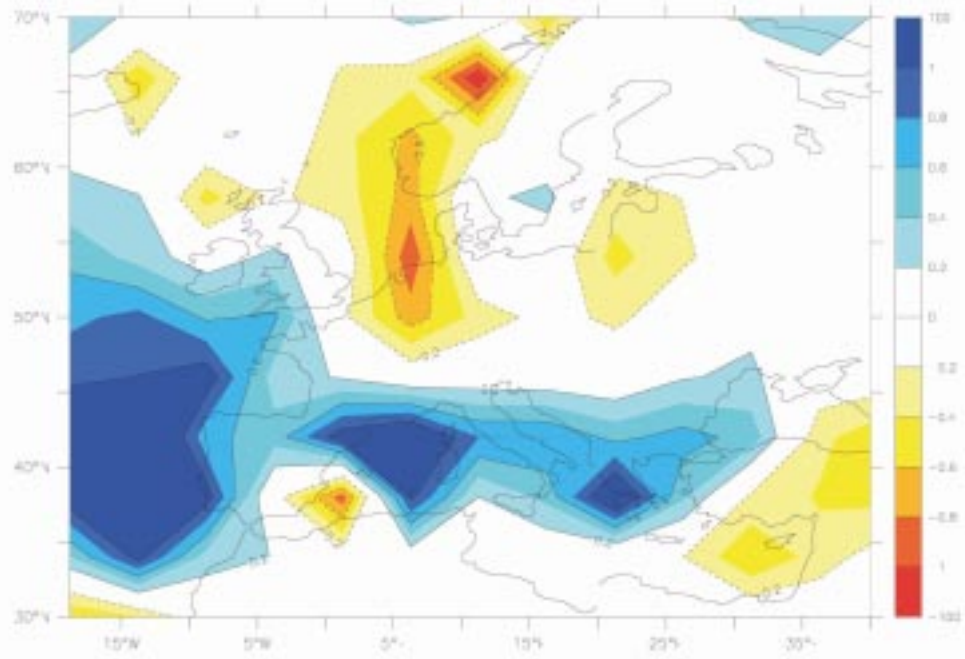


(c)

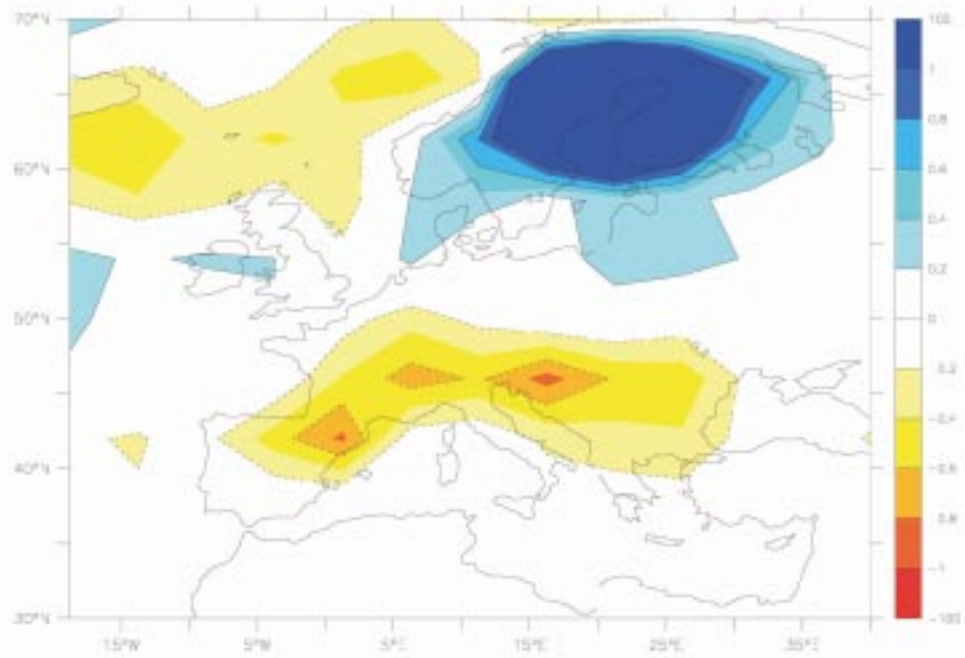


(d)

Figure 23: Caption at figure 23(a)



(c)



(d)

Figure 23: Caption at figure 23(a)

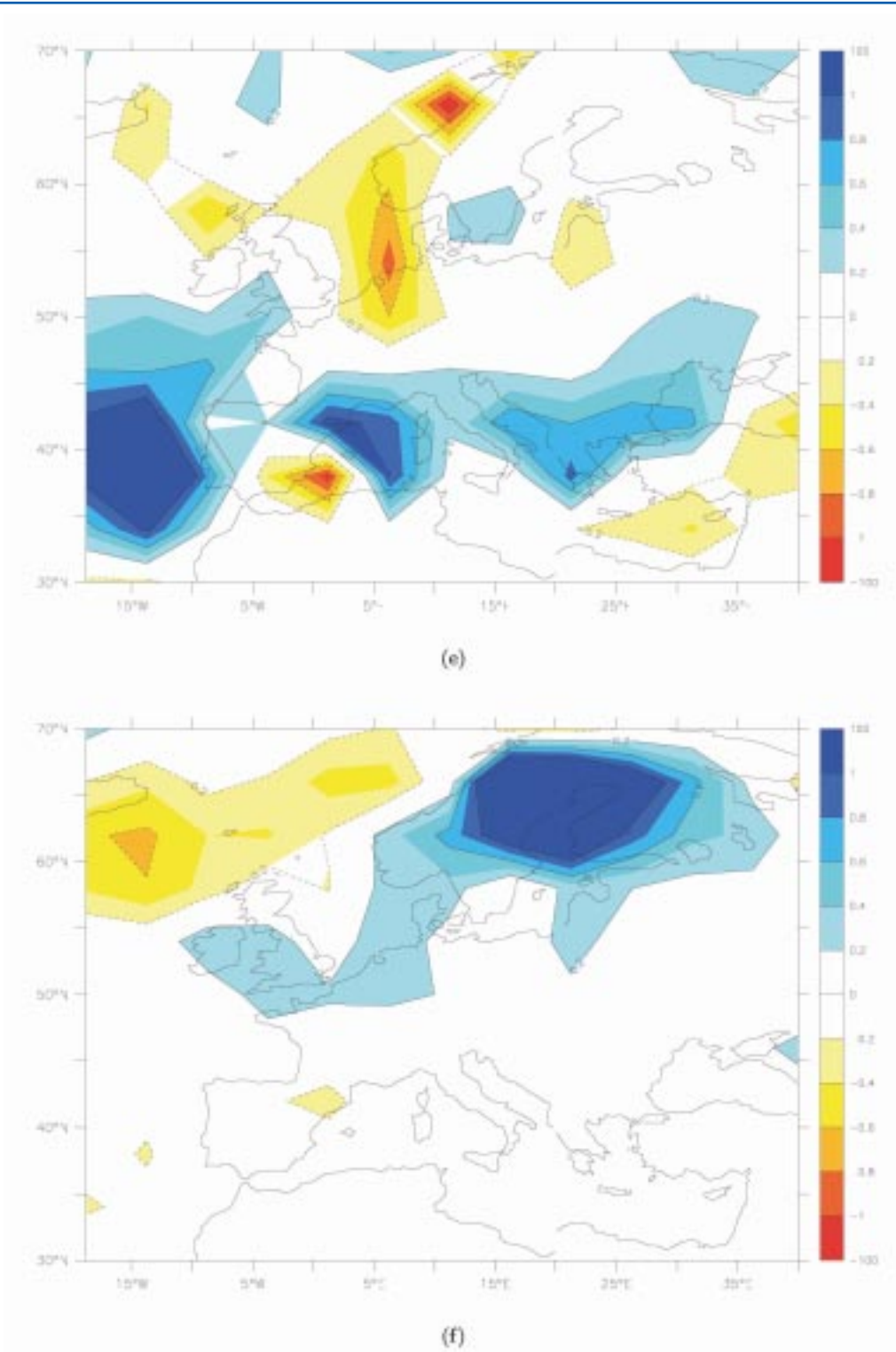
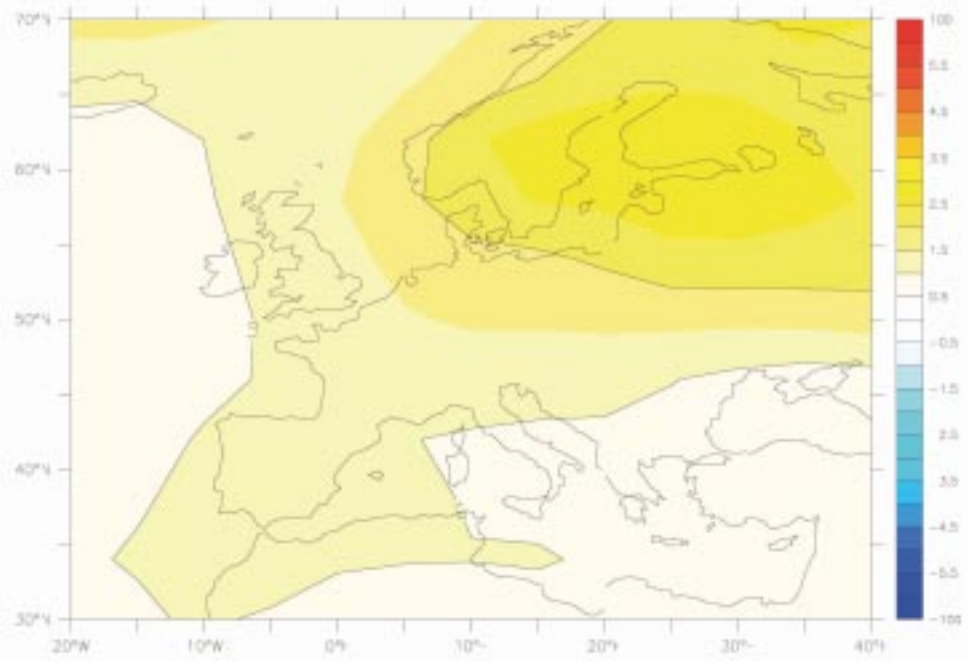
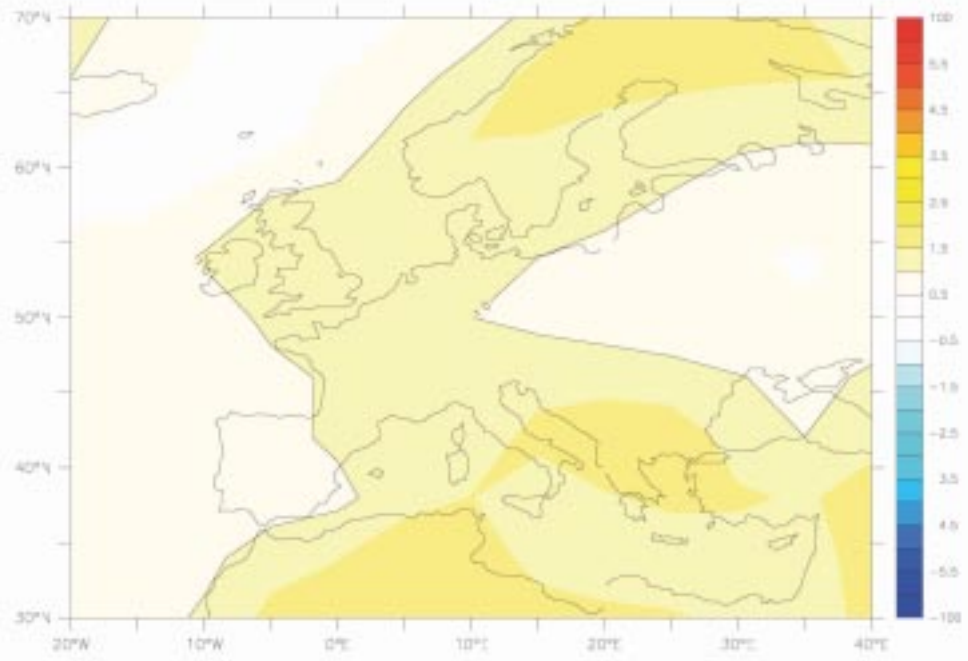


Figure 24: All fields are anomalies of experiment “C” (67kyr orbit, no Greenland ice sheet and CO₂=550ppmv) minus experiment “D” (67kyr orbit and no Greenland ice sheet). (a) 2m temperature in DJF, and in (b) JJA. (c) 2m temperature over Europe in DJF, and in (d) JJA. (e) Precipitation over Europe in DJF and in (f) JJA. Temperatures are in °C and precipitation in mmday⁻¹.



(c)



(d)

Figure 24: Caption at figure 24(a)

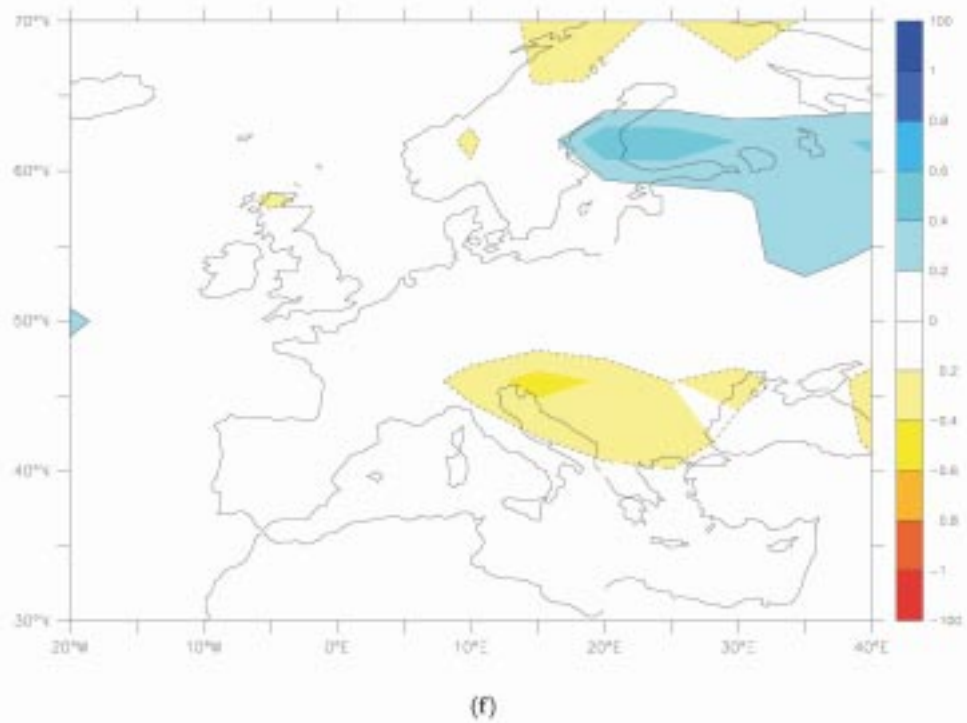
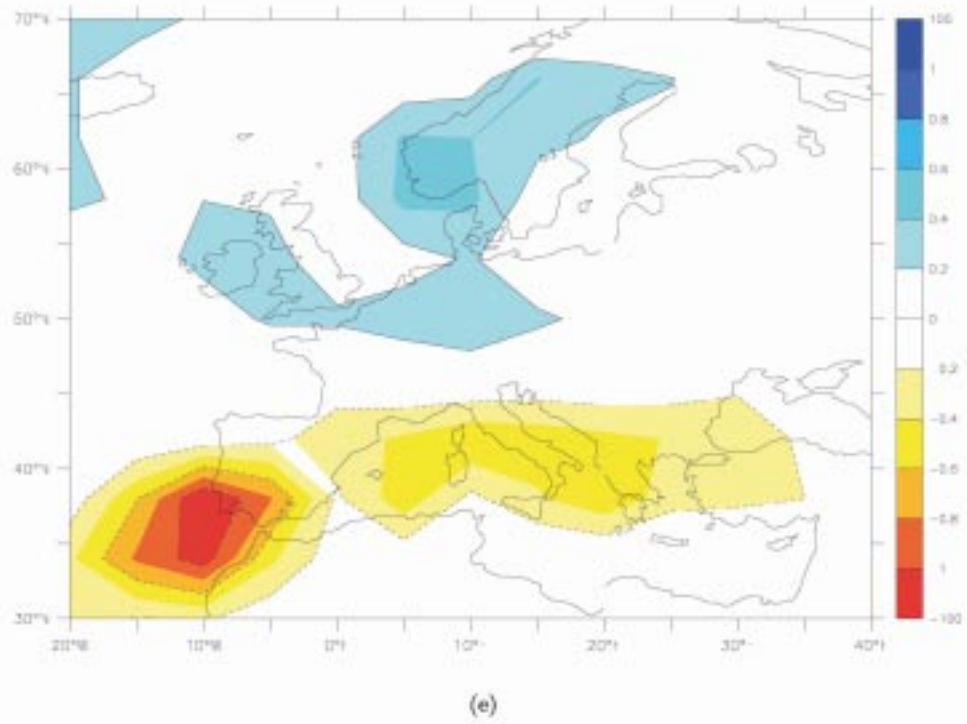
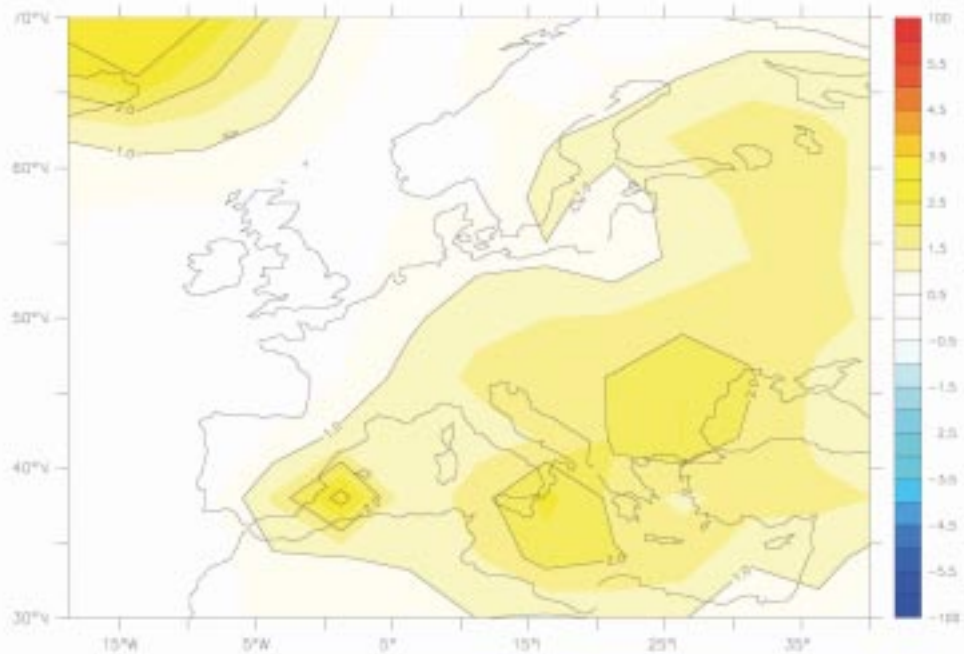
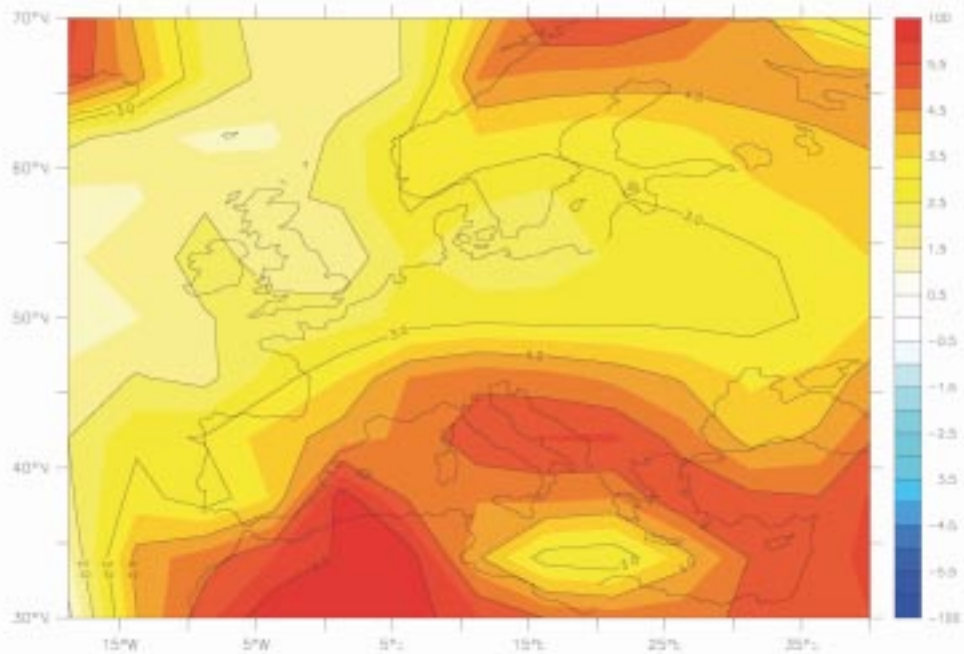


Figure 24: Caption at figure 24(a)

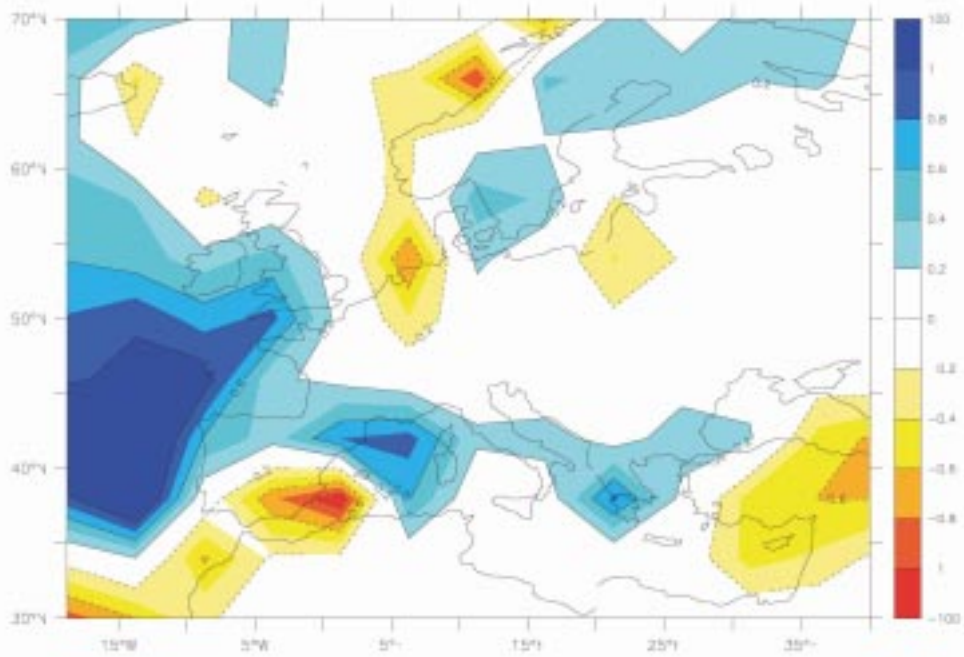


(a)

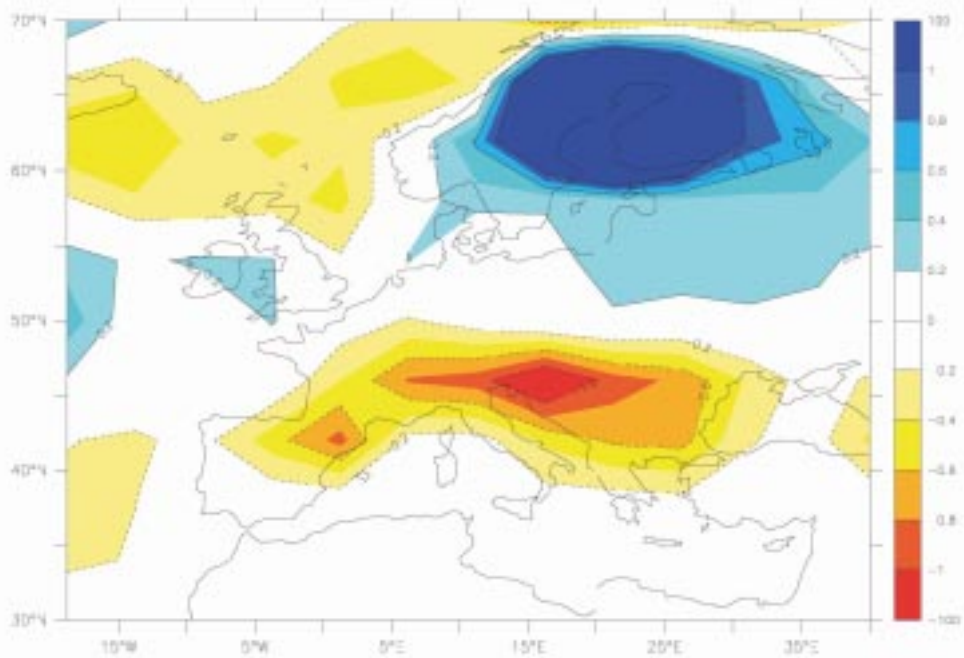


(b)

Figure 25: All fields are anomalies of experiment "C" (67kyr orbit, no Greenland ice sheet and $CO_2=550ppmv$) minus experiment "Baseline". (a) 2m temperature over Europe in DJF, and in (b) JJA. (c) Precipitation over Europe in DJF and in (d) JJA. Temperatures are in $^{\circ}C$ and precipitation in $mmday^{-1}$.

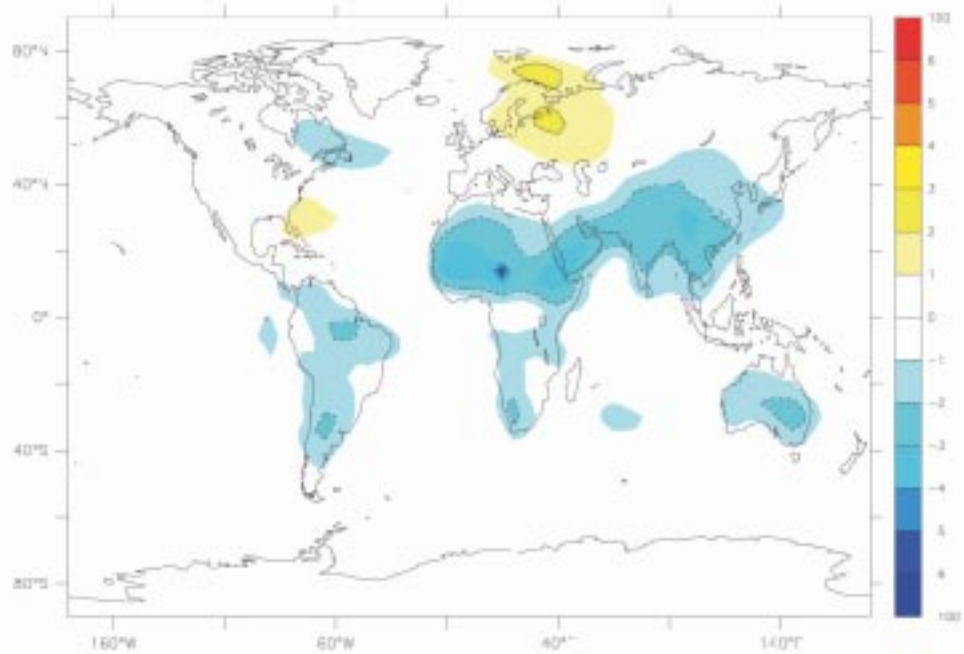


(c)

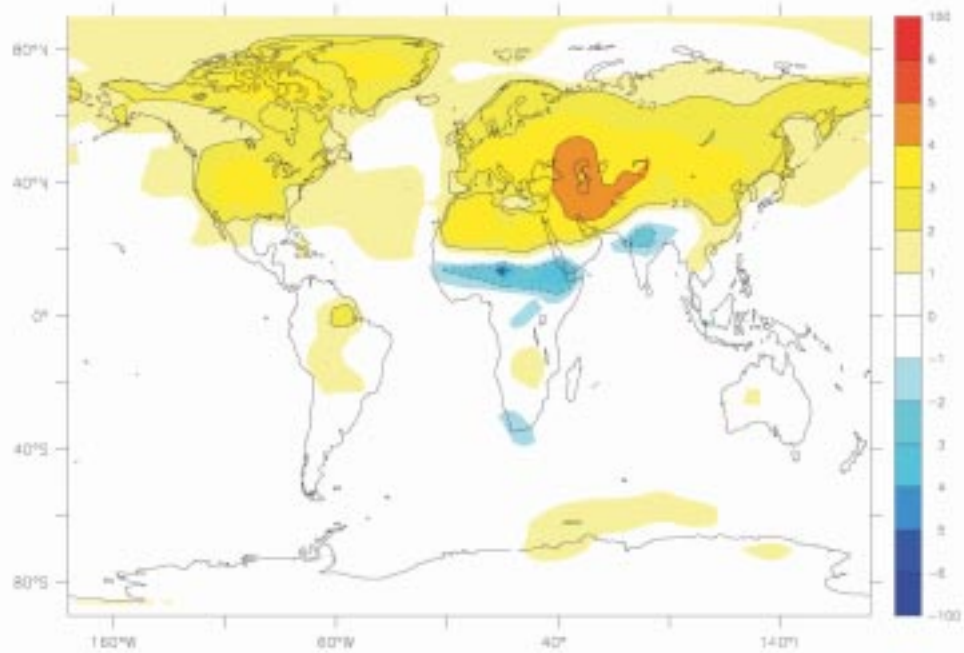


(d)

Figure 25: Caption at figure 25(a)



(a)



(b)

Figure 26: All fields are anomalies of experiment “C” (No Greenland ice sheet, $CO_2=550ppmv$ and 67kyrAP orbit) minus experiment “B” (No Greenland ice sheet and $CO_2=550ppmv$). (a) 2m temperature in DJF, and in (b) JJA. (c) 2m temperature over Europe in DJF, and in (d) JJA. (e) Precipitation over Europe in DJF and in (f) JJA. Temperatures are in $^{\circ}C$ and precipitation in $mmday^{-1}$.

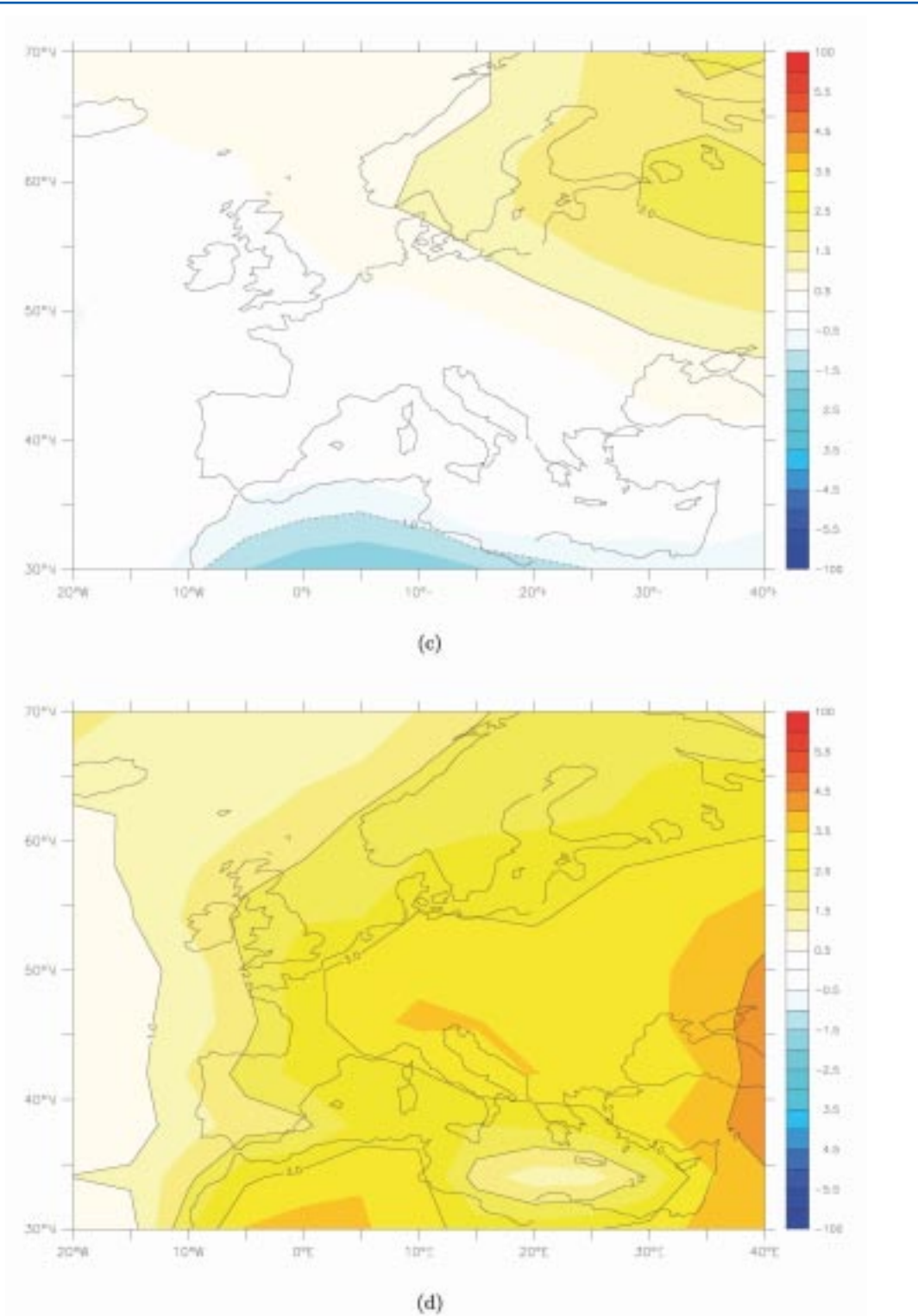
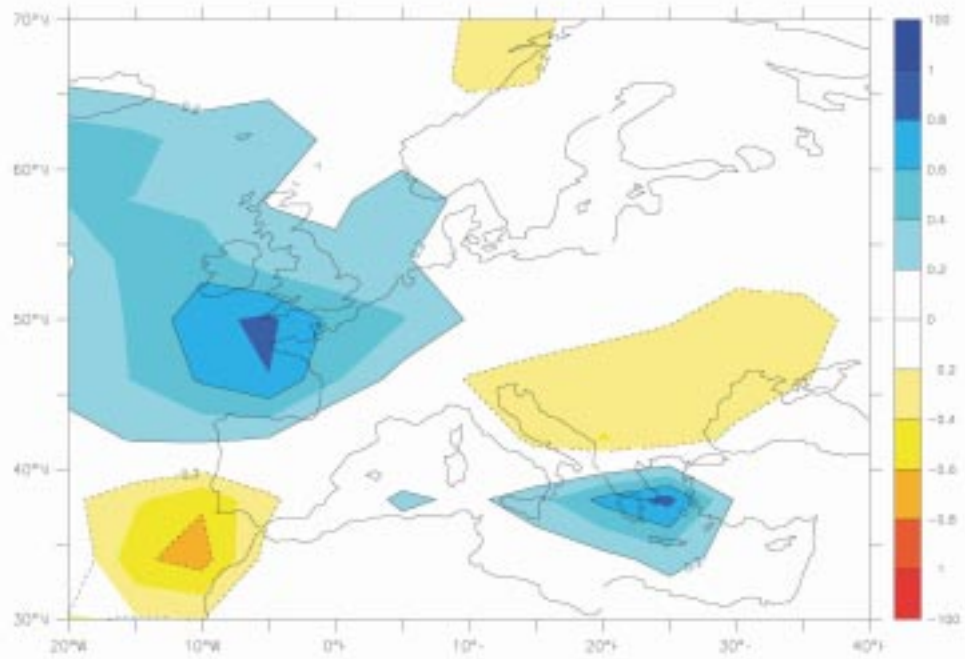
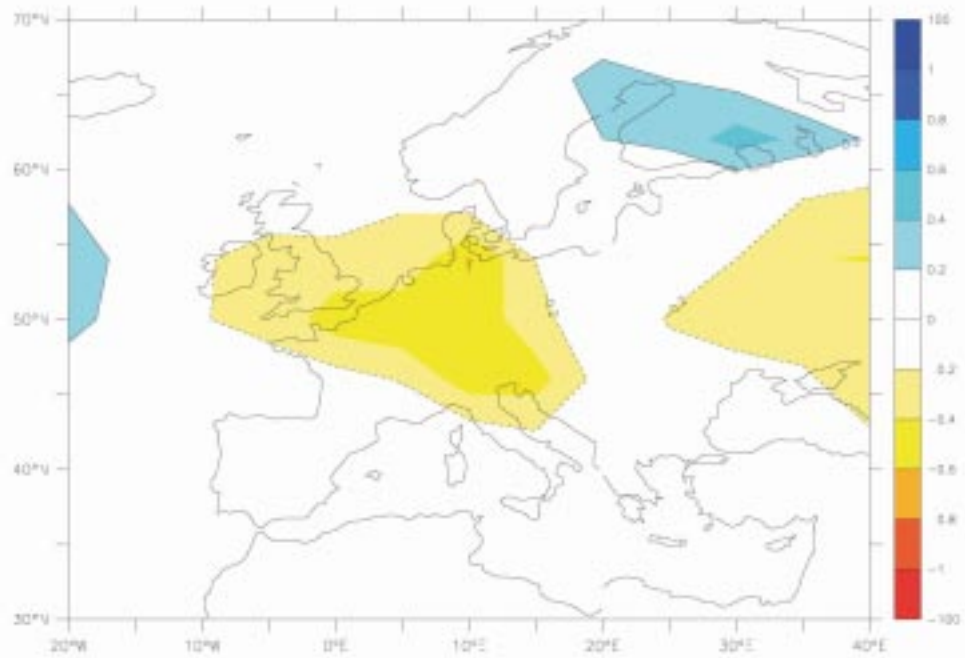


Figure 26: Caption at figure 26(a)



(e)



(f)

Figure 26: Caption at figure 26(a)

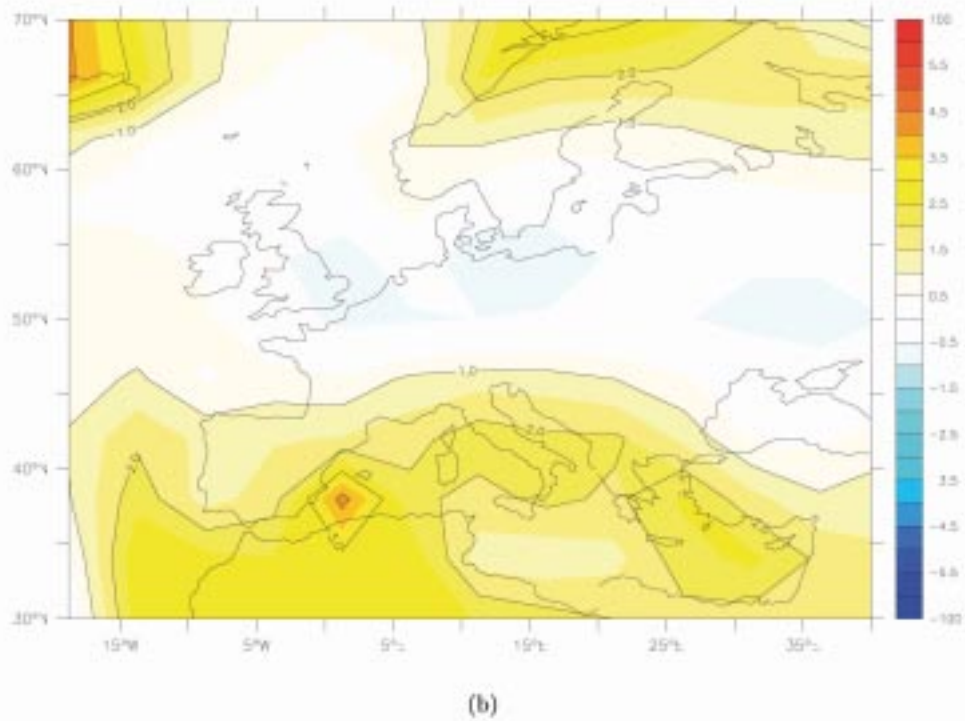
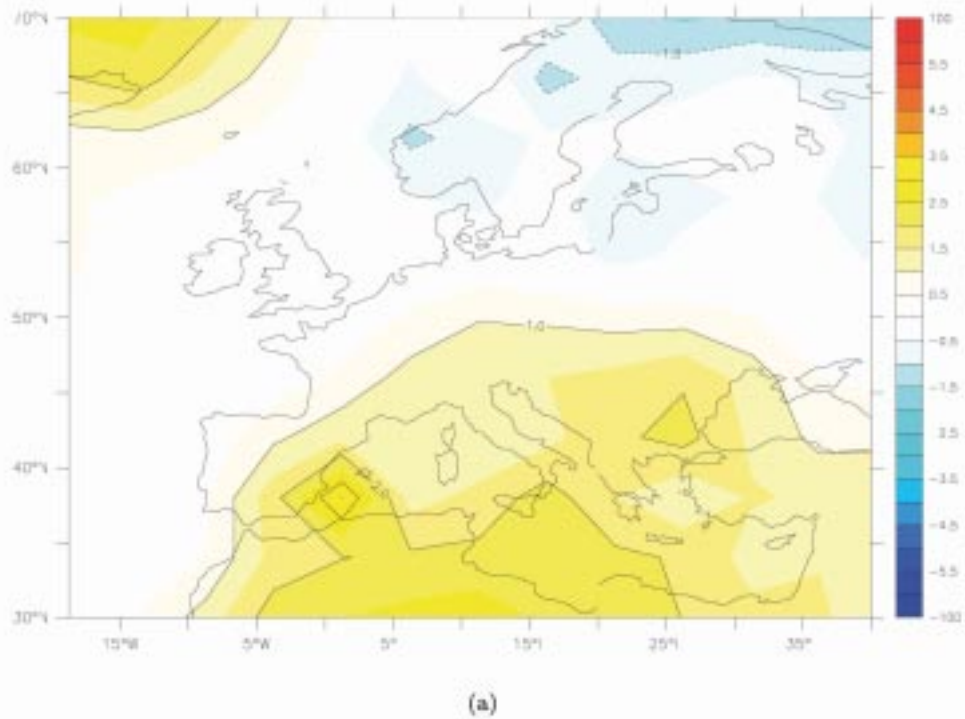
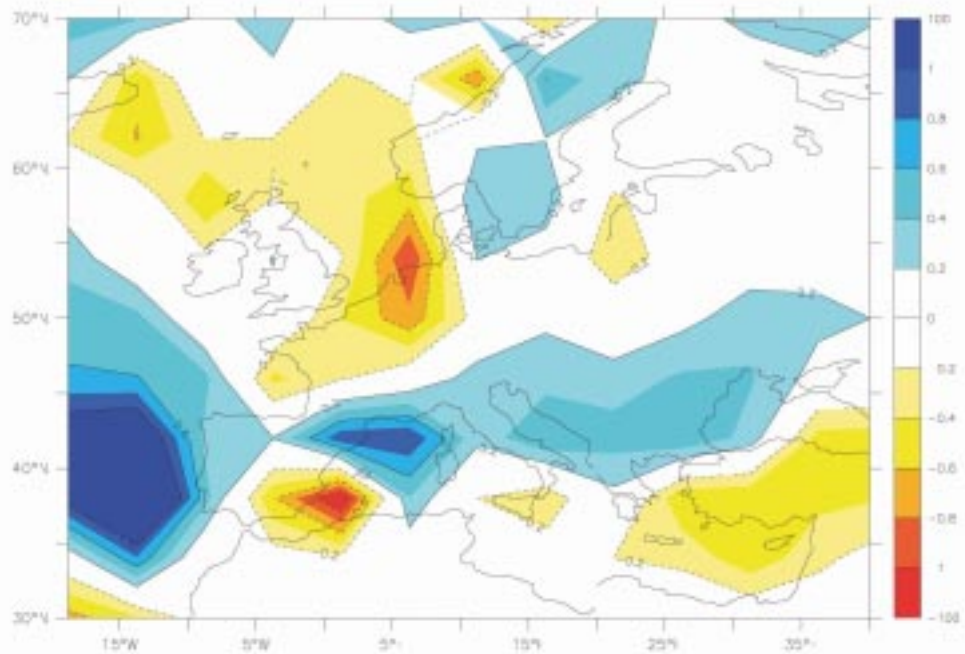
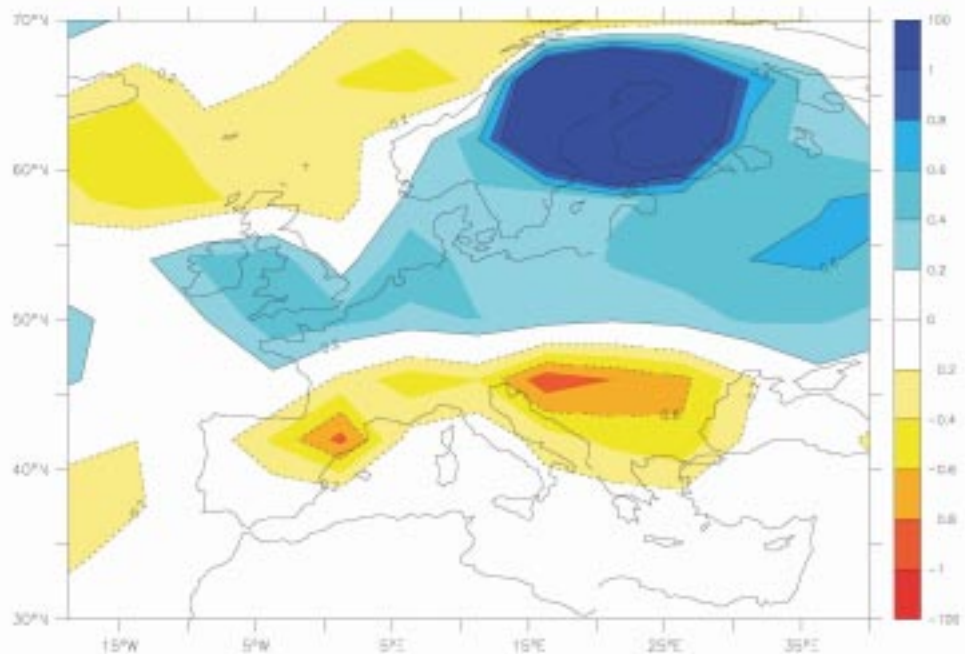


Figure 27: All fields are anomalies of experiment “B” (No Greenland ice sheet and $\text{CO}_2=550\text{ppmv}$) minus experiment “Baseline”. (a) 2m temperature over Europe in DJF, and in (b) JJA. (c) Precipitation over Europe in DJF and in (d) JJA. Temperatures are in $^{\circ}\text{C}$ and precipitation in mmday^{-1} .

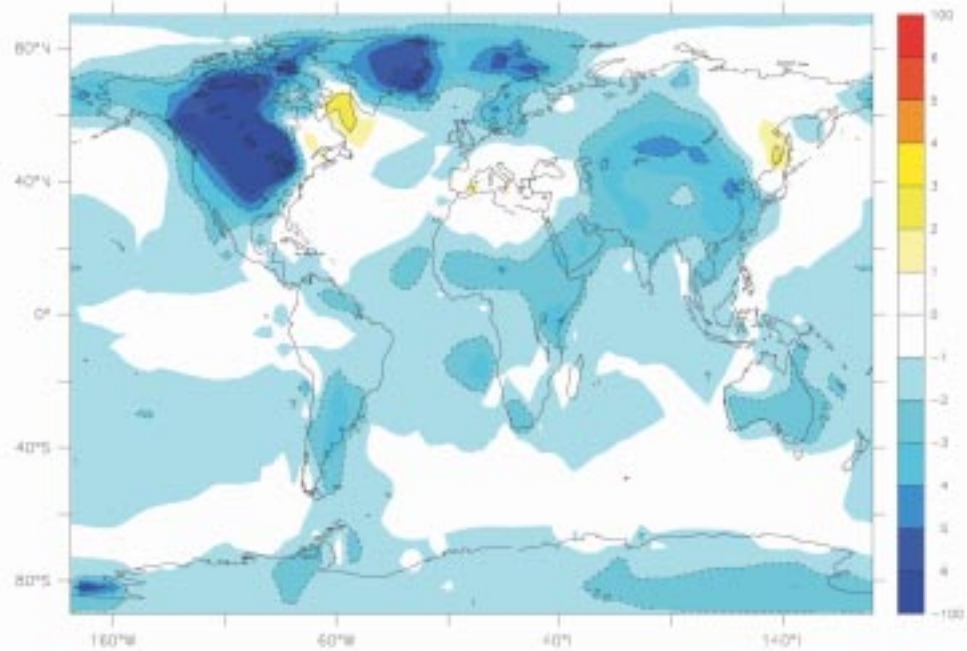


(c)

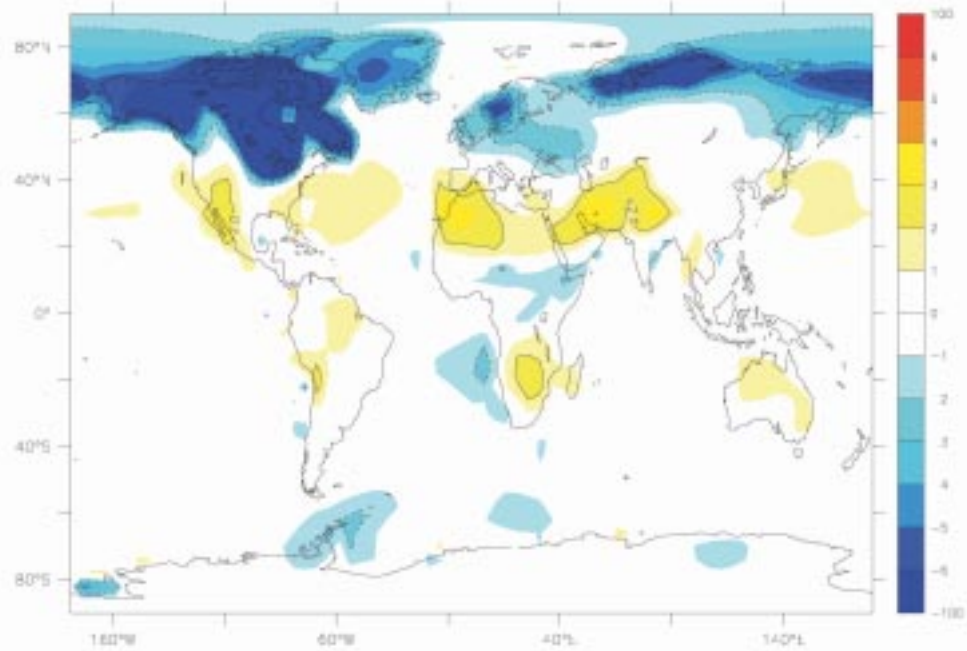


(d)

Figure 27: Caption at figure 27(a)

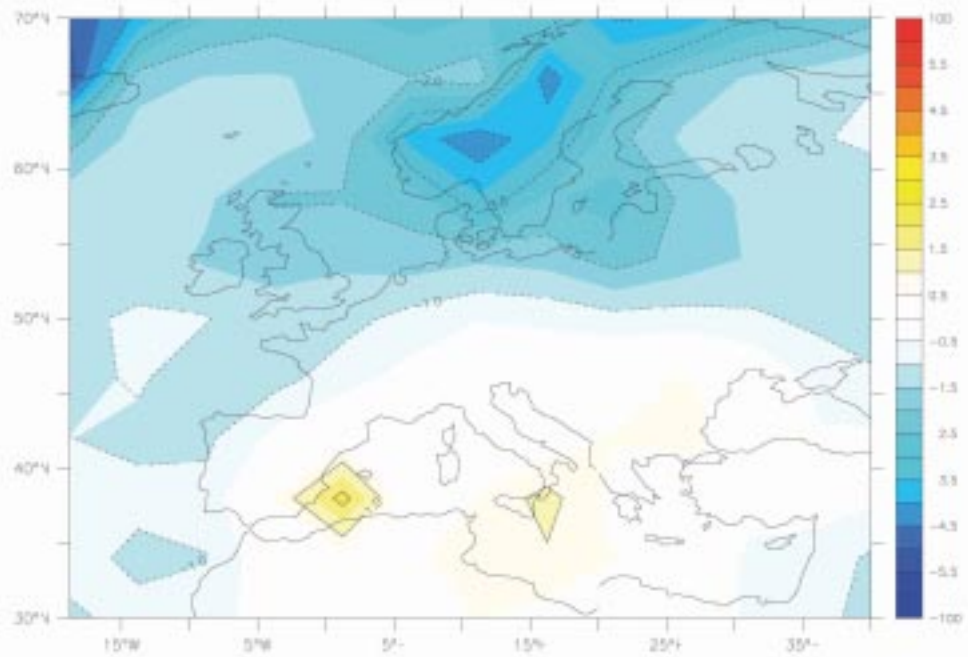


(a)

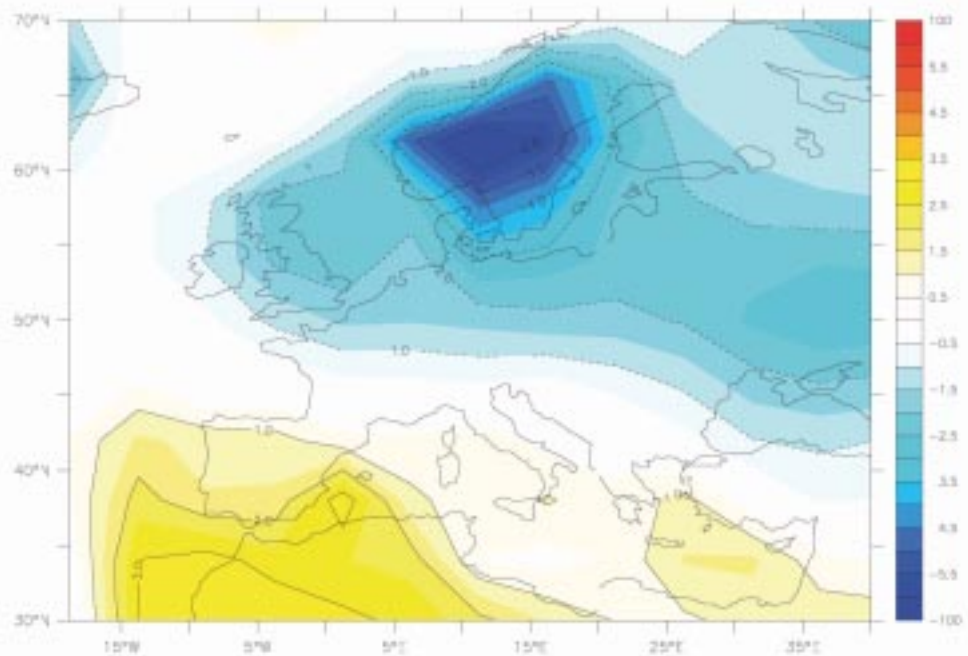


(b)

Figure 28: All fields are anomalies of experiment “F” (Increase northern hemisphere ice sheets, $CO_2=280ppmv$, and 178kyrAP orbit) minus experiment “Baseline”. (a) 2m temperature in DJF, and in (b) JJA. (c) 2m temperature over Europe in DJF, and in (d) JJA. (e) Precipitation over Europe in DJF and in (f) JJA. Temperatures are in $^{\circ}C$ and precipitation in $mmday^{-1}$.



(c)



(d)

Figure 28: Caption at figure 28(a)

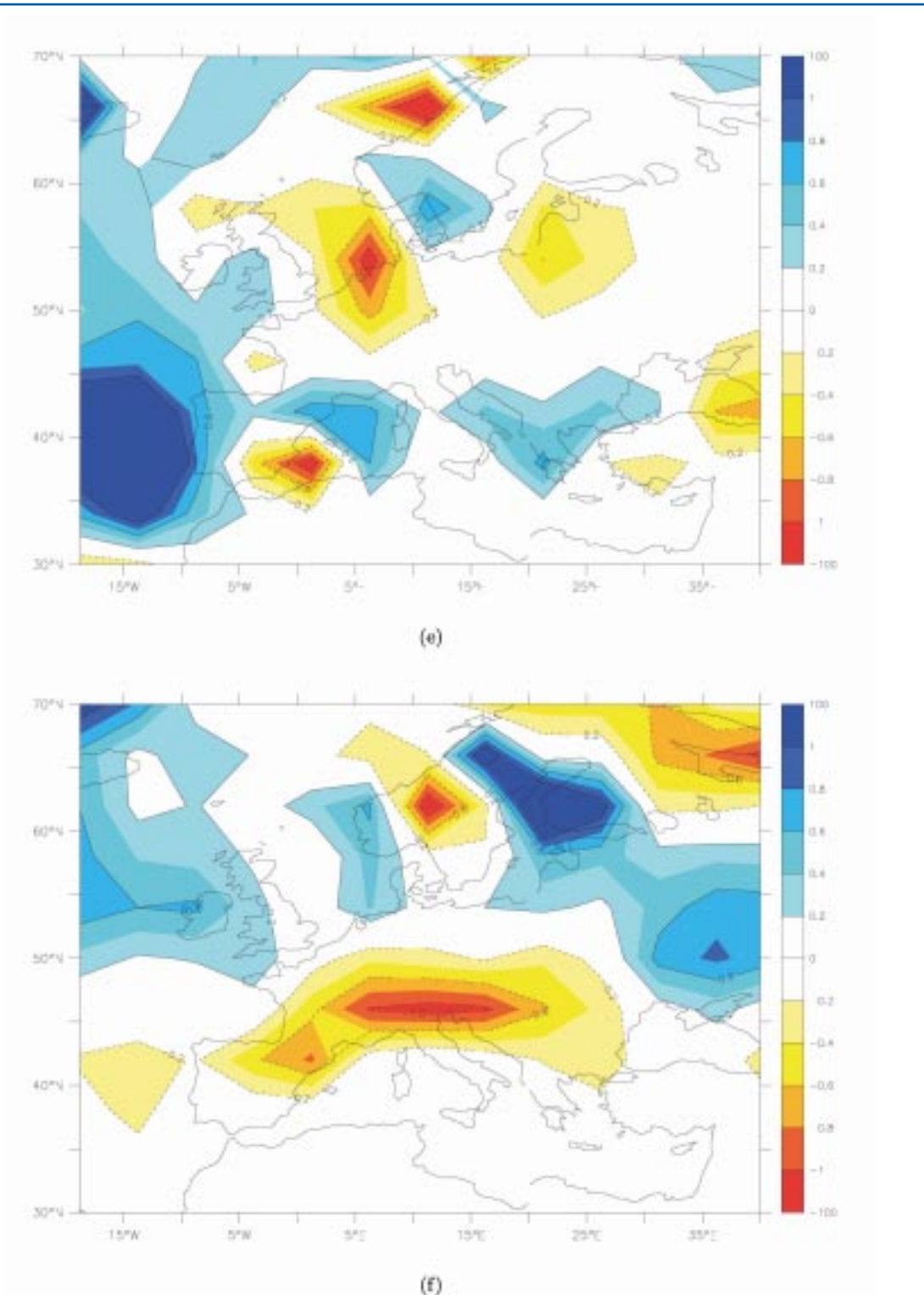


Figure 28: Caption at figure 28(a)

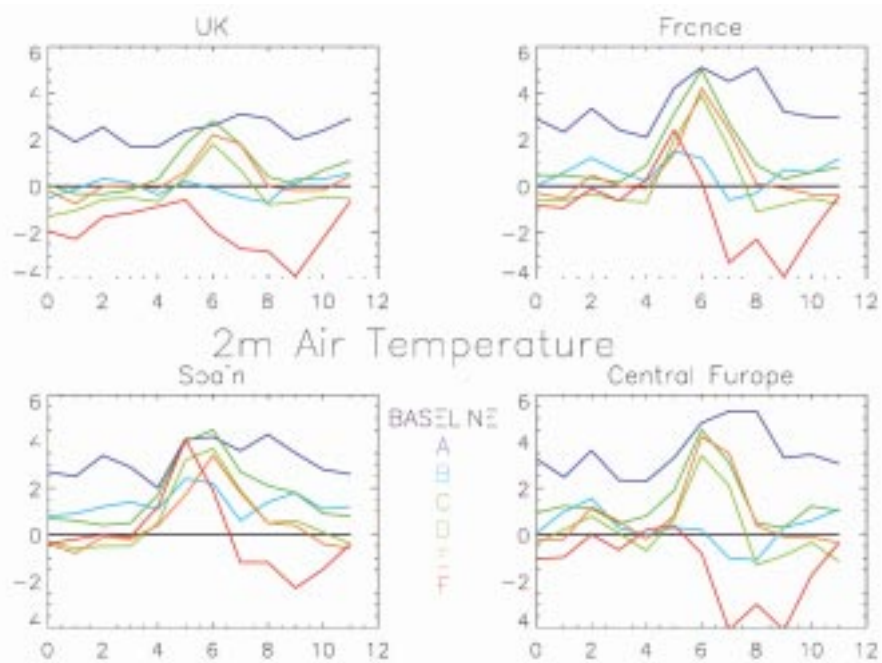


Figure 29: Monthly timeseries of 2m temperature, over the regions of the UK, France, Spain, and Central Europe, from the BIOCLIM simulations “A” to “F”. All series are anomalies from the Baseline simulation. Units are °C.

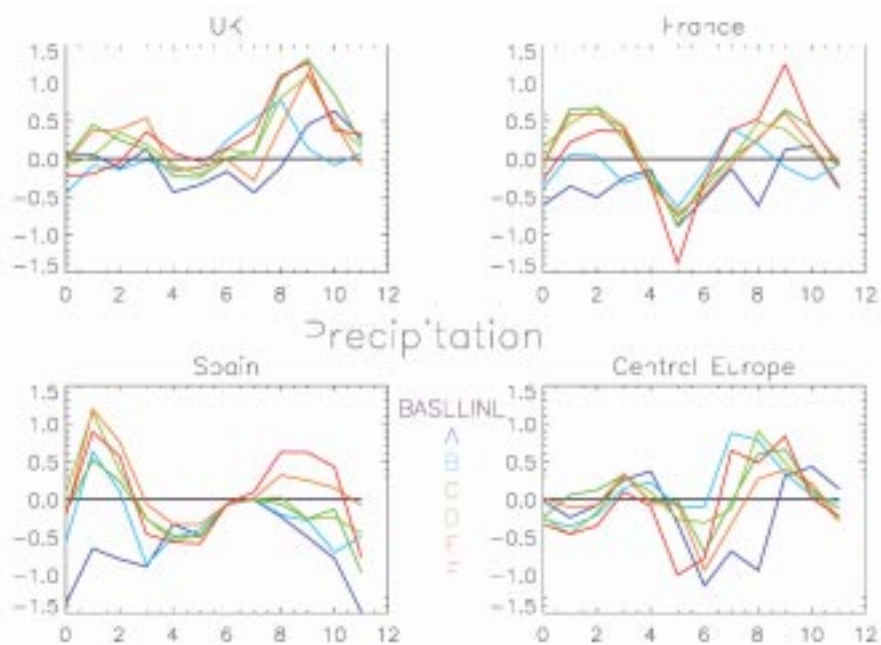


Figure 30: Monthly timeseries of precipitation, over the regions of the UK, France, Spain, and Central Europe, from the BIOCLIM simulations “A” to “F”. All series are anomalies from the Baseline simulation. Units are mmday⁻¹.

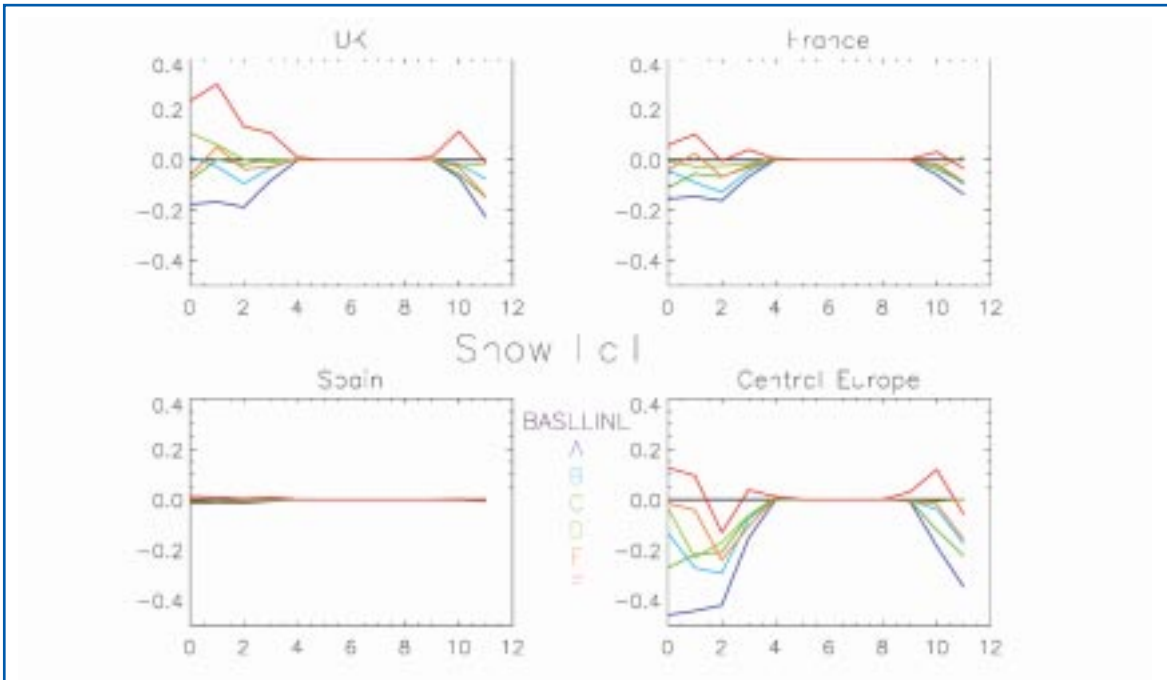


Figure 31: Monthly timeseries of snow fall, over the regions of the UK, France, Spain, and Central Europe, from the BIOCLIM simulations "A" to "F". All series are anomalies from the Baseline simulation. Units are mmday⁻¹.

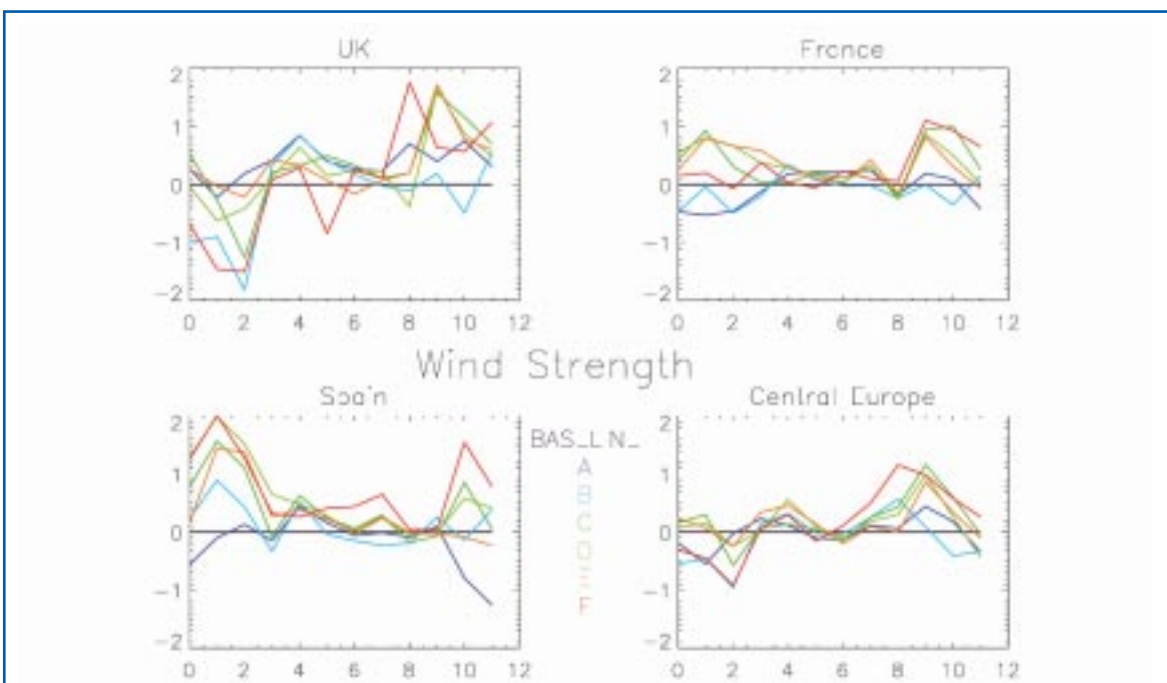


Figure 32: Monthly timeseries of lowest model level wind speed, over the regions of the UK, France, Spain, and Central Europe, from the BIOCLIM simulations "A" to "F". All series are anomalies from the Baseline simulation. Units are ms⁻¹.

3*CO₂ Simulated Vegetation (Simulation A)

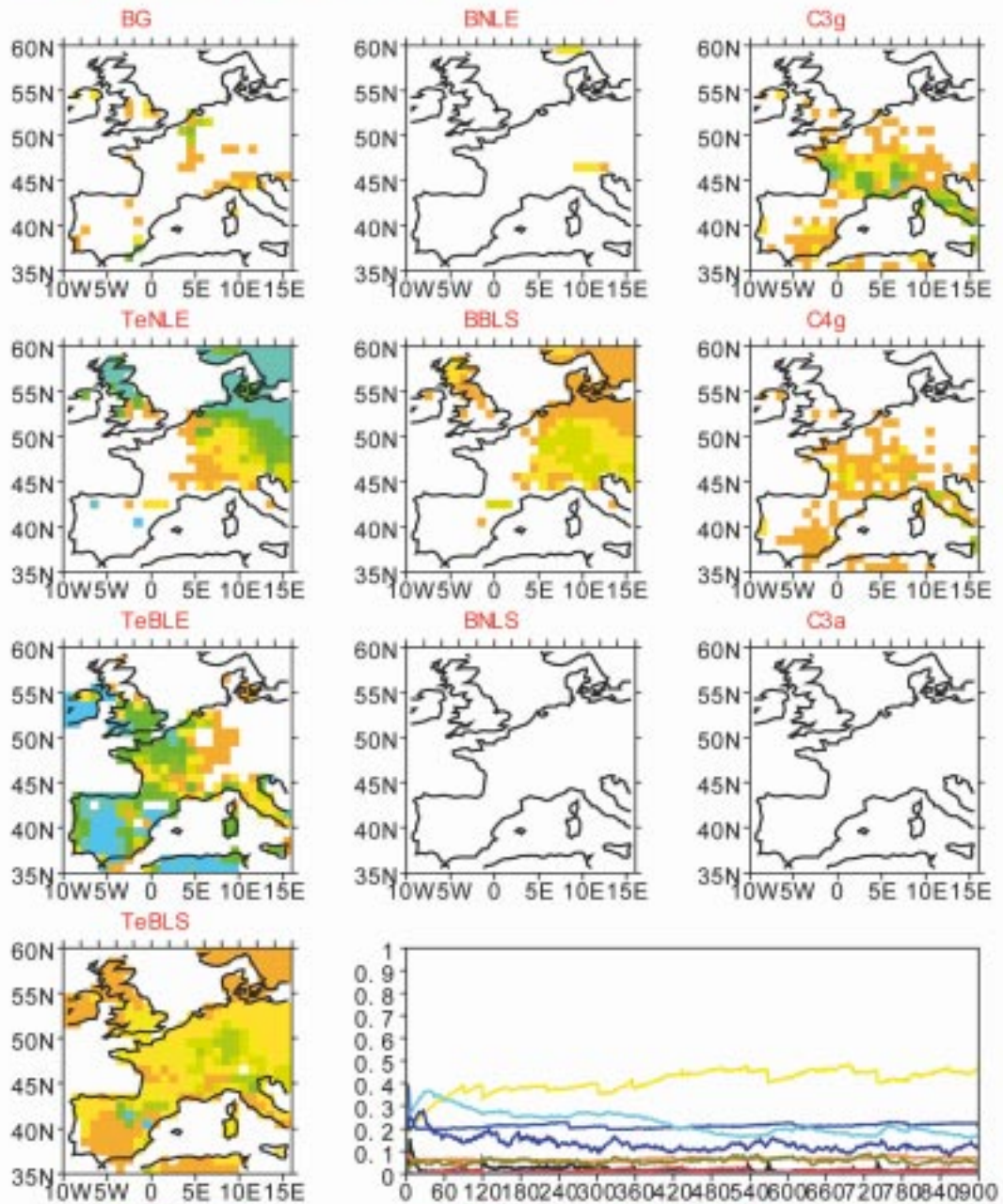


Figure 33: (a) Simulated potential distribution of Plant Functional Types over Europe under a 3*CO₂ climate (from the IPSL_CM4_D simulated "A" climate). The lower right graph corresponds to the time evolution of the area occupied by each PFT, averaged over Europe, for the 900 years simulation. Color legend is displayed separately (figure 6(b)). (b) Time evolution of the litter humidity (top graph) and the fire return frequency (bottom graph) simulated by ORCHIDEE using as atmospheric forcing the present-day observed CRU climatology (black lines) and the IPSL_CM4_D simulated 3*CO₂ climate (simulation "A" ; grey lines).

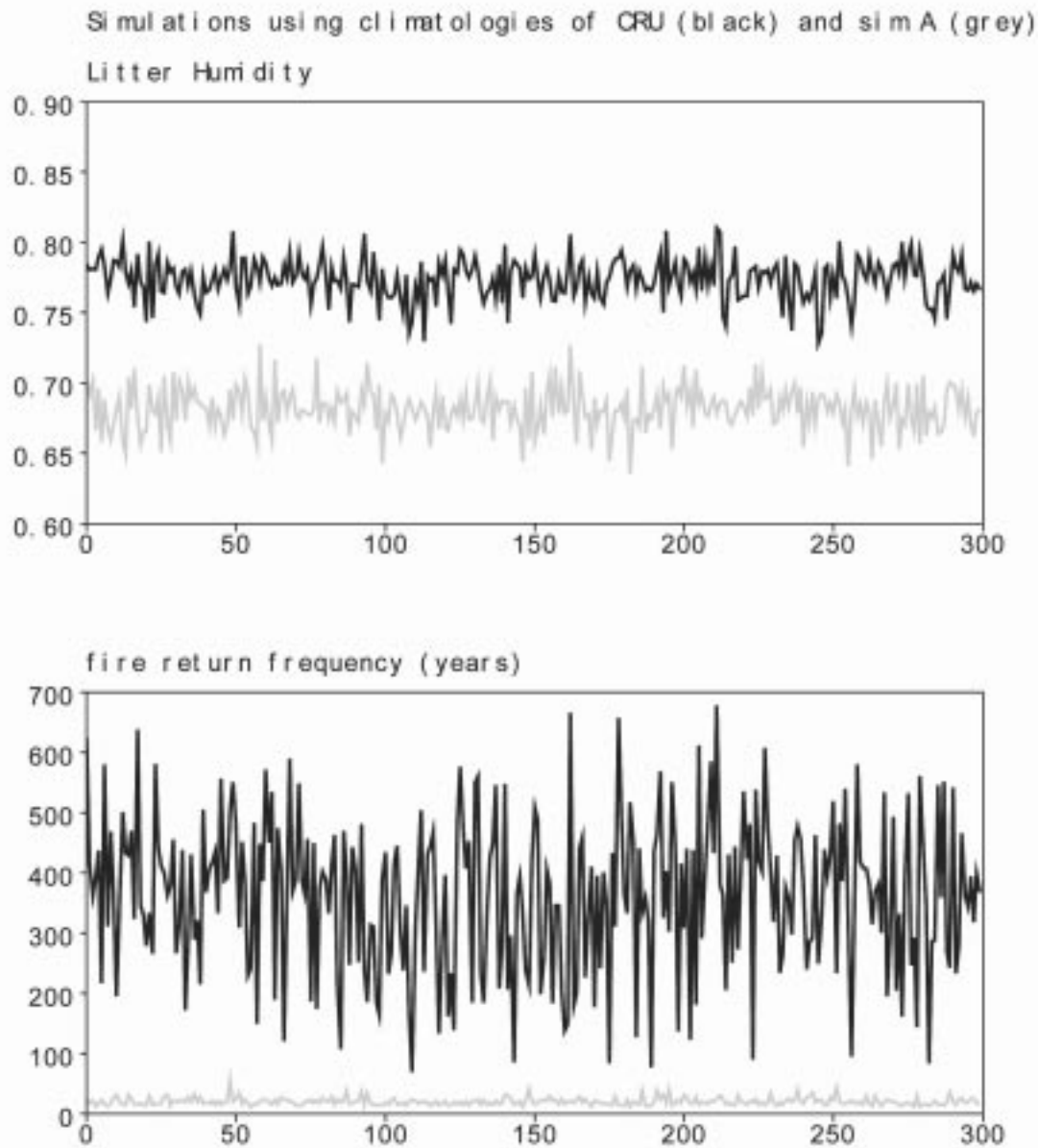
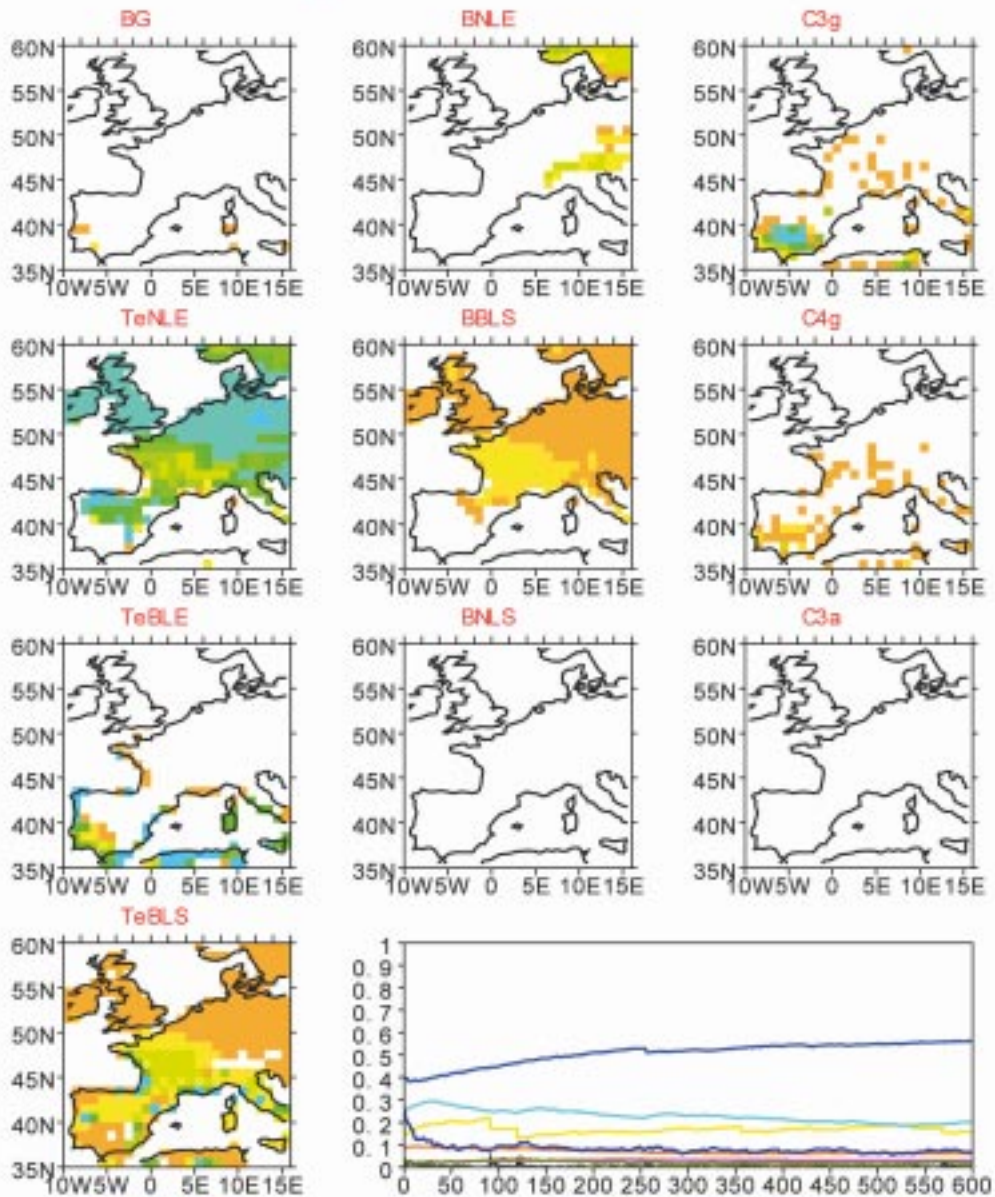


Figure 33: Caption at figure 33(a).

67 kyr AP Simulated Vegetation (Simulation E)



(a)

Figure 34: (a) Simulated potential distribution of Plant Functional Types over Europe 67kyrAP (from the IPSL_CM4_D simulated “E” climate: $CO_2=350ppm$ and presence of Greenland ice sheet). The lower right graph corresponds to the time evolution of the area occupied by each PFT, averaged over Europe, for the 600 years simulation. Color legend is displayed separately (figure 6(b)). (b) Time evolution of the litter humidity (top graph) and the fire return frequency (bottom graph) simulated by ORCHIDEE using as atmospheric forcing the present-day observed CRU climatology (black lines) and the IPSL_CM4_D simulated 67kyrBP climate ($CO_2=350ppm$ and presence of Greenland ice sheet ; simulation “E” ; grey lines). (c) Seasonal evolution of 6 surface variables simulated by IPSL_CM4_D (rainfall, ambient air temperature, ambient air specific humidity) or by ORCHIDEE (evapotranspiration, litter humidity, fire return frequency) averaged over Europe, for observed present-day climatology and the IPSL_CM4_D simulated 67kyrAP future climate “E”.

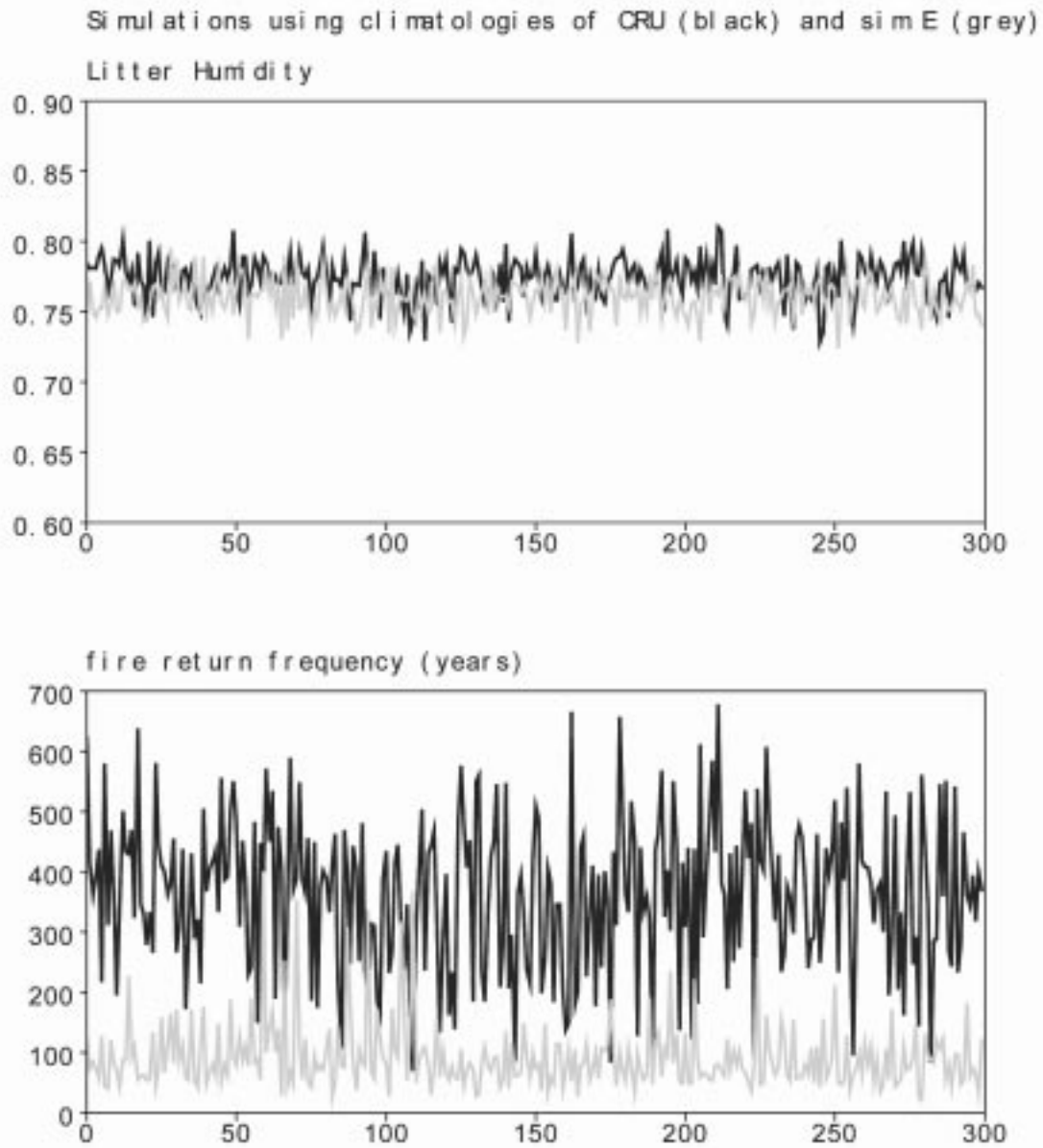


Figure 34: Caption at figure 34(a).

Surface climate averaged over Europe

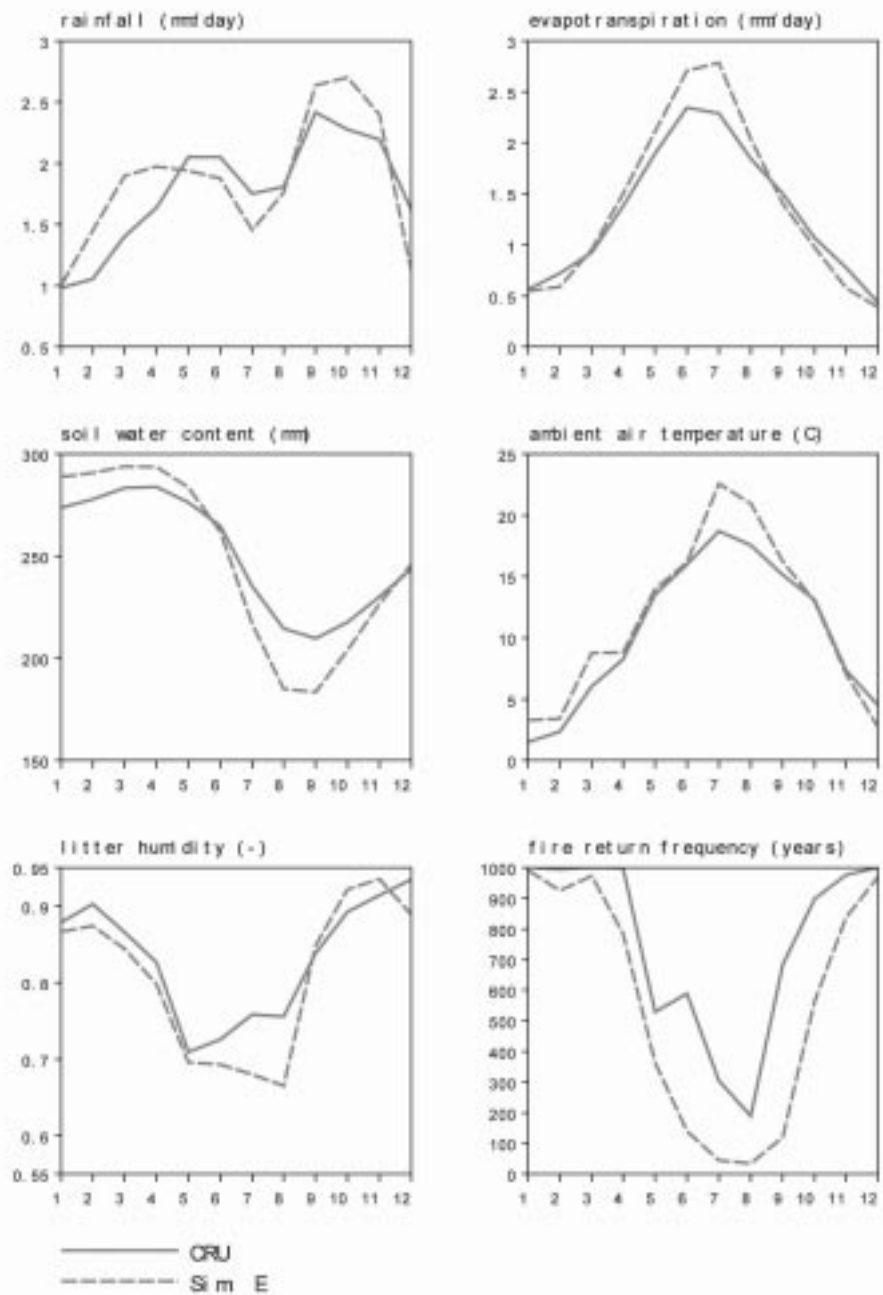


Figure 34: Caption at figure 34(a).

67 kyr BP Simulated Vegetation (Simulation D, no Greenland; CO₂=350ppm)

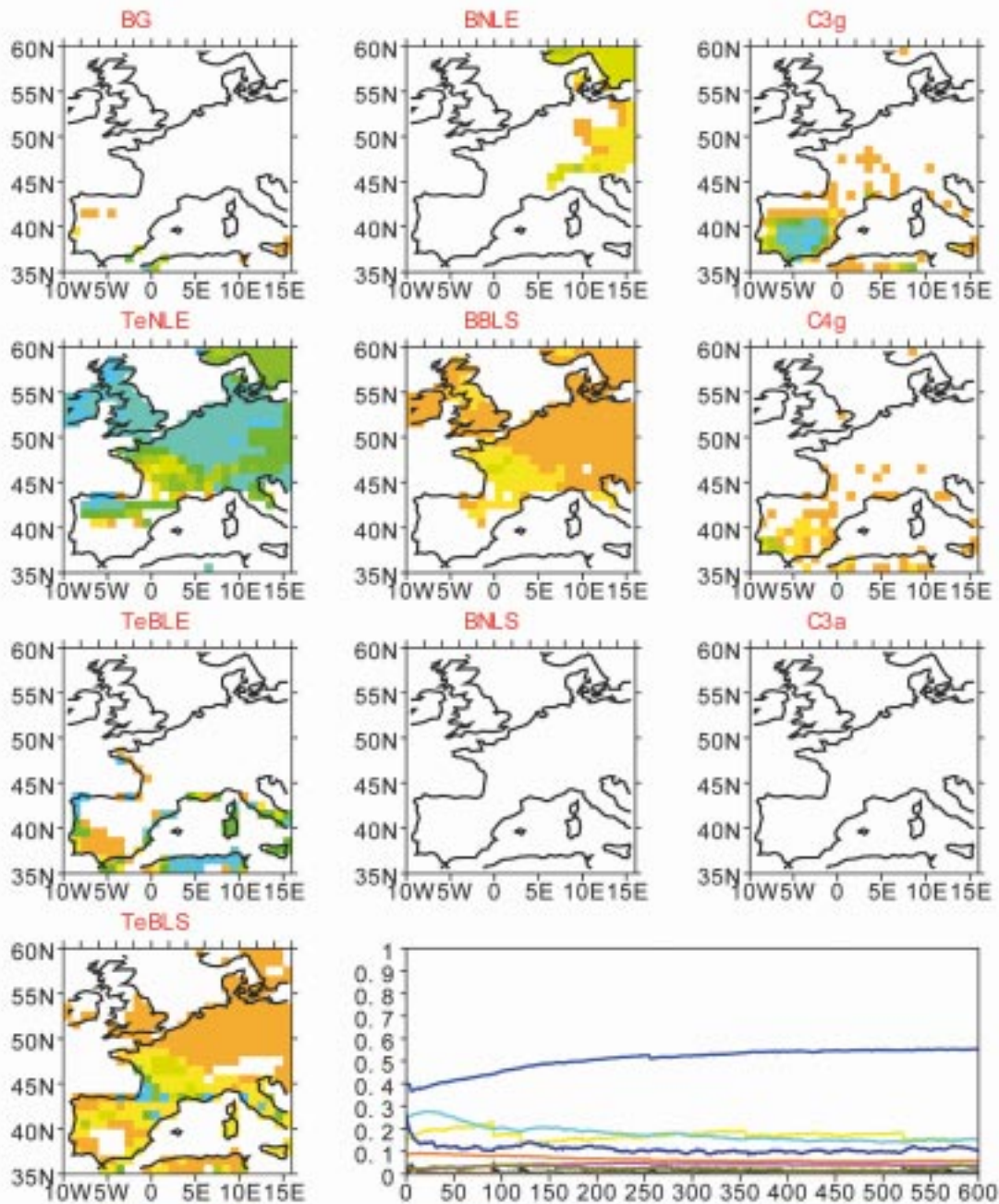
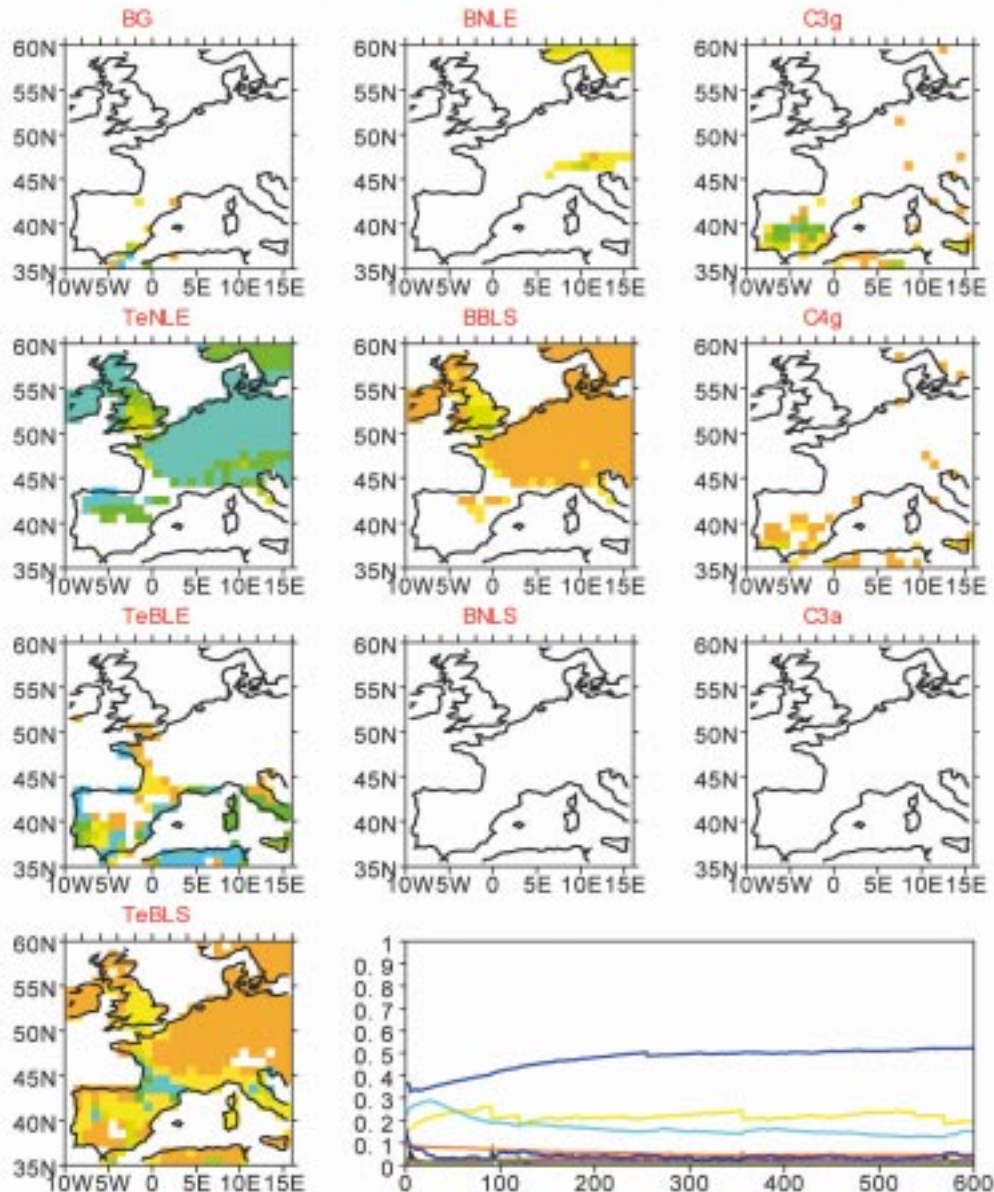


Figure 35: Simulated potential distribution of Plant Functional Types over Europe 67kyrBP (from the IPSL_CM4_D simulated "D" climate ; CO₂=350ppm and no Greenland ice sheet). The lower right graph corresponds to the time evolution of the area occupied by each PFT, averaged over Europe, for the 600 years simulation. Color legend is displayed separately (figure 6(b)).

67 kyr AP Simulated Vegetation (Simulation C, no Greenland, CO₂=550ppm)



(a)

Figure 36: (a) Simulated potential distribution of Plant Functional Types over Europe 67kyrAP (from the IPSL_CM4_D simulated “C” climate: CO₂=550ppm and no Greenland ice sheet). The lower right graph corresponds to the time evolution of the area occupied by each PFT, averaged over Europe, for the 600 years simulation. Color legend is displayed separately (figure 6(b)). (b) Seasonal evolution of 6 surface variables simulated by IPSL_CM4_D (rainfall, ambient air temperature, ambient air specific humidity) or by ORCHIDEE (evapotranspiration, litter humidity, fire return frequency) averaged over Europe, for observed present-day climatology and the IPSL_CM4_D simulated 67kyrAP future climate “E”. (c) Time evolution of the litter humidity (top graph) and the fire return frequency (bottom graph) simulated by ORCHIDEE using as atmospheric forcing the present-day observed CRU climatology (black lines) and the IPLS_CM4_D simulated 67kyrBP climate (CO₂=550ppm and no Greenland ice sheet ; simulation “C” ; grey lines).

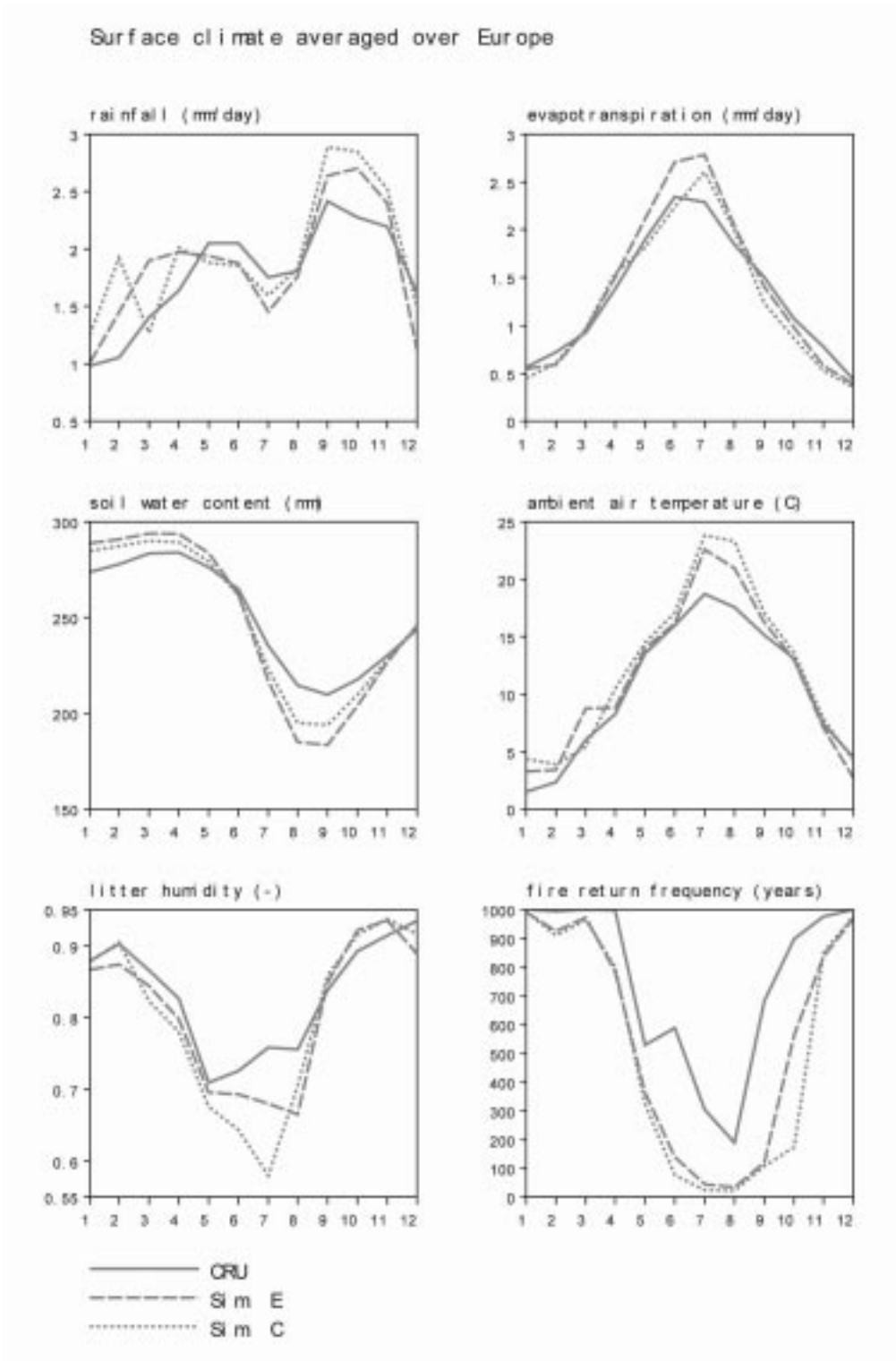
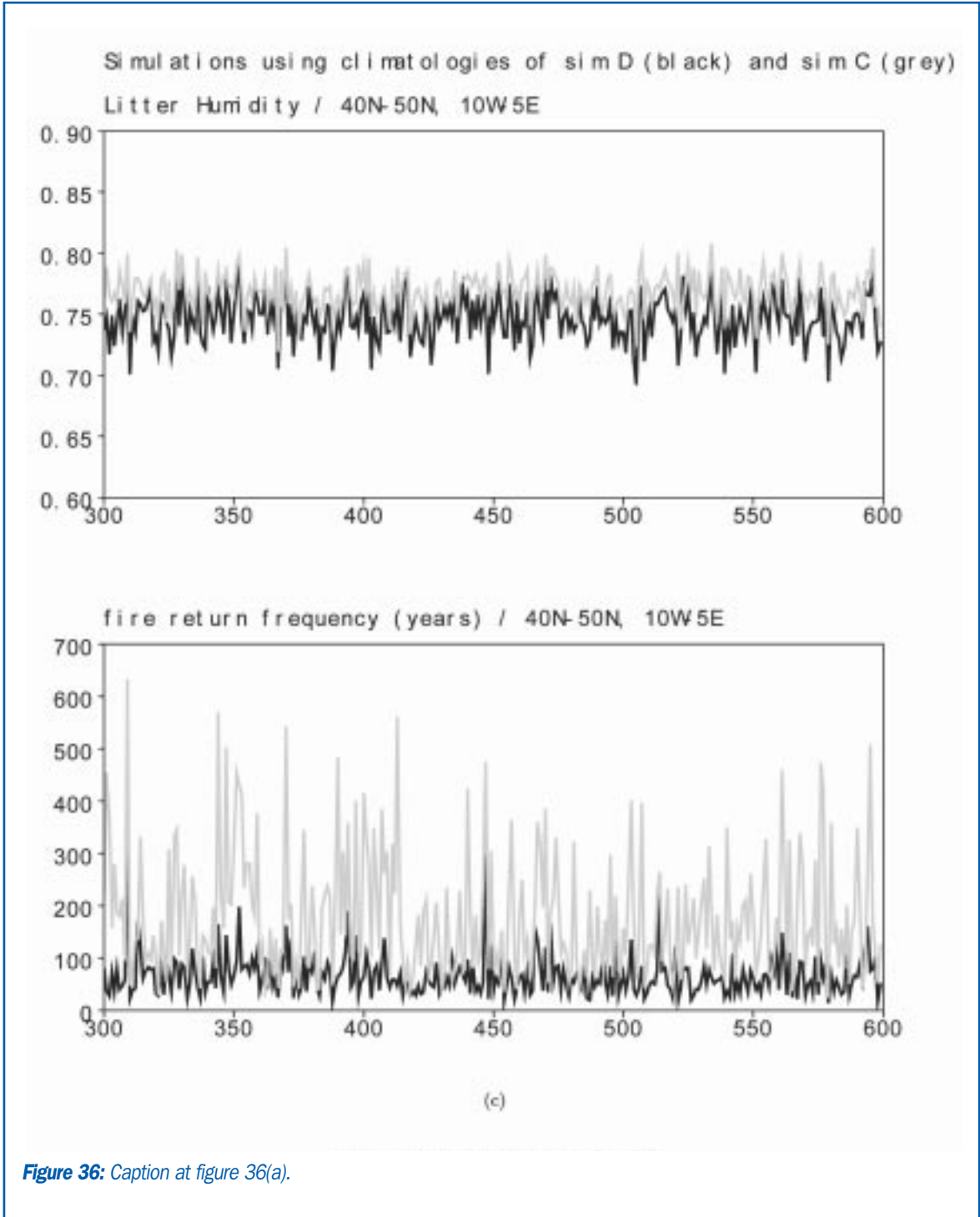


Figure 36: Caption at figure 36(a).



No Green and Simulated Vegetation (Simulation B)

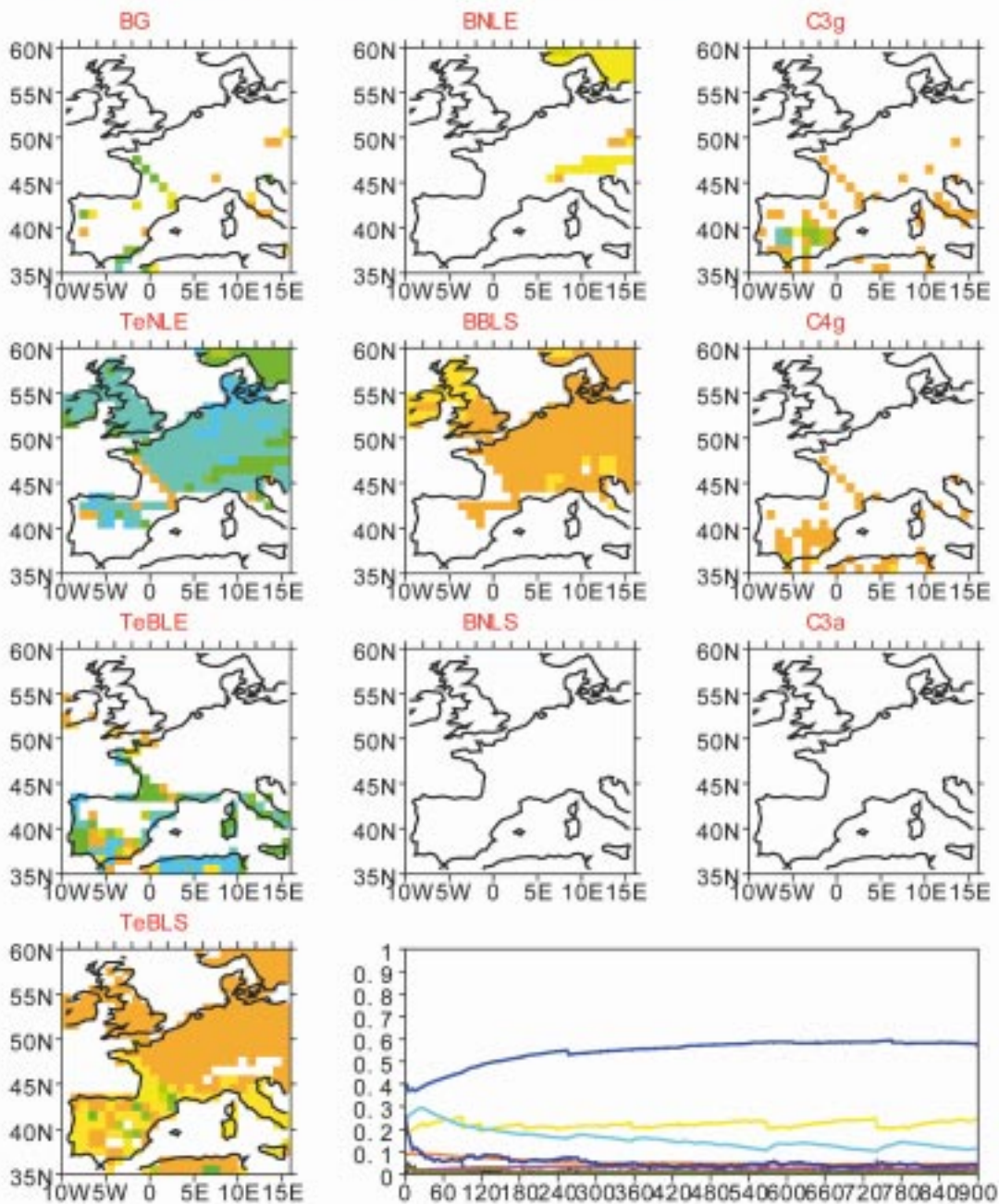


Figure 37: Simulated potential distribution of Plant Functional Types over Europe in a future no Greenland ice sheet climate (from the IPSL_CM4_D simulated “B” climate ; CO₂=550ppm, no Greenland ice sheet and present-day orbital configuration). The lower right graph corresponds to the time evolution of the area occupied by each PFT, averaged over Europe, for the 900 years simulation. Color legend is displayed separately (figure 6(b)).

178 kyr BP Simulated Vegetation (Simulation F)

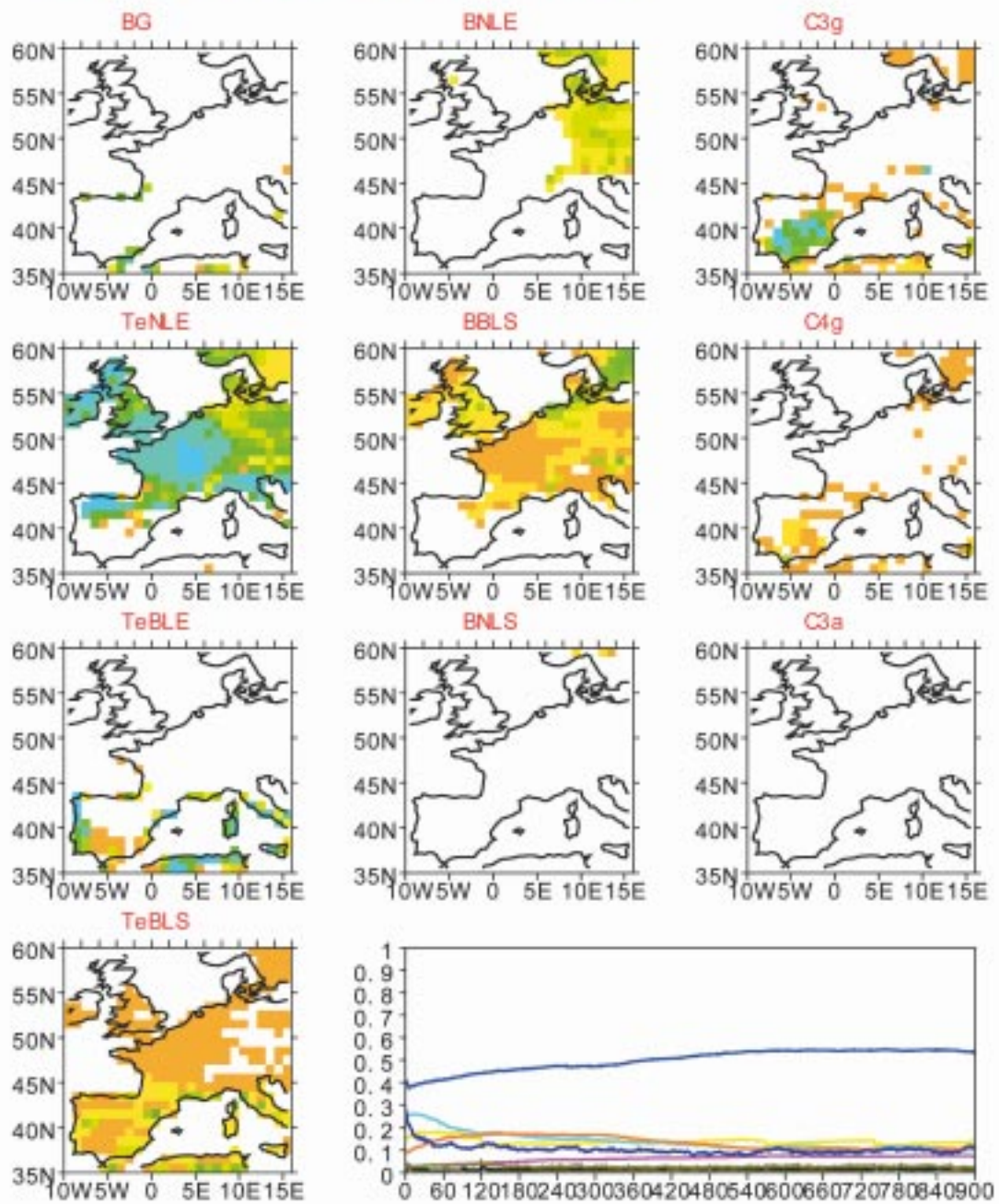


Figure 38: Simulated potential distribution of Plant Functional Types over Europe 178kyrBP (from the IPSL_CM4_D simulated "F" climate). The lower right graph corresponds to the time evolution of the area occupied by each PFT, averaged over Europe, for the 900 years simulation. Color legend is displayed separately (figure 6(b)).

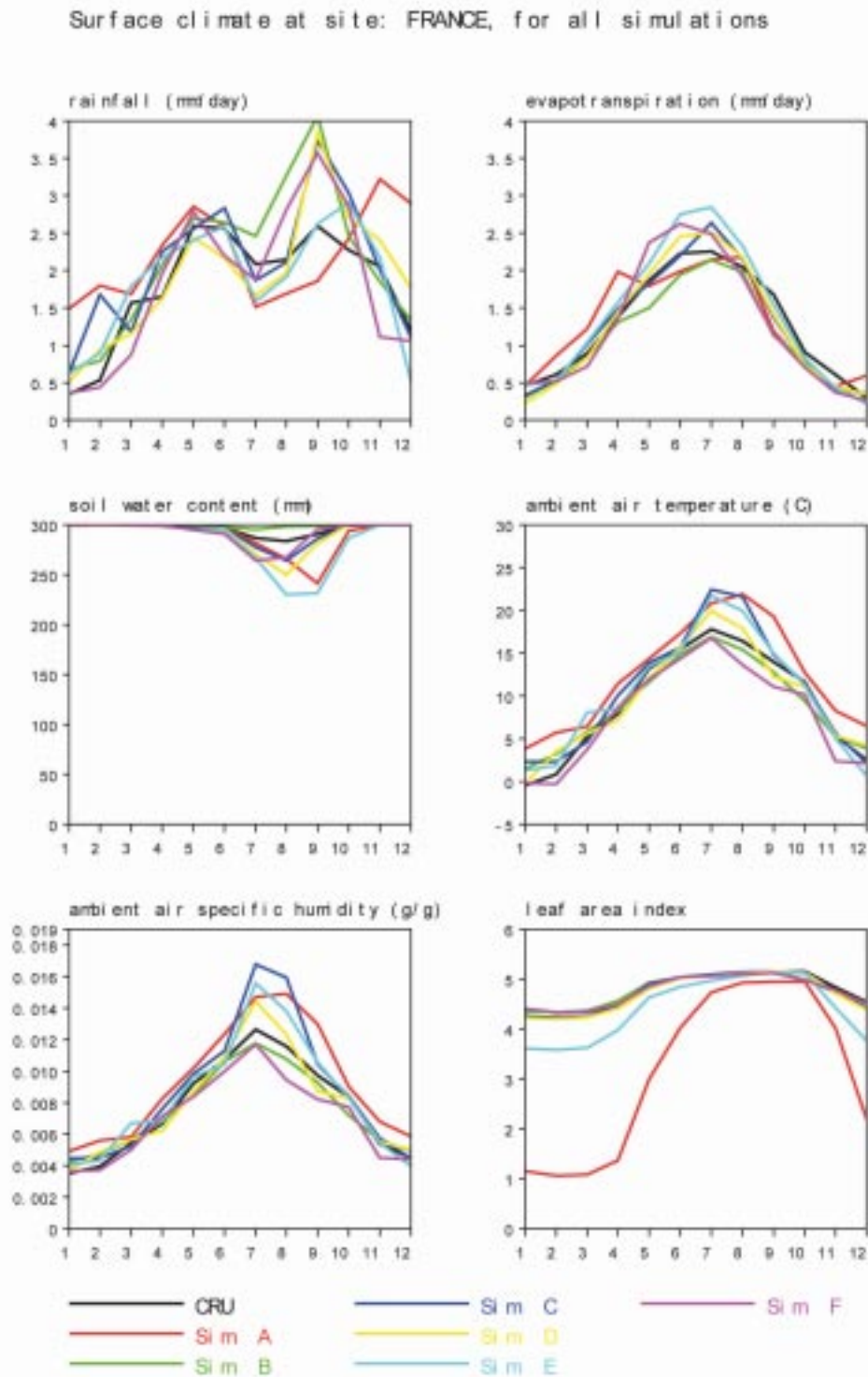


Figure 39: Surface climate at the French study area (48.5N, 5.5E): seasonal evolution of 6 surface variables simulated by IPSL_CM4_D (rainfall, ambient air temperature, ambient air specific humidity) or by ORCHIDEE (evapotranspiration, soil water content, leaf area index), for present-day climatology and fall future climated simulated by IPSL_CM4_D.

Surface climate at site: SPAIN, for all simulations

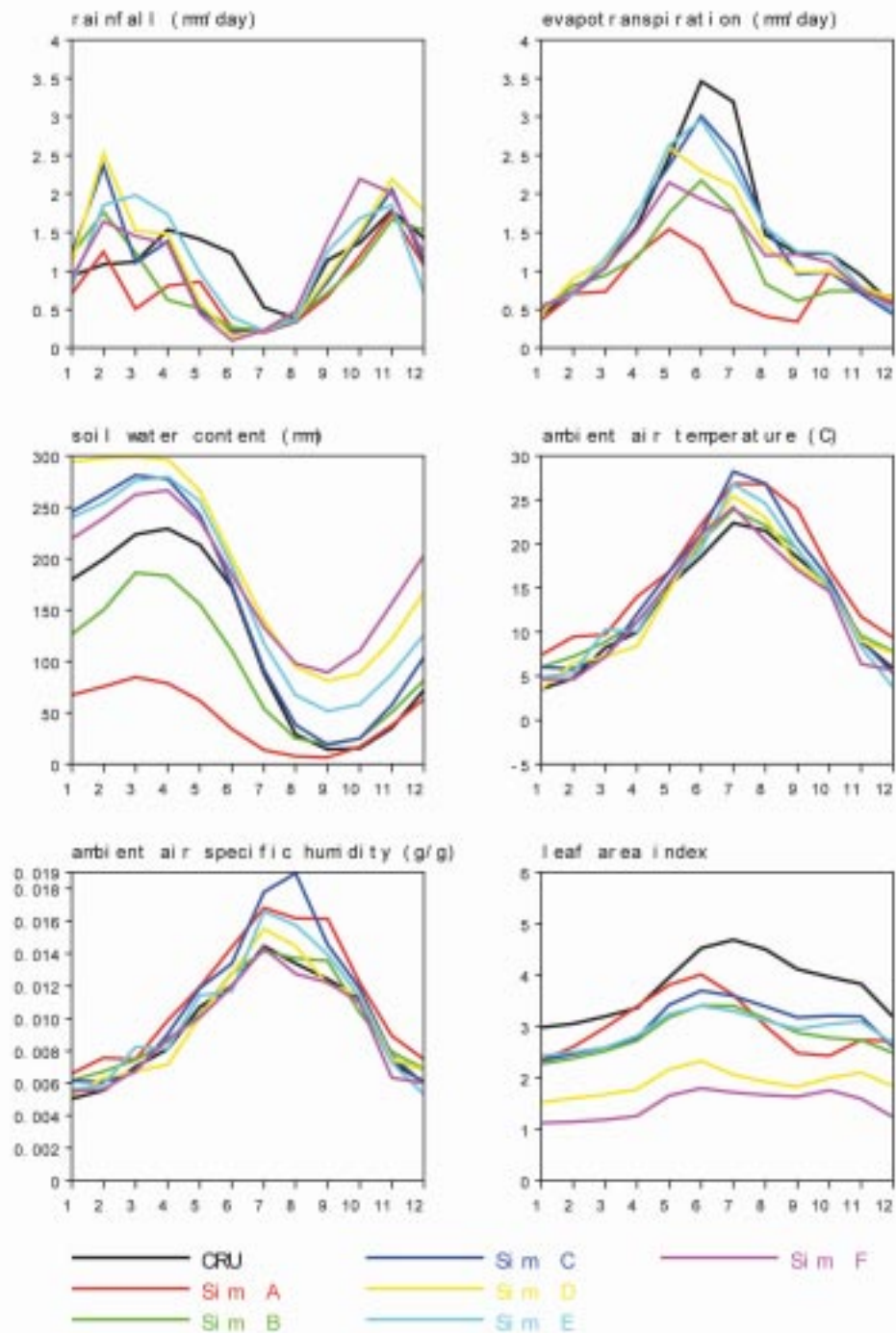
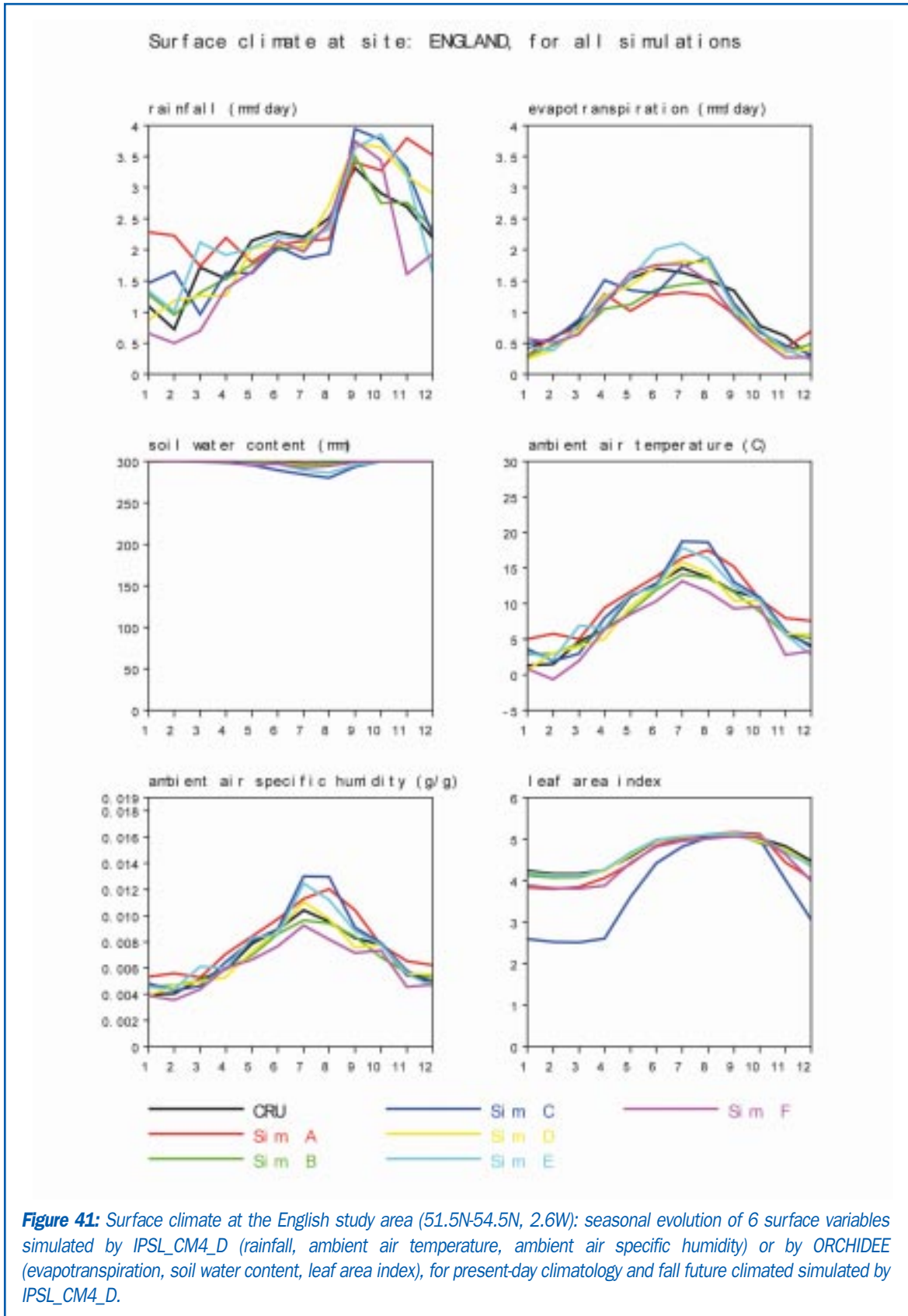


Figure 40: Surface climate at the Spanish study area (38N-41.5N, 1.3W-6.3W): seasonal evolution of 6 surface variables simulated by IPSL_CM4_D (rainfall, ambient air temperature, ambient air specific humidity) or by ORCHIDEE (evapotranspiration, soil water content, leaf area index), for present-day climatology and fall future climated simulated by IPSL_CM4_D.



Surface climate at site: CZECH, for all simulations

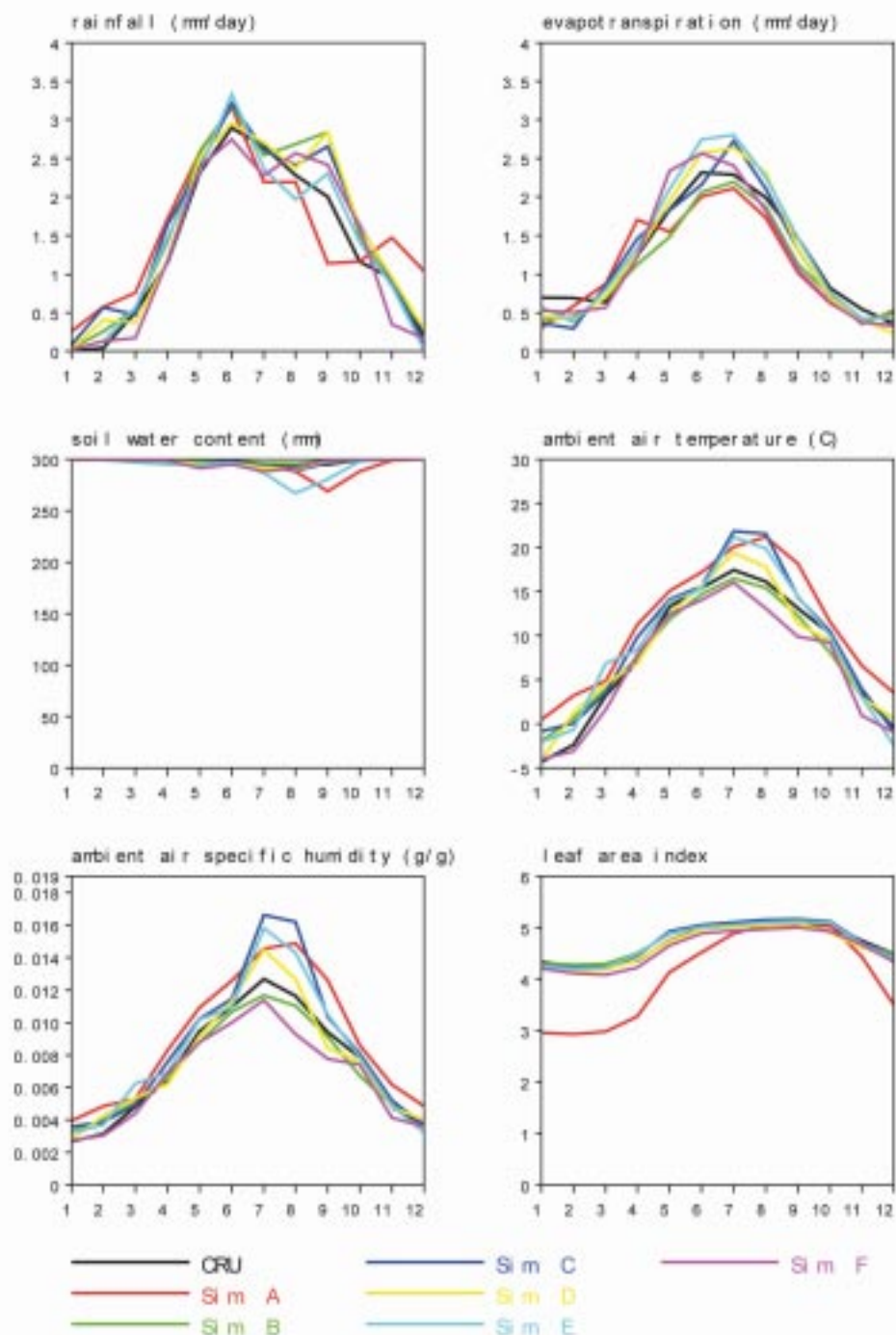
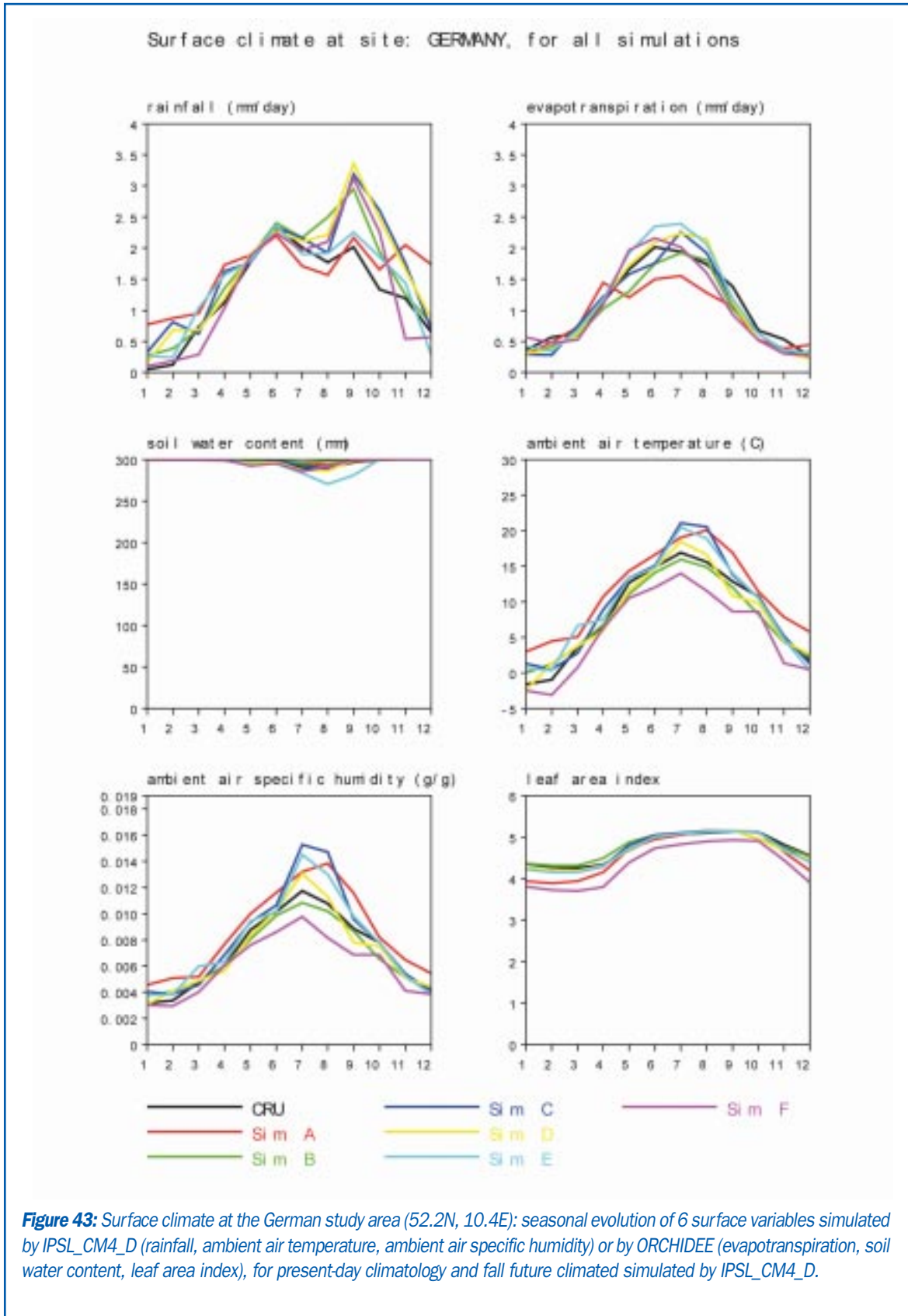


Figure 42: Surface climate at the Czech study area (48.9N-49.5N, 15E-15.6E): seasonal evolution of 6 surface variables simulated by IPSL_CM4_D (rainfall, ambient air temperature, ambient air specific humidity) or by ORCHIDEE (evapotranspiration, soil water content, leaf area index), for present-day climatology and fall future climated simulated by IPSL_CM4_D.





For further information contact:

BIOCLIM project co-ordinator, **Delphine Texier**

ANDRA, DS/MG (Direction Scientifique - Service Milieu Géologique)

Parc de la Croix Blanche - 1/7, rue Jean-Monnet - 92298 Châtenay-Malabry Cedex - FRANCE

Tél.: +33 1 46 11 83 10

e-mail: delphine.texier@andra.fr

web site: www.andra.fr/bioclim/